THESIS

DESIGN OF DURABLE DE-ICING, SUPERHYDROPHOBIC, SUPEROLEOPHOBIC COATINGS

Submitted by

Darryl Lewis Beemer

Department of Mechanical Engineering

In partial fulfillment of the requirements

For the Degree of Master of Science

Colorado State University

Fort Collins, Colorado

Summer 2015

Master's Committee:

Advisor: Arun K. Kota

Travis Bailey
Ketul Popat

ABSTRACT

DESIGN OF DURABLE DE-ICING, SUPERHYDROPHOBIC, SUPEROLEOPHOBIC COATINGS

This work looks at the issue of ice accretion on surfaces and efforts to reduce this ice accretion and the subsequent ice adhesion strength in order to make ice removal easier and more cost effective for wider implementation. Ice accretion on various surfaces is a major economic and safety issue for a variety of industries, including air travel, power production and transmission, maritime shipping, and more. While efforts have been taken to diminish ice accretion and subsequent ice adhesion strength, existing technology is limited in its ability to prevent ice accretion in a wide range of conditions and to then have a low ice adhesion strength once ice has accumulated on a surface.

With the background of icing and solid mechanics of ice removal in mind, materials were developed to exhibit a low ice adhesion strength while maintaining the durability characteristic of a non-sacrificial coating. After development and testing, it was found that the developed materials exhibited an adhesion strength lower than any currently available technology, with extended durability under both ice removal and mechanical abrasion conditions.

As a secondary effort, an initial exploration into the development of durable superomniphobic surfaces was performed in order to reduce and/or prevent adhesion of water-based paint and a low surface-tension fluid to various surfaces. Development of a variety of surface types (spray coated layered and mixed surfaces, etched stainless steel surfaces, and more) was performed, with initial results providing an encouraging path forward for future development of this durable coating work.

ACKNOWLEDGEMENTS

While the individuals that have assisted the author in creating this work and in life are too numerous to include in this section, the author would like to acknowledge the following individuals who have directly helped with this work.

Thank you to all undergraduate students who helped with testing, including Ari Metzger, Josh Murabito, Corrie Noah, and Robbie Mitchell. Thank you to all fellow graduate students and the whole research group, particularly Sanli Movafaghi, Hamed Vahabi, Sailaja Eluri, and Wei Wang, for always having good ideas and for providing a forum to pass ideas around. Thank you to all of the help from other research groups, particularly the Chuck Henry group for their assistance with optical profilometry measurements and the Travis Bailey group for their help with rheometry testing. Thank you to the Khetani and Kipper research groups for sharing lab space and wonderful discussion. Thank you to the thesis committee for providing guidance and suggestions during the research process. Thank you to Dr. Arun Kota for all of the hours and effort in advising this work and for helping guide a soothing path forward in times of trouble.

Thank you to you, the reader, for taking the time to read this work and appreciate the work that went into this document. Nothing is worth writing if no one will read it, so thank YOU.

Finally, the author would like to acknowledge all of his wonderful friends and family for all of their love and support throughout the work and in life. Thank you for the inspiration and for sharing the message of 1 Corinthians 13:13 daily.

TABLE OF CONTENTS

1. INTRODUCTION

Repellent surfaces have received great attention in the last few decades for their many applications in a variety of industries, including energy production/transmission, transportation, consumer products, medical devices, and more due to continued improvement in production and imaging technology allowing for the creation and analysis of advanced material surfaces. While the creative capacity of human-kind will ensure the continued discovery of innovative ways to implement engineered repellent surfaces, a few examples are presented here. More serious applications for repellent surfaces include self-cleaning,[2, 4-12] antifouling,[13-21] stain-resistant clothing,[7] drag reduction for internal and external flow,[22-24] fog harvesting for water collection as the world faces a continual water crisis,[25-29] locomotion of floating micro-robots,[30-34] corrosion prevention,[35-37] separation of liquids,[38-41] lab-on-chip sensor controls,[42-44] and many more.[45-50] Repellent surfaces have also been developed to try to prevent ice from adhering to a variety of surfaces, with varying degrees of success. [51-77] Since ice can still adhere to anti-ice surfaces under certain conditions, other de-ice materials have also been developed to make ice removal easier than on normal surfaces.[56, 60, 78-93] The current work was performed with the goal of developing surfaces for improving the removal of ice (de-icing) from surfaces exposed to extreme arctic conditions, preventing water-based paint from fouling surfaces exposed to moderate abrasion, and preventing the fouling of low surface tension fluids on production equipment for the food industry.

2. FACILE, DURABLE DE-ICE COATINGS

2.1. Introduction and Literature Review

Ice accretion on airplanes, ships, shipping facilities, photovoltaic cells, and power lines is a severe physical and economic hazard. For example, when ice accumulates on the exposed surfaces of airplanes it can lead to an undesirable increase in drag, decrease in lift, and reduced visibility.[56, 94] Consequently, technologies that can delay ice formation (i.e., anti-icing) and facilitate rapid, facile removal of ice build-up (i.e., de-icing) are highly essential for various industries.[60, 95-97] Typically, passive technologies are preferred over active technologies which are more complex and have higher capital costs and energy demands.[60, 98, 99] Over the past decade, noticeable progress has been made towards the development of anti-icing and de-icing coatings. However, it is noteworthy that anti-ice surfaces are only effective for a limited period of time; ice can eventually build-up on most any surface exposed to harsh conditions (e.g., frigid temperatures and high humidity).[51-77] Current passive de-icing technologies are either environmentally hazardous, lack durability, or display high ice adhesion strengths above 20 kPa.[56, 60, 78-93] Therefore, an ideal long-term solution is to design passive de-icing surface coatings with extremely low ice adhesion strength and high durability so that ice can promptly and repeatedly de-bond from coated surfaces under natural forces such as gravity and wind drag.

Recent years have seen a surge in slippery de-icing coatings with extremely low ice adhesion strength (10 kPa reported) which arises from the sacrificial nature of the liquid coating as mechanical ice removal sheds off some of the liquid coating, exposing the underlying structure. [79, 100-104] Yet, mechanical durability remains a significant hurdle for the practical application of the de-icing coatings under development.

From previous work, it has been found that increasing the thickness, lowering the bulk modulus, and decreasing the surface energy of a material can all decrease adhesion of biological and man-made

adherents.[15, 105-112] Kendall's 1971 analysis of adhesive failure of elastic solids has been further developed for shear adhesive failure and simplified into a general form for shear adhesive stress (τ), based on the work of adhesion between the two adhered objects (W_a), the material bulk modulus of elasticity (G), and the coating thickness (t).[113, 114]

$$\tau \propto \sqrt{\frac{W_a * G}{t}} \quad (1)$$

Yet, there is not currently a systematic study on the correlation between these parameters and the resulting material durability under ice removal conditions, which is important for the practical application of de-icing coatings.

In this work we demonstrate for the first time that silicone-based coatings with carefully tailored properties exhibit extraordinary de-icing performance, including extremely low ice adhesion strengths (< 7 kPa and < 15 kPa for coatings with thicknesses of 1.35 mm and 200 μm, respectively) and excellent mechanical durability (withstanding at least 1000 abrasion cycles). We believe that these mechanically robust surfaces with extremely low ice adhesion strength provide a long-term and universal solution for de-icing operations in various industries.

2.2. Materials/Methods/Experiments

As adhered ice was removed under shear loading on a thin film that primarily sees shear forces, the shear storage modulus (G') was used to represent the bulk modulus (G). The modulus was controlled by varying the molecular weight and amount of silicone oil "plasticizer" in the PDMS base of varying molecular weights, while the surface energy of all materials was held constant (Figure 6.1). The influence of thickness on ice adhesion strength was controlled by varying the speed for spin-coating the material on glass substrates. By varying the ratio and molecular weight of the base and plasticizer PDMS oil along with coating thickness, an ice-removal coating was developed that exhibited an ice adhesion strength down to ~5 kPa for a surface 1.35 mm thick, and ~10 kPa for a 200 μm thick surface with good durability under ice removal and mechanical abrasion.

2.2.1. *Material Preparation, Thickness/Roughness Measurements*

In the present work, we chose to study polydimethylsiloxane (PDMS) based coatings because the environmentally friendly material's bulk modulus and thickness properties can be readily tuned while retaining the same surface chemistry between surfaces.[18, 44, 115-117] Samples were prepared by mixing the reactive base PDMS with the trimethyl-terminated plasticizer oil based on the desired percentage based on weight, with all mixtures cross-linked in a 10:1 ratio of base to cross-linker, as advised by the supplier. The samples were completely degassed under vacuum (Figure 6.7) to remove all gas bubbles produced during mixing then immediately spin-coated onto glass slides for sufficient time to allow even spreading using a Specialty Coating Systems G3P-8 Spin coater (Figure 6.42). Samples were then fully cured at 70 ^{o}C on a hot plate, well below the boiling temperature of the material components. A Zygo ZeScope optical profilometer was used to measure the thickness and roughness of each sample in at least three separate locations. The spin speed of each material was tuned to produce samples with a consistent thickness. Thickness-controlled samples were coated to a thickness of 200 μm, with all thicknesses controlled to ±20 μm (section 6.6.2).

2.2.2. *Rheometry Procedure*

Rheological analyses were performed using a TA Instruments ARES Rheometer using 8mm parallel plate geometry (Section 6.4). This geometry was chosen in order to provide enough pressure to the soft samples for adequate strain detection. All samples were tested with a 2-5% strain offset and output torque ranging from 0.2-4.5 g-cm (with an equipment threshold sensitivity of 5 mg-cm). Dynamic strain sweeps were performed between 0.1% and 10% to determine where the material showed a linear modulus response, indicating the appropriate strain percentage to use for the dynamic frequency sweeps, which were then performed to calculate the average rheological properties in the frequency range of 10 to 100 rad s^{-1}. All tests were performed at -20 ^{o}C using the TA Instruments convection oven under nitrogen gas.

2.2.3. Ice Adhesion Strength Testing

Ice adhesion strength was measured by clamping samples onto an internally fabricated mounting plate attached to an electric Peltier cooling plate (TECA model AHP-150CPHC with TC-3400 controller) at a temperature of -18 °C (±2 °C). The as-manufactured polished side of a square plastic cuvette with a side length of 1 cm was placed onto the surface of the sample, then 250 µL of DI water was added into the cuvette and allowed to completely freeze hard to ensure a liquid layer did not exist between the ice and the surface.

Linear shear removal testing was performed at a constant rate of 5 cm min^{-1} using a Kent Scientific GenieTouch syringe pump with a strain gauge firmly mounted on top. The translation rate was held constant at a moderate rate relative to other studies that have demonstrated a rate dependence for elastic adhesion.[86, 108, 118, 119] Due to this rate dependence, it is suggested that all studies regarding ice removal report the loading rate. Two strain gauges were used depending on the adhesion strength for the material: a Mark-10 model M3-2 for increased sensitivity of loads under 10 N (100 kPa) and a Mark-10 model M3-20 for loads under 100 N (1,000 kPa). A probe 1 mm thick and 12.5 mm wide was used to squarely load the ice block, with the probe placed as close to the coating as possible without contacting the surface (within 1 mm). The load was applied well below the center of gravity of the ice block to minimize normal forces at the ice-coating interface. Samples were loaded over a distance of 1.5 cm to ensure complete removal of the ice from the coating, with force vs. time and the maximum force recorded using MESUR Lite software (version 1.3, Mark-10 Corporation).

The following equation is used to calculate the ice adhesion strength (IAS), where F is the measured force and A is the ice-coating adhesion area (1 cm^2).

$$IAS = \frac{F}{A} \quad (2)$$

The average of the first three removal trials of at least three samples for each material was utilized to develop the initial ice adhesion strength for each material.

After ice block removal, effective ice removal durability was tested by repeating the adhesion strength test until 30 tests were reached and it was clear that the sample would not fail in a time reasonable for durability experimentation under these testing conditions.

2.2.4. Linear Taber Abrasion Method

Further durability testing was performed using a Taber Industries linear abraser, with a stroke length of 1 inch, load of 350 grams, head diameter of 1 inch, pressure of 6.7 kPa, and a speed of 25 cycles min^{-1} (Section 6.5). Buehler CarbiMet 2 sandpaper was used for abrasion tests, with abrasive replaced at least every 250 tests, with more frequent replacement if any contamination of the abrasive was seen. 400/P800 grit sandpaper was initially used as its RMS roughness was similar to the mildly abrasive CS-10 abrasive from Taber Industries, and 180/P180 grit sandpaper was chosen as it provided a slightly higher RMS roughness than the Taber Industries H-18 abrasive (Figure 6.4). Both the CS-10 and H-18 abrasives are commonly used for durability testing of coatings, particularly for ASTM D4600. The linear abraser was used as specimens of various sizes could be easily clamped and tested, allowing for ice adhesion testing after abrasion consistent with that done before abrasion.

2.3. Results and Discussion

2.3.1. Confirmation of Test Setup

After spin-coating preparation, samples were securely clamped on a Peltier cold stage, bringing the surface to -18 ± 2 ^{o}C, well below the melting temperature of water, where the sample was allowed to reach thermal equilibrium before deionized (DI) water was frozen completely into a hard block of ice to ensure there was not a liquid layer between the material and frozen ice block (Figure 2.1B). [81]

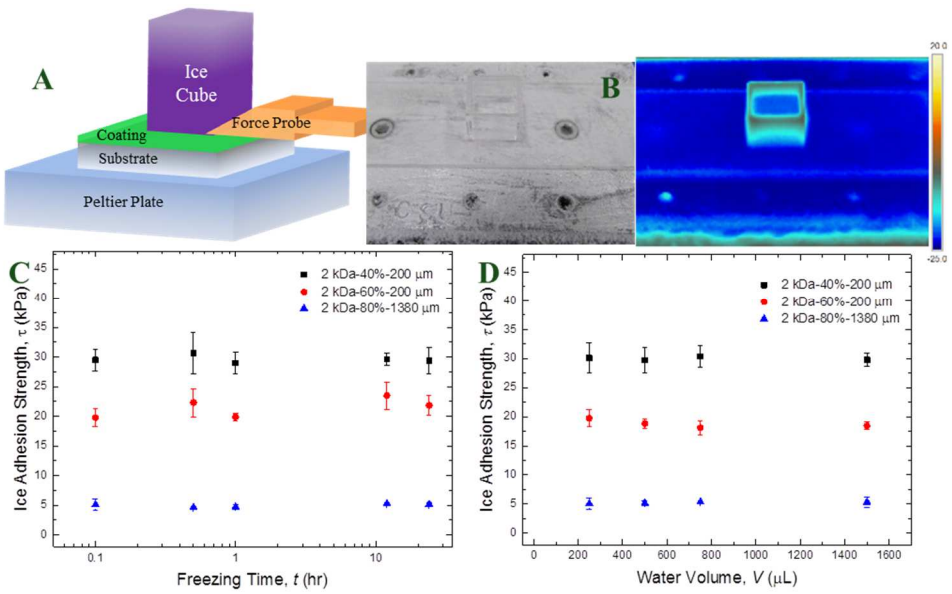

Figure 2.1: A) Schematic of ice adhesion strength test setup. B) Image of frozen water in cuvette on coated slide mounted to Peltier Plate and Forward-Looking Infrared (FLIR) image of frozen test setup. C) Variation of freezing time to confirm testing procedure. D) Variation of freezing water volume to confirm testing procedure.

As seen in Figure 2.1B, infrared imaging and a thermocouple (not shown) mounted onto a hole tapped into the Peltier plate were used to ensure the consistent freezing temperature for ice removal tests, with both the surface and the top of the ice cube well below 0 ^{o}C. There were no obvious changes in ice adhesion strength when tested at various freeze times ranging from several minutes to several hours (overnight, Figure 2.1C). Similarly, no obvious change in ice adhesion strength was seen when the frozen DI volume in a constant cross-section cuvette was also varied to ensure a lack of pressure effect due to the column of water during freezing (Figure 2.1D). Volume was varied from the minimum for full surface coverage (250 µL) to nearly an order of magnitude higher (1.5 mL). Indeed, the pressure increase over the range of fluid heights tested is minute compared to atmospheric pressure (84.12 kPa to 84.24 kPa, with an atmospheric pressure of 84.1 kPa at the altitude of 5,250 feet (1600 meters) in Fort Collins, CO). For consistency, all tests were conducted at -18 ± 2 ^{o}C with a DI water volume of 250 µL (or a fluid height of 2.5 mm for the 1 cm^2 cuvette) and a strain rate of 5 cm min^{-1}.[56]

2.3.2. *Modulus and Thickness Variation*

The coating adhesion strength was initially controlled by varying the molecular weight and percent of silicone oil in a material with constant molecular weight of vinyl silicone base (Figure 6.2).

From this, it was found that as high of a percentage of lower molecular weight plasticizer in the base material (without being overly-tacky material upon curing) resulted in the lowest ice adhesion strength results (Figure 2.2A).

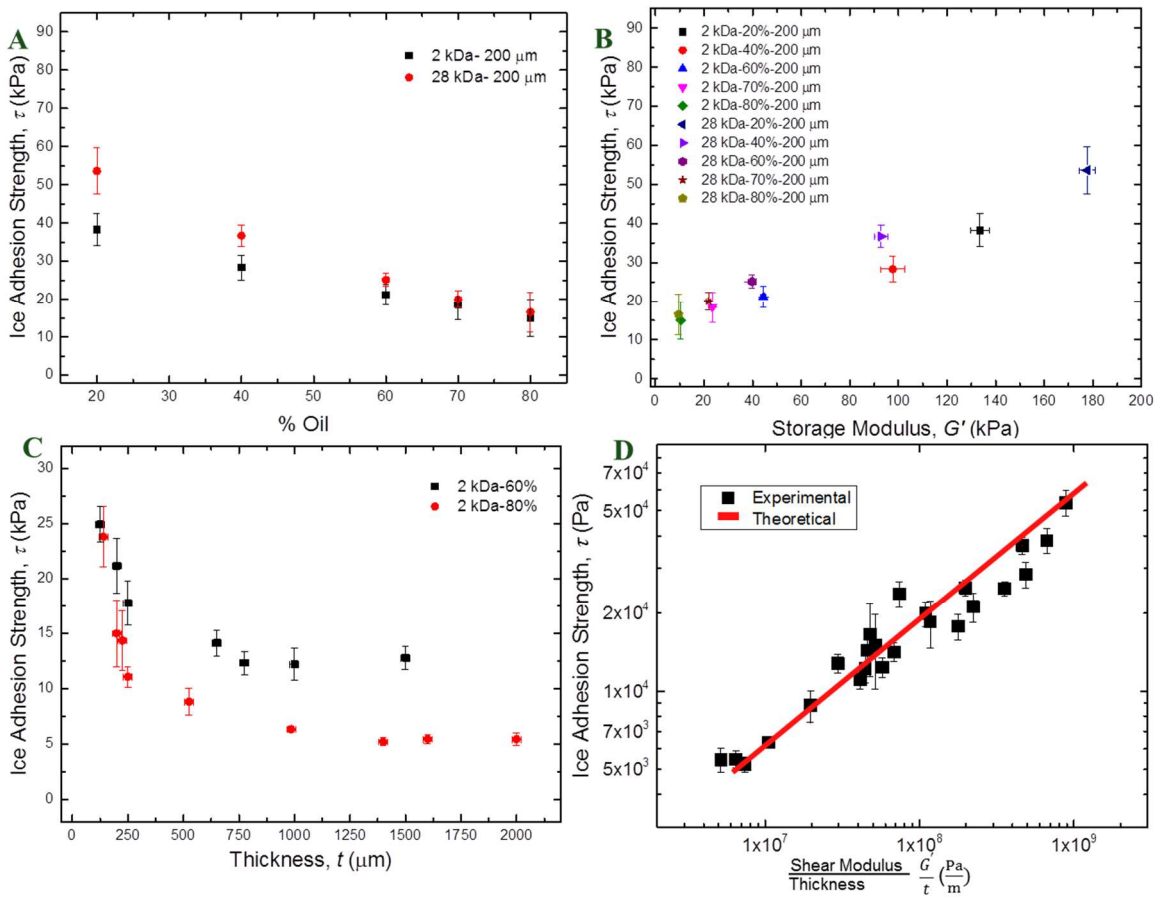

Figure 2.2: A) Ice adhesion strength for varying percentages of different molecular weight oils (2 kDa oil- black circles; 20 kDa oil- red squares) at 200 µm. B) Ice adhesion strength varying with shear modulus at 200 µm. C) Ice adhesion strength for 60% and 80% oil materials with varying thickness. D) Log-log plot of data (black squares) and theoretical curve fit of (G′/t)^0.5 (red line).

As all tested materials had a storage modulus (G', solid-like, in-phase response) around 10 times the loss modulus (G'', liquid-like, out-of-phase response), the storage modulus was chosen to represent the linear elastic system. Materials were held at a constant thickness in order to compare the adhesion

strength to storage modulus, with a finding that lower modulus materials resulted in lower adhesion strengths (Figure 2.2B). Two of the lowest adhesion strength materials were tested at varying thicknesses to determine if increasing the amount of bulk material would further decrease the ice adhesion strength. It was found that IAS decreased with increasing coating thickness, with a plateau at around 1 mm for the lowest IAS sample (~5 kPa, Figure 2.2C). Recognizing that both modulus and thickness were affecting the IAS, we compared IAS to modulus over thickness (G'/t), and successfully found that this data matched the previous theoretical models for general adhesion to a thin material, even with use of shear ice removal and the shear storage modulus (Figure 2.2D).

2.3.3. Coating Durability

Since the durability of de-ice coatings is their greatest barrier to widespread use, repeated ice adhesion strength tests were performed to compare developed coatings to liquid-based, sacrificial coatings. All tested samples exceeded 30 icing and de-icing cycles without any visible effect on performance (Figure 2.3A).

As de-icing cycles are not the only durability need of

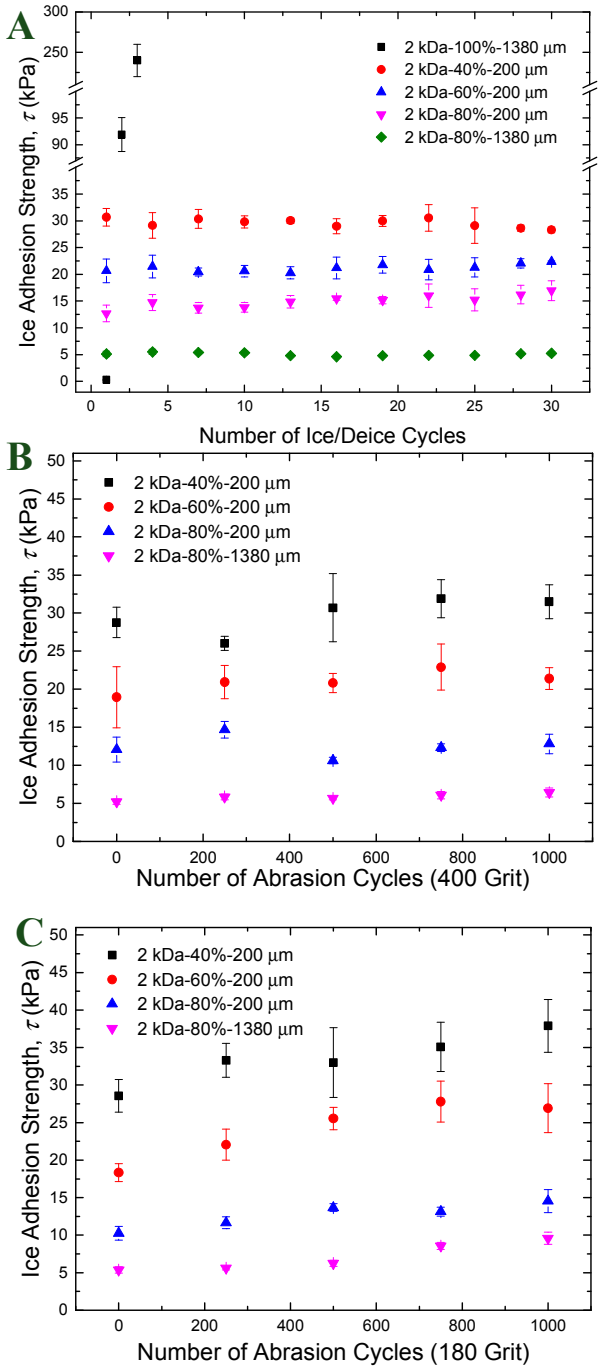

Figure 2.3: A) Endurance shear ice removal tests showing no change after 30 trials for non-sacrificial coatings. B) Ice adhesion strength after 400/P800 grit sandpaper abrasion cycles. C) Ice adhesion strength after 180/P180 grit sandpaper abrasion cycles.

de-icing coatings, accelerated life testing using linear abrasion with sandpaper was performed on the materials with lowest adhesion strengths. Grit sizes were chosen based on RMS roughness measurements of common abradants for accelerated life testing (Figure 6.4). Abrasion with 400/P800 grit sandpaper, (slightly lower roughness) did not show an increase in adhesion strength even after 1000 abrasion cycles (Figure 2.3B).

Grit size was increased to 180/P180 to provide a heavier abrasive action to test the limits of the material. Due to the heavier abrasive action, adhesion strength was seen to increase over the 1000 abrasion cycles tested, even though thickness did not decrease greatly (Figure 2.3C**,** Table 6.1).

2.4. Conclusion

From testing, it was determined that materials should be selected based on their desired application-specific performance parameters, including coating thickness, desired ice adhesion strength, and abrasive durability. The best performing material had an adhesion strength around 12 kPa at 200 µm, and decreased to 5 kPa when thickness was increased to 1.35 mm. This material was prepared from testing that showed that increasing the percent of lower molecular weight oil in a high molecular weight base vinyl silicone resulted in the lowest ice adhesion strength material developed, with good durability under both de-icing operations and mild abrasive action with sandpaper.

3. DURABLE SUPERHYDROPHOBIC SURFACES

3.1. Literature Review

3.1.1. Contact Angle

Surface wettability is the primary defining factor for a surface's repellence of any liquid, and is usually characterized by the surface's contact angles and contact angle hysteresis.[45, 120] Smooth surfaces are fundamental for the further understanding of all repellent surfaces, and the focus the earliest wetting analyses. For a smooth surface, Young's relation[121] defines the equilibrium contact angle (θ_Y) for any liquid:

$$\cos(\theta_Y) = \frac{\gamma_{SV} - \gamma_{SL}}{\gamma_{LV}} \quad (3)$$

Here, γ is the interfacial tension and subscripts S, L, and V refer to the solid, liquid, and vapor phases, respectively. γ_{SV} is often referred to as the solid surface energy and γ_{LV} is often referred to as liquid surface tension. This equation arises from the force balance for a liquid droplet contacting a flat, non-textured and non-reactive solid surface, and can be visualized in Figure 3.1 with the contact angle being the angle between the tangent to the liquid-vapor interface and the tangent to the solid-liquid interface at the triple phase contact line, measured through the liquid:

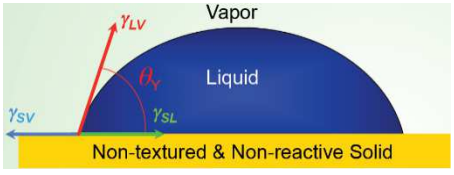

Figure 3.1: Schematic of energy balance at the triple-phase contact point for a liquid drop on a flat surface.[3]

It is generally accepted that surfaces are classified as hydrophobic when the measured contact angle, θ > 90° and hydrophilic when θ < 90° (Section 9.2). As evident from Young's equation, lower solid surface energy materials provide higher contact angles while higher surface energy materials have lower contact angles. Thus, lower surface energy materials are preferred for repellent-surfaces, with a hierarchy of

repellent surfaces dependent on the surface functional groups. This hierarchy is dominated by fluorinated and perfluorinated materials, along with some other polymers and copolymers.[120]

3.1.2. Work of Adhesion and Contact Angle Hysteresis

The contact angle hysteresis (CAH) for a surface is the second parameter for analyzing surfaces as it accounts for the fact that some rose-pedal-effect surfaces [6, 122-124] can have high contact angles but still trap a drop and prevent it from being removed from the surface while other lotus-leaf-effect surfaces [2, 4, 12, 22, 125-127] cause drops to readily roll off. Due to inhomogeneity of contaminants, roughness, and surface chemistry, drops do not interact consistently on all parts of a surface, leading to certain portions of a surface having greater contact angles than others. This inhomogeneity is accounted for by contact angle hysteresis, which is defined as the difference between the advancing (maximum) and receding (minimum) contact angles for a surface (Figure 3.2).[128, 129] Ideally, repellent surfaces would have minimal to no CAH as they would have minimal defects and surface adhesion would not be energetically favorable; however, real surfaces will always have some degree of CAH.

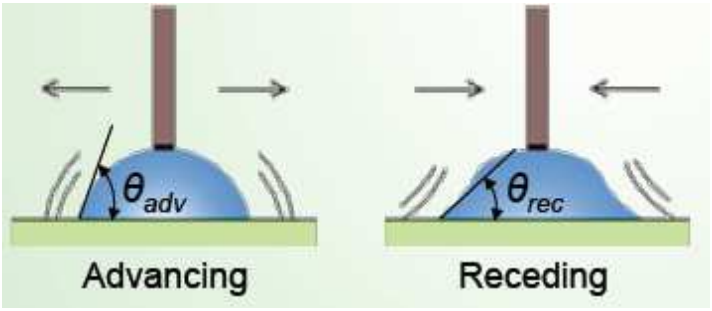

Figure 3.2: Schematic of advancing and receding contact angle measurements for a liquid drop.[3]

Contact angle hysteresis is a measure of the energy dissipated in moving a drop across a surface.[130, 131] Liquids in contact with a surface have a certain work of adhesion W_{ad} that dictates the motion of a drop and many other surface physics phenomena. This work of adhesion is based on the Young-Dupré equation developed by Thomas Young in 1805 and Monsieur Athanase Dupré in 1869, as their respective equations must be combined to develop a measurable relationship:

$$W_{ad} = \gamma_{LV}(1 + \cos\theta) \quad (4)$$

This work of adhesion comes from the difference of internal energy between the initial un-wetted and final wetted states. In the situation where the liquid completely wets the solid surface (θ = 0), W_{ad} = 2 γ_{LV}. It is also noteworthy that the Young-Dupré Equation should usually be evaluated with the receding contact angle as this is the angle where the work of adhesion is finally overcome and the drop retracts. However, the Young's contact angle, which is the equilibrium contact angle that must be between the advancing and receding angles is also commonly used for evaluating this equation.

$$\cos(\theta) = \frac{\gamma_{SV} - \gamma_{SL}}{\gamma_{LV}} \qquad \gamma_{LV}\cdot\cos(\theta) = \gamma_{SV} - \gamma_{SL}$$

$$W_{ad} = E_i - E_f \qquad E_i = \gamma_{SV} + \gamma_{LV} \qquad E_f = \gamma_{SL} \qquad W_{ad} = \gamma_{SV} + \gamma_{LV} - \gamma_{SL}$$

Final energy (solid contacting liquid) will be less than the initial energy (solid in vapor and liquid in vapor) due to energy minimization, and work of adhesion must me positive.

Substituting in Young's equation for contact angle:

$$W_{ad} = \gamma_{LV} + \gamma_{LV}\cdot\cos(\theta) = \gamma_{LV}(1 + \cos(\theta)) \qquad W_{ad} = \gamma_{LV}(1 + \cos(\theta))$$

Figure 3.3: Derivation of the Young-Dupre equation for work of adhesion of a liquid on a surface.

3.1.3. Furmidge Sliding/Rolling- Depinning

A common method for evaluating surfaces in field application was provided by Furmidge via the analysis of droplet roll/slide-off angle. When a drop initially placed on a level surface rolls off after the surface is tilted to an angle α, contact angles for the surface can approximated with MacDougall-Ockrent and Furmidge's equation:

$$sin\alpha = \frac{\gamma_{LV} w(\cos\theta_R + \cos\theta_A)}{\rho g V} \quad (5)$$

Here, a displaced drop is approximated as having a rectangular contact line (as seen in Figure 3.4) with triple phase contact line width w, drop volume V, fluid density ρ, and gravitational acceleration g. The roll-off angle can also be used to approximate the contact angle hysteresis when imaging technology is not available for measuring the advancing and receding contact angles.

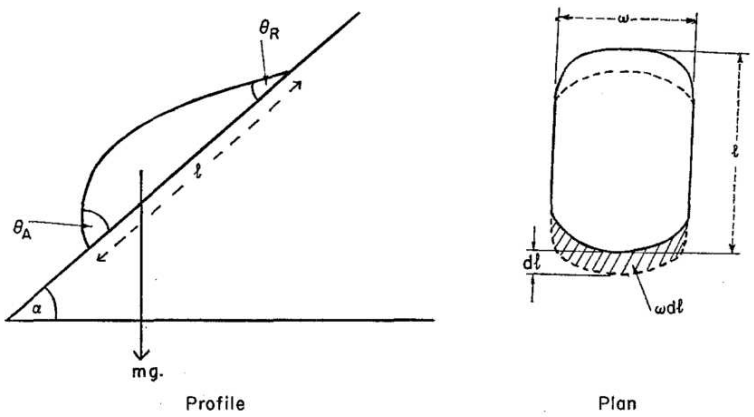

FIG. 4. Profile and plan view of drop during sliding without acceleration.
θ_A—advancing contact angle
θ_R—receding contact angle
l—overall length of drop
w—overall width of drop

Furmidge, 1962, 316

Figure 3.4: Schematic of drop during sliding. [132]

3.1.4. Lotus Effect and Introduction to Superhydrophobic Surfaces

Superhydrophobic surfaces were initially inspired by the water repellence of wool fibers in the textile industry[133] and the historic knowledge of the repellence of lanolin-coated wool by shepherds, weavers, and colonial ship-builders[134]; then further expanded upon following scanning electron microscope analyses of the surface of the self-cleaning, superhydrophobic lotus leaf.[2, 4, 22, 126] All of these analyses saw that textured surfaces performed better than flat surfaces, with the texture combining with low surface energy materials to provide quality water repellence. From these studies a new classification of superhydrophobic surfaces was developed, with it generally accepted that superhydrophobic surfaces must exhibit an apparent contact angle that is greater than 150° and exhibit CAH < 5°, as these are the bounds where droplets are very readily removed from the surface.

However, the maximum contact angles reported for a water droplet on a non-textured surfaces is in the 120°-130° range [135, 136], meaning that chemistry is currently limited in its ability to create superhydrophobic surfaces alone. Instead, surface texturing is needed to create an air-solid composite surface that can use air (or any vapor) to help hold the droplet up. Before getting into the physics of this texturing, it is necessary to make a distinction about the local Young's contact angle and the apparent

contact angle for a surface. As liquids contact textured surfaces in a complex, composite manner, the apparent contact angle which is the macroscopic contact angle visible with most photographic imaging techniques is used for analysis of textured surfaces. Some textured surfaces will still exhibit local contact angles that follow Young's contact angle for a flat surface, but these local contact angles are constrained to the micro and even nano-texture, and do not fully represent the composite, textured surface (Figure 3.5).

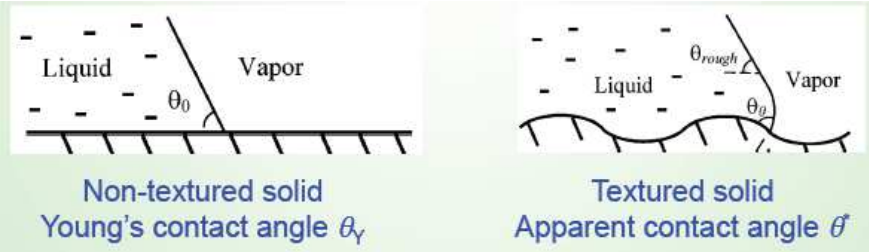

Figure 3.5: Young's contact angle on a flat surface and local Young's contact angle and apparent contact angle on a textured surface.[137]

3.1.5. Wenzel State

Robert Wenzel performed one of the earliest analyses of textured surfaces in looking at the wetting behavior in the production of waterproofing fabrics and the use of emulsions for depositing the waterproofing agents onto porous fabrics[138]. Wenzel considered that any real solid surface will have a greater surface area than a perfectly flat surface due to surface roughness, and developed the roughness factor, r, that is the ratio of the actual surface area to the geometric (or projected flat) surface area.

$$r = \frac{SA_{Actual}}{SA_{Projected}} \tag{6}$$

Note that since all surfaces have a degree of surface roughness, r will always be greater than unity; however, polished and other reasonably flat surfaces, (such as flat glass, silicon wafers, and mirror-polished metals) are reasonably modeled with roughness factors of r = 1.

Wenzel furthered this analysis by considering the effect that increased surface area of texture has on fluid contact angles, with the fluid completely penetrating the surface texture. The Wenzel equation, given below, gives the apparent contact angle, θ_W^*, as a function of the roughness factor, r, and the flat surface contact angle, θ:

$$\cos(\theta_W^*) = r\cos(\theta) \quad (7)$$

From observation of this equation, it is seen that the wetting/de-wetting propensities of flat surfaces get enhanced when drops fully wet textured surfaces. In the Wenzel state, if the solid has a positive wetting tendency and equilibrium contact angle θ < 90°, then the apparent Wenzel contact angle is $\theta_W^* < 90°$ and lower than the equilibrium contact angle. Conversely, de-wetting surfaces with θ > 90° would see increased apparent contact angles $\theta_W^* > \theta > 90°$. This relation holds due to basic surface area, with twice as much surface area per unit geometric area providing twice as much energy content for the drop to interact with. For wetting surfaces, this correlates with twice as much surface area to spread on while de-wetting surfaces have the same amount of surface area in half of the geometric area to have the same energy as on a flat surface, causing drops to elevate above the surface with a higher contact angle than the flat surface.

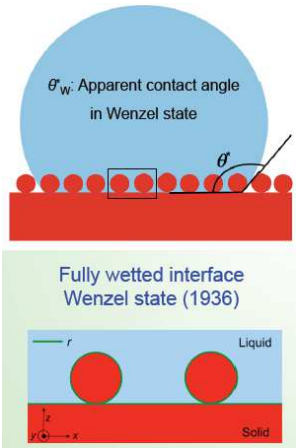

Figure 3.7: Schematic of a liquid drop in the Wenzel state on a textured surface.[3]

3.1.6. *Cassie-Baxter State, Spacing Ratio, Robustness Factor*

Superhydrophobic surfaces utilize incomplete wetting of surface roughness to elevate liquid droplets into the Cassie-Baxter state where there is a composite solid-liquid-vapor interface at the surface, like with a duck's feathers.[133] Cassie and Baxter expanded on Wenzel's work by considering that surfaces are not always completely wet, but rather that textured

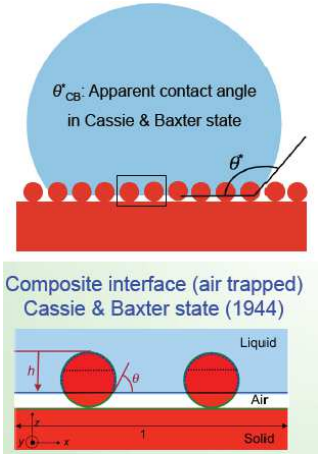

Figure 3.6: Schematic of a liquid drop in the Cassie-Baxter state on a textured surface.[3]

surfaces can have air supporting the droplet as well.

When a drop partially wets a textured surface in the Cassie-Baxter state, the liquid contacts the solid with a surface area of A_1 and energy $A_1(\gamma_{SL}- \gamma_{SV})$ and a solid-air interface of area A_2 and energy $A_2\gamma_{LV}$. The net energy of the static, partially wetted drop with contact angle accounted for provides the Cassie-Baxter equation for the apparent contact angle θ^*_{CB} on a partially-wetted textured surface:

$$cos\theta^*_{CB} = f_{SL}cos\theta + f_{LV}cos\pi \quad (8)$$

Due to geometric manipulation, this equation can be rewritten as:

$$cos\theta^*_{CB} = r_\phi \phi_S cos\theta + \phi_S - 1 \quad (9)$$

Here, r_ϕ is the ratio of the actual solid-liquid interfacial area to the projected solid-liquid interfacial area, ϕ_S is the ratio of the projected solid-liquid interface area to the total projected area for a unit of contact area, f_{SL}=$r_\phi \phi_S$ or the ratio of the actual solid-liquid interfacial area to the total projected area, $f_{LV} = 1 - \phi_S$ or the ratio of the liquid-vapor interfacial area to the total projected area. f_{SL} is considered the solid fraction of the interface with f_{LV} considered the vapor fraction of the composite drop interface. These parameters are geometrically-dependent, as calculations for their values are based on repeating unit cells for the texture.

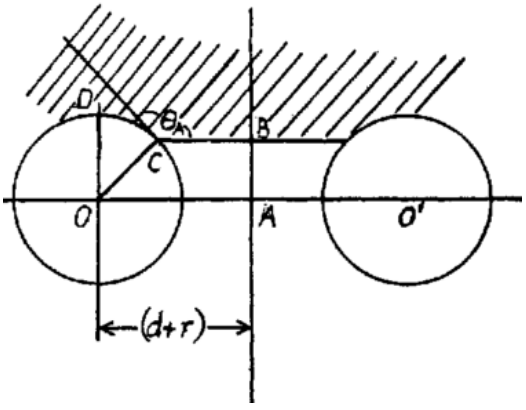

Figure 3.8: Schematic of the Cassie-Baxter state for a cross-section of a unit of a continuous, circular texture. [133]

Considering extreme cases for the Cassie-Baxter equation shows how surfaces can be designed. First, consider that the texture is completely wet by the liquid. In this case, $f_{LV} = 0$ and this equation simply

becomes the Wenzel relationship, with its enhanced dependence on surface chemistry. On the other hand, if the drop is essentially solely supported by air, $f_{SL} = 0$ and the θ^*_{CB}=180°, as a free-falling drop with negligible drag would exhibit in its fully spherical shape. Thus, it can be seen that decreasing the solid fraction and increasing the vapor fraction of the interface produces surfaces with higher contact angles.

The solid and vapor fractions above can be controlled by altering the geometry and spacing of surface texture. The dimensionless spacing ratio, D* can be used to design surfaces and find the apparent contact angle for a particular geometry and surface chemistry.[139, 140] For example, Kobaku considered discrete spherical particles evenly spaced in a hexagonal planar structure on a surface and solved the Cassie-Baxter equation for the apparent contact angle θ^* as[140]:

$$cos\theta^* = -1 + \frac{1}{D^*}[\frac{\pi}{2\sqrt{3}}(1 + cos\theta)^2] \quad (10)$$

Where θ is the Young's contact angle, and D* = $[(R+D)/R]^2$, with R being the radius of the spherical particle and D being half the inter-particle spacing. Due to the inverse relationship of D*, higher values of D* (increased space between small particles) result in higher apparent contact angles. Therefore, it is advantageous to increase the spacing of texture to decrease the solid-liquid interfacial area when trying to repel liquids.

Increasing the spacing ratio does come at a cost, though, and that cost is in the form of higher vulnerability to droplets breaking through the texture due to external pressure from gravity, wind, or other sources. The robustness factor, A* was developed to account for a surface's sensitivity to applied pressure [139]:

$$A^* = \frac{P_{breakthrough}}{P_{ref}} \quad (11)$$

Where $P_{breakthrough}$ is the pressure required to force a transition from the non-wetting Cassie-Baxter state into the wetted Wenzel state, and P_{ref} is a characteristic reference pressure based on the liquid surface tension and capillary length[132]. While calculating the spacing ratio and robustness factors is specific for

individual geometries, they serve as guides for the general design criterion that surfaces have as wide of spacing as possible for specific breakthrough pressure requirements.

3.1.7. Hierarchical Structure

Patankar's analysis of the superhydrophobic lotus leaf recognized that the surface of the leaf has a double structured rough surface with a coarse-scale rough structure of visible protrusions and a second, fine-scale hairy texture covering the entire structure, including the coarse texture.[2]

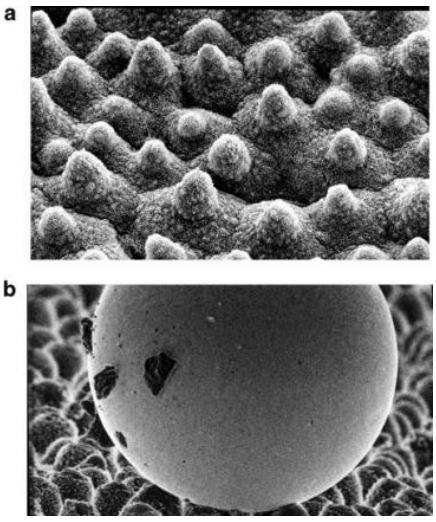

Figure 3.9: A) SEM image of the hierarchically textured surface of a lotus leaf. B) SEM image of a mercury drop in the Cassie-Baxter state on the surface of a lotus leaf. [1, 2]

It was found that this hierarchy of texturing (which also appears in other biological systems) was important for superhydrophobic surfaces as it allowed increased robustness of surfaces as the coarse roughness could remain in the Cassie-Baxter state even in times when the fine scale of roughness may get fully wetted to a local Wenzel state.[9, 120, 141] Hierarchical structures allow multiple thermodynamically stable states for a fluid, allowing for increased droplet stability on a surface. Herminghaus presented an analysis of a hierarchical structure, along with a recursive form of the Cassie-Baxter equation that can be compounded for multiple length scales[142]:

$$cos\theta_n^* = f_{SL,n} cos\theta_{n-1} - f_{LV,n} \quad (12)$$

Here, n is the number of the length scale for which the apparent contact angle is being calculated. The recursive Cassie-Baxter relationship utilizes the apparent contact angle of preceding texture scales, providing a compounding effect for contact angles that enhances contact angle along with drop stability.

3.1.8. Summary of Literature Review

With these fundamentals, many superhydrophobic surfaces have been prepared by varying texturing and surface chemistry; however, durability of these surfaces is a continual challenge given the

importance of maintaining multiple microscopic length scales of texture. Metals are common materials for industrial application due to their high strength and durability, so work has been done to make metallic surfaces highly repellent while trying to retain the durable nature of the base material. Coatings for a variety of surfaces are also very common for industrial application as they allow for complex surfaces to be rendered repellent in a cost-effective and (usually) simple manner. However, the low surface-energy nature of superhydrophobic surfaces makes adhesion and cohesion between the surface, substrate, and any functional particles difficult. While work has been done in improving the durability of superhydrophobic surfaces, the creation of superhydrophobic surfaces that can maintain their performance under potentially extreme conditions of many ideal applications is a constant goal for surface engineers. There has been varying success in producing durable superhydrophobic surfaces in a variety of manners and materials.[34, 120, 143-157] Superhydrophobic stainless steel surfaces are more difficult to produce, resulting in fewer works for stainless steel, with fewer reporting durability results [158-162]. This work sought to produce a surface for both spray-coat application stainless steel modification that could maintain a sufficient degree of repellence even after surface abrasion.

3.2. Seed Drying Problem Definition

A producer of agricultural seed processing equipment specializing in fluidized bed equipment for seed coating and drying for coating seeds with herbicides, pesticides, and other seed-enhancing technology contacted our research group to try to solve an issue with the seed coating fluid (and, consequentially, coated seeds) adhering to their equipment and reducing system efficiency. This work was trying to develop coatings for flat vertical seed-directing walls as well as horizontal metal meshes used to hold the seeds up and allow air to pass through and dry the coated seeds. Given the vibrational flow characteristics leading to moderate abrasion of surfaces, coatings not only have to provide adequate hydrophobicity to repel the water-based coating paints but also withstand high abrasion cycles for a

moderate amount of time. Repellence for approximately 3 months is a good durability target to avoid the costs associated with having to frequently stop operation to rejuvenate the surfaces.

3.3. Materials/Methods/Experiments

A durable spray-coated material was developed to apply to any surface along with an etching and surface functionalization process to make the stainless steel (grades 304 and 430) surfaces superhydrophobic. Additionally, abrasion testing systems were created for in-house accelerated-life and simulation of application abrasion durability analysis of surfaces under conditions similar to those likely to be experienced in application. Cost analyses and operational suggestions were also provided in order to determine the feasibility of developed methods in application (Figure 8.8).

3.3.1. Spray Coating

Initial conceptualization for a material mixture that could experience high abrasion while retaining surface repellency were centered on highly adhesive materials that could serve as carriers for additives functionalized to provide the desired hydrophobicity. Initial tests were performed with JB Weld adhesive and Tile Clad commercial epoxy from Sherwin Williams with silanized silica particles. While these surfaces were durable to scratching, they did not have the desired repellency due to the high surface energy of the metal and epoxy chemistries, even with the added hydrophobic particles. During these tests, the spray coating and mixing methods were continually improved for optimal texture and surface durability. Additionally, polymeric materials were also tested, including Fluorolink cross-linkable material and Tecnoflon; however, these materials did not provide the durability and repellence needed for application.

As the surfaces were not providing adequate hydrophobicity, a fluorinated polyurethane (FPU, Luxecolor 4FVBA-800 from Helicity Technologies) was chosen to serve as the matrix material due to its highly adhesive nature and low surface energy from fluorinated polyols (Section 8).

Subsequently, fluorination of silica nanoparticles (F-SiO_2) was developed by dispersing fumed silica particles in a solution of hexane and (heptadecafluoro-1,1,2,2-tetrahydrodecyl) trichlorosilane (HpDF-TCS, silane) which was mixed for 3 days to allow complete hydrolysis of the surface for the formation of covalent bonds between the perfluorosilane and silica particles. It was then found that removal of hexane through centrifugation (350g for 10 minutes, Figure 8.2) and subsequent ultrasonic particle dispersion in chloroform allowed a more even dispersion of nanoparticles with fewer large conglomerations than when sprayed while dispersed in hexane. This dispersion in chloroform allowed greater control of surfaces, allowing FPU and F-SiO_2 mixtures to be analyzed based on relative concentrations and spraying methods. Early testing showed that some highly superhydrophobic surfaces lacked durability as many surfaces were powdery, with the nano and micro particles necessary for the hierarchical texture not well adhered to the surface. Given the micro and nano-scales of the texturing, minimal contact area is available for adhesion with underlying adhesives. To try to increase adhesion between functional particles and the surface, the particles were mixed with the adhesive and sprayed as a single material in order to coat the particles with enough binding agent to provide durability while trying to retain the surface texture and low surface energy necessary for superhydrophobicity.

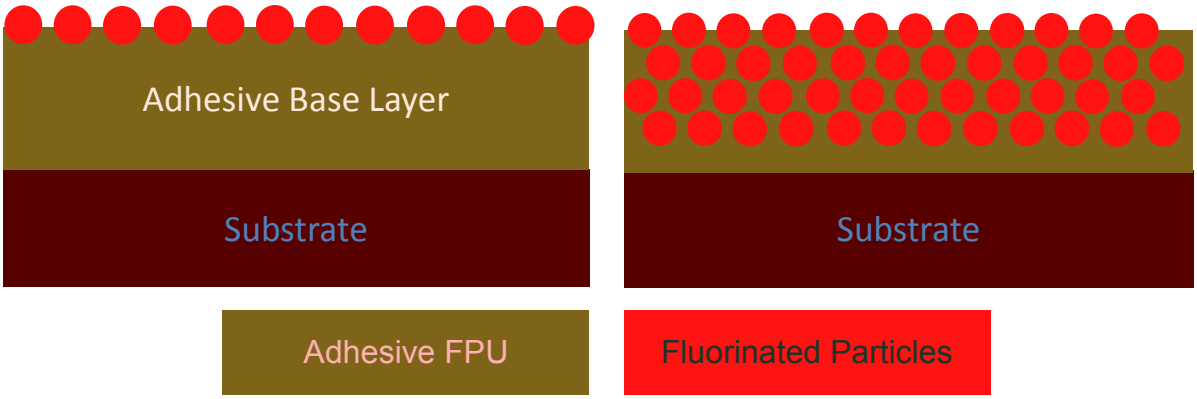

Figure 3.10: Layered (left) and mixed (right) surface schematics.

Layered surfaces were also prepared by applying a film of flat FPU followed by pure F-SiO_2 dispersed in chloroform, which evaporated in the spraying process leaving the F-SiO_2 particles to impact the FPU and create a top layer of low surface-energy, textured particles.

3.3.2. Stainless Steel Etching

While developing spray coating materials, a subsequent effort was made to texturize and functionalize stainless steel used in the drying system in order to simply modify the existing setup. Stainless steel grades 304 and 430 are the main metals used in the seed-drying system, so etching processes were developed for each of these to induce hydrophobic texturing. To speed up research iteration cycles, materials were specified to enable quick metal shearing to desired sizes by ordering metal thinner than 18 gauge and in sheet sizes that would minimize waste and costs. Additional research into improving the durability of these metals was also done to further enhance the surface durability and operation life before revitalization (Section 7).

Early etching trials showed that as-received metal surfaces (from McMaster-Carr) were difficult to etch uniformly and consistently. It was theorized that this was due to surface hardening from the cold-rolling preparation process creating residual stresses at the surface that decreased the surface's available sites energetically favorable for chemical etching. To try to reduce residual stresses and improve etching, abrasive blasting was performed with #8 glass beads at a pressure of 60 psi and a distance of 1 inch

(2.54 cm) from surfaces. This bead blasting procedure produced visibly uniform, scratch free surfaces. Bead blasted samples were completely washed using ethanol in an ultrasonic bath in order to remove any residual silica particles or other contaminants prior to etching.

It was found that this bead blasting step was indeed critical for the effective etching of all stainless steel samples, with a stark contrast in the etching results between abrasively blasted samples and as-received samples. A standardized procedure for abrasive blasting was developed (including the use of a sample-holding fixture) for uniform, rapid production of samples for testing (Section 7.3).

Etching of SS304 was initially performed with iron chloride solution ($FeCl_3$, Section 7.2) and hydrofluoric acid (HF, Section 7.1) in the hopes that the different etchants would etch at different size scales. Initial tests found that $FeCl_3$ was not an adequate etchant due to its propensity to etch large circular (mm sized) pits non-uniformly across the surface. Under high concentration, high temperature, and/or long etching times, $FeCl_3$ would even etch holes completely through the material. Additionally, successful etching with HF rendered this etchant as the only etchant necessary for making SS304 superhydrophobic following vapor phase silanization. Etching was performed at elevated temperature (50 ^{o}C) and at room temperature (27 ^{o}C), with comparable results for the two processes. As room-temperature etching is far more controllable and scalable, it was chosen as the preferred method for continued refinement of the etching process.

Following etching, stainless steel surfaces were silanized with HpDF-TCS to deposit a low surface energy perfluorinated layer on the surface to create the double effect of texture and low surface energy necessary for superhydrophobic surfaces. Vapor phase silanization was performed immediately following etching by exposing the surfaces to oxygen plasma for 15 minutes before being placed on a hot plate at 125 ^{o}C with 100 µL of silane per square inch of metal surface with glass bowl isolating the silanization environment from the ambient (Section 7.1.4). Silanization occurred for 1 hour, then samples were quickly rinsed with DI water and placed back on the hot plate to dry for 5 minutes.

Following washing with acetone, ethanol, and DI water, contact angles were measured using a contact angle goniometer (Section 9.2).

3.3.3. Corn Mixer Abrasion

A standard 3.5 gallon cement mixer (CM) from Harbor Freight (Item #67536) was used to simulate accelerated seed abrasion by tumbling seeds over surfaces mounted collinearly along the interior of the CM, with the surfaces rotating under the center of 5 pounds of washed, uncoated shell corn (Section 8.7). Due to the hardness and sharp edges of the corn seed and their tumbling nature and depth (4-5 times deeper than seeds flowing in operation), this test provided a heavy abrasion baseline to compare samples by. The degree of acceleration to which this test mimics what might be seen in actual application (Figure 8.13Figure 8.13: Oliver Manufacturing seed dryer.[184]).

Seeds and the coating paint were not provided, so shell corn used after washing with water and detergent to completely remove all dust and chaff, then complete rinsing and drying prior to testing. While most of the chaff and contaminants were removed, it is practically impossible to completely clean corn (Figure 8.10). This washing was performed to simulate the state of seeds in application, as these seeds will be fairly clean with some contaminants still likely present. Chaff was removed during testing through holes in the mixer that were large enough for produced chaff to drop out but small enough to retain the whole corn. Additionally, a fan was used to occasionally gravimetrically clean chaff out of a stream of corn poured from the mixer into a bucket. With the presence of liquid during the coating operations, it is likely that abrasion could be different in operation compared to the developed testing method. It is probable that the abrasion would be less intense in application than in the developed test method, but this will be verified with results from on-site testing of model surfaces. CM tumbling tests of samples mounted with adhesive strips were performed for 1 hour, with contact angles for DI water measured before and after abrasion. Additionally, observations of the surfaces were made to gauge how much material was removed and contaminants were added. Due to the dual nature of material

removal and chaff deposition (which was difficult to remove) and the desire to simply maintain hydrophobicity, contact angles and hydrophobic performance were used as the main criterion for surface performance.

3.3.4. Corn Shaker Abrasion

In an attempt to more directly simulate the conditions that surfaces would experience in application, a shaking mixer was tilted and fitted with a seed containment structure and seed hopper to slowly flow seeds over the shaking surfaces of interest (Section 8.8). The internally fabricated feeder system allowed flow control depending on the desired application. For testing purposes, washed corn (same corn as above) was shaken over the surfaces of interest at a flow rate of 10 min gal^{-1} for 1 hour at an angle of 5^{o}.

Pending results from on-site testing, it is believed that the corn abrasion test methods can provide an adequate application-specific test method for similar projects in the future (with changes in abradants used) in dynamic environments similar to those experienced during every-day use of hydro/omniphobic surfaces and that these test methods provide a valuable tool for future analysis.

3.4. Results and Discussion

It should be noted that the following results and discussion are preliminary works, with further development and testing needed to improve surfaces for more effective implementation. However, they serve as an adequate initial exploration.

FPU and F-SiO_2 mixtures were tested at varying ratios to compare the effect of having more functionalized particles in the mixture on initial contact angles and contact angles after corn abrasion. Higher FPU: F-SiO_2 ratios correspond to more FPU in the mixture with the thought that this would improve durability by having more adhesive material surrounding each particle, with the potential sacrifice of repellence due to the higher surface energy of the FPU compared to the F-SiO_2 particles

(Figure 8.6). Inversely, low ratio mixtures with more particles were considered to increase repellence while potentially decreasing durability.

Testing showed that, by-and-large, lower ratio mixtures did indeed have higher contact angles but also less durability than higher ratio mixtures. Contact angles were measured before and after CM and shaker abrasion for 1 hour on all samples. Table 3.1 summarizes the results for a controlled study of F-SiO_2 concentration for samples before as well as after CM and Shaker abrasion tests.

Table 3.1: DI Water contact angles before and after washed corn abrasion on mixed surfaces.

Mixed Surfaces	**Before Abrasion**			**CM Abrasion**			**Shaker Abrasion**		
FPU:F-SiO_2 (% F-SiO_2), mg F-SiO_2/mL Chloroform	CA Adv	CA Rec	CAH	CA Adv	CA Rec	CAH	CA Adv	CA Rec	CAH
100% Flat FPU, 0% F-SiO_2	96	59	37	100	70	30	103	66	36
30:1 (3.2%), 30 mg/mL	136	64	73	107	43	64	111	55	57
22.5:1 (4.3%), 30 mg/mL	155	153	2	141	112	28	143	113	31
15:1 (6.2%), 30 mg/mL	148	142	6	150	141	9	141	128	14
10:1 (9.1%), 30 mg/mL	154	148	6	148	73	74	141	123	19
10:1 (9.1%), 200 mg/mL	151	134	17	141	93	48	147	131	16
5:1 (16.7%), 200 mg/mL	152	136	16	70	20	50	149	124	24

Solely looking at initial contact angles, it is tempting to identify the 9.1% mixture as the best surface developed. However, in considering the reduction of the receding contact angle following shaker and concrete mixer abrasion it can be seen that the increased amount of F-SiO_2 made this surface more powdery than the 6.2% mixture, resulting in decreased durability. As the receding contact angle is critical for repelling fluids, the decrease in receding contact angle with abrasion renders this surface less effective than the 6.2% surface. While all surfaces saw a reduction in contact angles, they still outperformed the flat FPU in general repellence, with exception of the 3.2% mixture. This surface had advancing angles greater than FPU, but receding angles less than the flat FPU, suggesting that this surface was fully wet, with the Wenzel equation enhancing the surface's repellent (advancing angle) and philic (receding angle) properties. Thus, for decreasing adhesion, it is suggested that textured surfaces

only be used if they can retain a Cassie-Baxter state. Otherwise, these surfaces will have even more adhesion.

The layered surfaces were prepared thinking that the highly adhesive uncured FPU would still provide enough adhesion to maintain decent durability without completely coating the particles on the nano-scale, allowing for enhanced phobicity. Since the F-SiO_2 has a lower surface energy than the cured FPU, allowing fluid to only contact F-SiO_2 texture would provide greater phobic properties, essentially shielding the FPU surface from fluids. Test results of these layered surfaces are summarized in Table 3.2:

Table 3.2: DI Water contact angles before and after washed seed abrasion on layered surfaces.

Layered Surfaces- DI Water	Before Abrasion			CM Abrasion			Shaker Abrasion		
(F-SiO_2 coverage, mg/mL in Chloroform); (FPU coverage)	CA Adv	CA Rec	CAH	CA Adv	CA Rec	CAH	CA Adv	CA Rec	CAH
100% Flat FPU	96	59	37	100	70	30	103	66	36
(5 mg/cm^2, 30 mg/mL); (155 mg/cm^2)	154	151	3	152	146	6	125	82	43
(7.5 mg/cm^2, 30 mg/mL); (155 mg/cm^2)	151	148	3	139	120	18	152	148	5
(10 mg/cm^2, 30 mg/mL); (155 mg/cm^2)	146	143	3	144	128	16	132	107	25
(20 mg/cm^2, 30 mg/mL); (155 mg/cm^2)	153	148	4	148	57	91	147	135	12

Similarly to the mixed surfaces, it was seen that an intermediate amount of F-SiO_2 was optimal for retaining hydrophobicity, though the layered surfaces exhibited high initial contact angles more consistently than the mixed surfaces, likely due to the reduced amount of FPU in contact with the liquid. However, at very low F-SiO_2 coverage (5 mg cm^{-2}) there was not enough textured F-SiO_2 to hold the liquid in the Cassie-Baxter state and it tended to wet the surface in the Wenzel state. While the 10 mg/cm^2 surface with a medium layer of FPU was the best layered surface after abrasion, damage had a greater effect on this surface than the best mixture surface. This aligns with the consideration that the layered surfaces only had adhesion between the F-SiO_2 and the FPU at specific points where the particles impacted the tacky FPU while the mixed surfaces had FPU surrounding the particles.

Etching 304 stainless steel with 48-50% Hydrofluoric Acid for only 10 minutes at room temperature followed by vapor phase silanization rendered a highly hydrophobic surface with hysteresis and contact

angles approaching their thresholds for superhydrophobic classification, with water drops readily rolling off of the surface. Negligible improvement was seen at increased time and temperature of etching, allowing for the scalable short, room temperature process to be used. Additionally, it was found that these surfaces could effectively repel water, although abrasion did slightly decrease contact angles, as seen in Table 3.3.

Table 3.3: DI Water contact angles on etched and silanized SS304.

HF Etch Temp	Etch Time	Advancing Contact Angle		Receding Contact Angle			Hysteresis		
°C	Minutes	Degrees		Degrees			Degrees		
50	20	160		147			13		
25	20	161		148			13		
25	10	160		145			15		
Etched Stainless Steel Surfaces	Before Abrasion			CM Abrasion			Shaker Abrasion		
HF Etch 25 °C	CA Adv	CA Rec	CAH	CA Adv	CA Rec	CAH	CA Adv	CA Rec	CAH
SS304 HF 10 min	157	136	22	134	112	21	152	123	29
SS430 HF 10 min	162	147	15	152	129	23	160	145	15

3.5. Conclusion

Defining what makes superhydrophobic surfaces highly durable is an issue of much debate and development, and also a very application-specific requirement. The inherently fragile nature of micro and nano-textured surfaces makes these surfaces difficult to make highly durable. However, for trying to develop durable coatings for the purpose of repelling water-based seed coating paint this work was able to preliminarily produce surfaces that could retain fair repulsion of water even following a heavy abrasion with application specific media, allowing for on-site testing of these materials for analysis and further development of both the surfaces and the testing process. Additionally, design, coating, and testing methods for FPU/F-SiO_2 and etched stainless steel surfaces were developed to enable their improvement with future research. In application, the balance between durability and performance must be considered and designed for.

4. DURABLE SUPEROLEOPHOBIC

4.1. Literature Review

4.1.1. Low Surface-Tension Liquids

Oleophobicity, the resistance to wetting by low surface tension liquids, such as oils, alcohols, or other organic solvents, uses the same contact angle and CAH ranges as hydrophobicity presented before to classify surfaces from superoleophilic to superoleophobic. However, oleophobicity is much more difficult than hydrophobicity in both natural and man-made surfaces. While there are many examples of natural superhydrophobic surfaces, there are rarely natural oleophobic surfaces, and no known natural superhydrophobic surfaces. Indeed, offshore oil spills are dangerous to maritime waterfowl as the oil can penetrate their otherwise waterproof wings and render the animals immobile and unable to escape the oil, hunt for food, and avoid hypothermia.[163] Dawn brand dish soap, a common household product, has even run advertisements with an adorable duckling highlighting their efforts to send thousands of bottles of their product to help aid workers clean birds soaked in oil spills.[164]

While the upper surface of the lotus leaf is only superhydrophobic and is wet by oils, other natural surfaces can indeed repel oils.[6] Oils can wet superhydrophobic surfaces due to the fact that oils have a lower surface tension than water, often below half the surface tension of water, resulting in Young's contact angles <<90°.

As described by Frederick Fowkes, liquids have two main interatomic forces that comprise the surface tension of any liquid: a polar component γ_{LV}^{p} and a dispersive component γ_{LV}^{d}.[165] Fowkes analyzed the surface tension of a fluid to be the sum of its polar and dispersive components:

$$\gamma_{LV} = \gamma_{LV}^{p} + \gamma_{LV}^{d} \quad (13)$$

The polar component of surface tension arises from highly attractive dipole-dipole and hydrogen bonding forces that polar fluids like water have, while the dispersive component is imparted by weaker

London dispersion and other non-polar forces inherent to all materials. Oils have very low surface tension compared to other fluids as they are usually non-polar molecules, resulting in less attractive hydrogen bonding and polar forces that hold higher surface tension fluids together. In the case of non-polar liquids, the polar component of surface tension will be equal to zero, resulting in a low value for surface tension. Similarly, surfaces also have polar and dispersive components of surface energy, γ_{SV}^{p} and γ_{SV}^{d}, respectively. Fowkes continued his analysis for the interfacial tension γ_{SL} between a non-polar surface and non-polar liquid as the sum of the geometric means of the tension in the interfacial region between the two interacting materials as:

$$\gamma_{SL} = \gamma_{SV} + \gamma_{LV} - 2\sqrt{\gamma_{SV}^{d}\gamma_{LV}^{d}} \quad (14)$$

Here, γ_{SV} is the total surface energy of the solid and γ_{LV} is the total surface tension of the liquid. Owens and Wendt furthered the analysis of the components of surface tension and energy and the subsequent interfacial energy of interaction by accounting for the polar components of surface forces.[166] Owens and Wendt provided this more general form of the equation for interfacial energy that accounts for liquids and solids that have both polar and dispersive components:

$$\gamma_{SL} = \gamma_{SV} + \gamma_{LV} - 2\sqrt{\gamma_{S}^{d}\gamma_{L}^{d}} - 2\sqrt{\gamma_{S}^{p}\gamma_{L}^{p}} \quad (15)$$

Again, γ_{SV} is the total surface energy of a solid, γ_{LV} is the total surface tension of a fluid, and superscripts d and p represent the dispersive and polar components, respectively. If either the solid or liquid are non-polar, then the last part of the Owens-Wendt equation is equal to zero and the equation simplifies to Fowkes' relation. These works not only allow for the measurement of the polar and dispersive components of surfaces and liquids, but also provide insight into the fact that the lack of polar forces usually results in lower surface tension fluids, and that even if there are polar forces along with dispersive forces, if they are both small the net surface tension can still be low. Thus, fluids with Young's contact angles << 90^{o} are classified as having low surface tension, even if they are not oils.

4.1.2. Necessity of Re-Entrant Texture

While the Cassie-Baxter state is desirable for superomniphobic surfaces, not all types of texture can provide this Cassie-Baxter state in low surface tension liquids.[120] Reentrant texture is described by an overhanging geometry for which a line drawn vertically from the base and passing through the side of the texture will pass through both the side and top. This reentrant texture is critical for producing superoleophobic surfaces as it allows for fluids with low contact Young's contact angles to go into a stable Cassie-Baxter state. Kota, et. al. provide a wonderful description of the necessity of reentrant texture using Figure 4.1. For textures with the same surface energy, the texture in Figure 4.1a is concave with a texture angle ($\psi > 90^o$) while the texture in Figure 4.1b is convex ($\psi < 90^o$) facing upwards. Both textures have liquids in Cassie-Baxter contact with local Young's contact angle θ, although θ is different for the two textures. If $\theta < \psi$, the net traction on the liquid-vapor interface is downward due to the capillary force promoting imbibition of the liquid into the solid texture, resulting in transition to the wetted Wenzel state. When $\psi > 90^o$, low surface tension fluids with $\theta < 90^o$ will be fully wetted as $\theta < \psi$. However, if a low surface tension fluid is in contact with a reentrant-textured surface with $\psi < \theta < 90^o$, the fluid can retain the repellent Cassie-Baxter state.

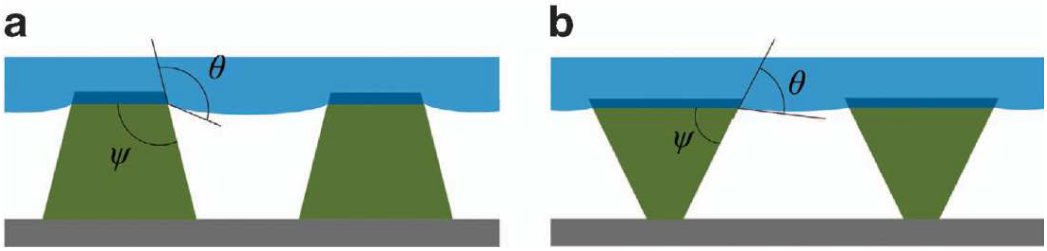

Figure 4.1: A) A schematic of a concave texture ($\psi>90^o$) showing a liquid droplet with $\vartheta>90^o$ in the Cassie-Baxter state. B) A schematic of a convex, reentrant texture ($\psi<90^o$) showing a lower suface tension liquid with $\vartheta<90^o$ in the Cassie-Baxter state. [120]

This overhanging reentrant texture and corresponding oleophobicity is observed in natural surfaces as well.[36] In-fact, no known naturally oleophobic surfaces have been discovered without some sort of reentrant texture. The springtail, a group of anthropods from the hexapod subphylum, lives in the

decaying material of soil surrounding plants, and has evolved to repel low surface tension fluids produced by decaying organic matter.[36] Analysis of the overhanging texture of springtails highlights that there are multiple equilibrium states for fluids of a variety of surface tensions contacting the springtail skin, as seen in Figure 4.2.

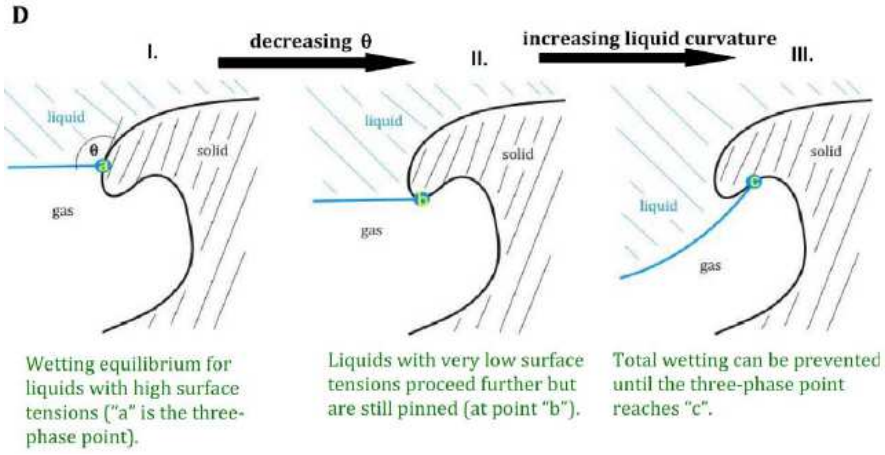

Figure 4.2: Equilibrium states for the wetting of springtail skin with reentrant texture. [36]

Just as it is a challenge for nature to create surfaces with a combination of reentrant texture and low surface energy in order to repel low surface tension fluids, researchers have difficulty creating oleophobic surfaces, much less superoleophobic surfaces. Ahuja also gave a good description of the role of reentrant texture in developing superoleophobic surfaces.[36] Researchers have still produced superoleophobic and superomniphobic surfaces with a variety of methods.[6, 7, 32, 38, 40, 45, 48, 50, 120, 139, 144, 151, 167-175] However, due to the low surface energy and complex reentrant texture requirements, these surfaces are normally created with powdery low surface energy materials that often coat fragile base materials, such as silicon wafers.[120] While many researchers have reported superoleophobic surfaces, fewer have added on an analysis of any sort of durability for their surfaces with durability testing performed in a variety of ways which often only minimally attack surfaces.[143-146, 149, 151-154, 173, 176-181]

4.2. Problem Definition

A food-service industry partner has had an issue with product loss due to a concentrate of their concentrate syrup adhering to process piping and equipment. The high-viscosity (58 cSt) and low surface-energy (27.5 mN m^{-1}) of this fluid make it very sticky and very difficult to repel. Additionally, it is desired that any coatings retain their durability for cost-effective implementation. The fluid flow provided is described in Figure 4.3 below, with a flow rate of 500 liters per minute in a 2 inch pipe resulting in a bulk flow of 4 meters per second.

Syrup Full-Scale Flow

$$U_{flow} := 500\frac{L}{min} \quad D_{pipe} := 2in \quad \mu_{fluid} := 0.58poise \quad \gamma_{fluid} = 27.5\frac{mN}{m} \quad \rho_{fluid} := 1300\frac{kg}{m^3}$$

$$A_f := \pi \cdot \frac{D_{pipe}^2}{4} \qquad V_f := \frac{U_{flow}}{A_f} = 4.112\frac{m}{s} \qquad Re_f := \frac{\rho_{fluid} \cdot V_f \cdot D_{pipe}}{\mu_{fluid}} = 4681.5$$

Figure 4.3: Full-Scale syrup pipe flow information.

4.3. Materials/Methods/Experiments

4.3.1. Surfaces

As the fluid dissolves most soluble plastics and durability is of interest, highly adhesive materials were considered for this application, similarly to the seed-adhesion surfaces. Much of the surface development was completed along with the seed-coating surfaces, with application specific testing. The low surface tension of this fluid would render many superhydrophobic surfaces useless, so some different tactics had to be used for making these surfaces. Specifically, the need for re-entrant texture and for low surface-energy correlated to the use of higher percentages of F-SiO_2 particles and multiple layered coatings (Figure 8.7).

As mechanical abrasion would not be experienced by these surfaces, a separate testing regime had to be prepared for analyzing the repellence of the syrup. Initial analysis of whether surfaces could potentially repel the fluid was performed by simply placing a drop on the surface. This pass/fail test was then followed with contact angle measurements using n-hexadecane (surface tension of 27.4 mN m^{-1}), which

was considered an adequate representative for measuring the contact angles of the low surface-tension syrup.

4.3.2. Syrup Repellence Testing

To test syrup repellence, a dipping test was prepared to submerge surfaces then pull them up and out of the fluid, with weights recorded before and after dipping to measure the amount of adhered fluid per unit area of the surface (Figure 8.16). While this test does not fully simulate the high flow seen in application, it provided a quick, facile method for early analysis of the repellence of surfaces for further development. Dipping exposed the surfaces to a complete film of liquid and associated hydrostatic pressure, as would be seen in application, instead of just droplets as used for contact angles. Dipping was performed at a constant rate of 5 cm min^{-1} for consistent shear on the surfaces by using a linear translation stage. Samples were submerged vertically with the top edge of the sample just below the surface, then immediately retracted for 60 seconds, allowing for the samples to be completely removed from the fluid by de-wetting action.

4.4. Results and Discussion

4.4.1. Hexadecane Contact Angles

Contact angle results for n-hexadecane on various surfaces are provided in Table 4.1.

Table 4.1: Hexadecane contact angles for mixed and layered surfaces.

Hexadecane Contact Angles			
Surface ID	CA Adv	CA Rec	CAH
Mixed Surfaces- FPU:F-SiO_2 (%F-SiO_2), F-SiO_2 mg/mL in Chloroform			
15:1 (6.2%), 30 mg/mL	139	105	34
10:1 (9.1%), 30 mg/mL	137	106	31
10:1 (9.1%), 200 mg/mL	129	101	28
5:1 (16.7%), 200 mg/mL	144	125	19
Layered Surfaces- (F-SiO_2 coverage, mg/mL in Chloroform); (FPU coverage)			
(5 mg/cm^2, 30 mg/mL); (155 mg/cm^2)	91	22	68
(7.5 mg/cm^2, 30 mg/mL); (155 mg/cm^2)	121	40	80
(10 mg/cm^2, 30 mg/mL); (155 mg/cm^2)	146	142	4
(20 mg/cm^2, 30 mg/mL); (155 mg/cm^2)	158	145	13

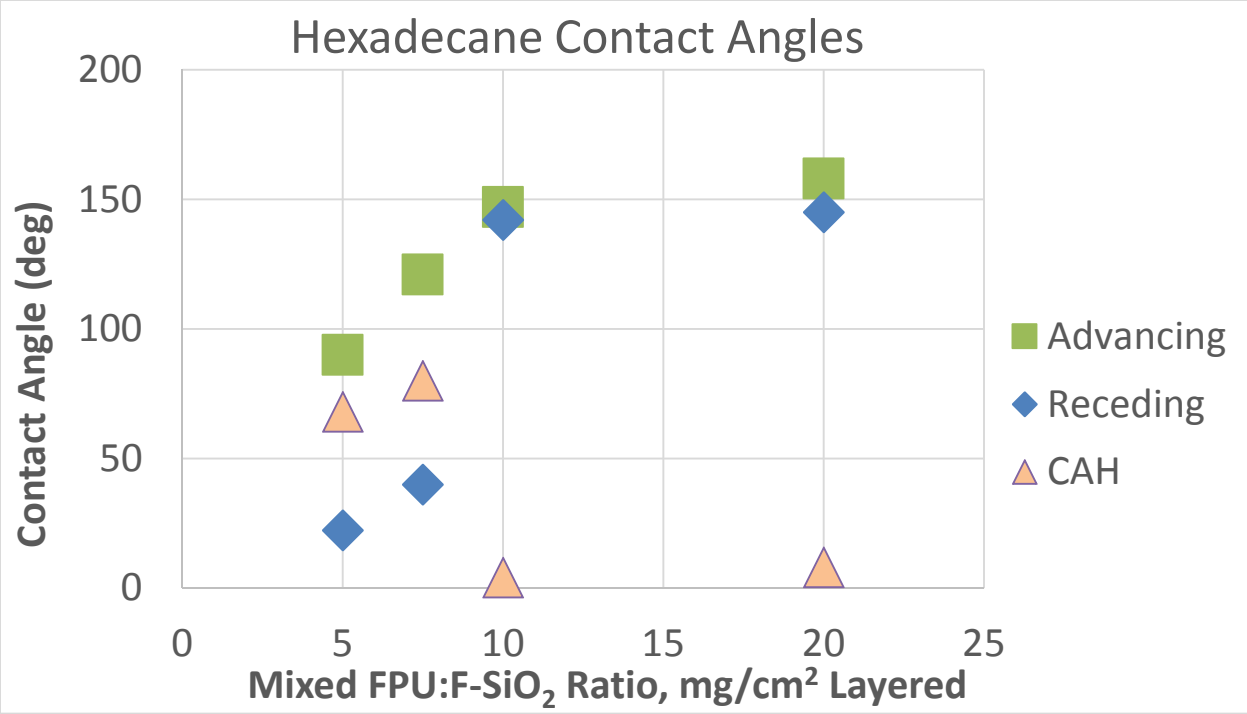

Figure 4.4: Hexadecane contact angles for layered surfaces.

It can be seen that these contact angles are lower than those for deionized water due to the lower surface tension of the hexadecane. Again, increasing the amount of F-SiO_2 for the surfaces increases the surface repellence. This is particularly evident for the layered surfaces, where low concentrations of F-SiO_2 lead to the surface exhibiting the wetted Wenzel state as there is not enough texture to hold a stable Cassie-Baxter state. Once 10 mg cm^{-2} of coverage is reached, however, a Cassie-Baxter state is achieved and the surface effectively repels the hexadecane due to enough texture for the breakthrough pressure to be greater than the gravitational force on the drop. Hexadecane contact angles for the layered surfaces are better than the mixed surfaces due to the lower relative surface energy of the uncoated F-SiO_2 particles than particles coated with the FPU in the mixed surfaces.

4.4.2. Dip Test Results

Dip tests results are summarized in Table 4.2:

Table 4.2: Syrup dip-testing adhesion results for various surfaces.

Syrup Dip Testing	
Surface	Adhesion/area
	mg/mm^2
Control Surfaces	
UED	17.5
FPU Flat	3.0
SS Bead Blast Silanized	3.0
SS Bead Blast Control	10.6
Mixed Surfaces- FPU: F-SiO_2 (%F-SiO_2), F-SiO_2 mg/mL in Chloroform	
5:1 (16.7%), 200 mg/mL	5.8
10:1 (9.1%), 30 mg/mL	4.3
15:1 (6.2%), 30 mg/mL	2.2
22.5:1 (4.3%), 30 mg/mL	21.3
30:1 (3.2%), 30 mg/mL	27.1
Layered Surfaces- (F-SiO_2 coverage, mg/mL in Chloroform); (FPU coverage)	
(20 mg/cm^2, 30 mg/mL); (155 mg/cm^2)	0.03
(10 mg/cm^2, 30 mg/mL); (155 mg/cm^2)	0.53
(7.5 mg/cm^2, 30 mg/mL); (155 mg/cm^2)	0.84

A commercially available product (Ultra-Ever-Dry©) was completely wet as the syrup dissolved the coating, with the texture increasing surface area for fluid to adhere to. Flat chemically modified surfaces exhibited less adhesion than a control stainless steel surface. Mixed coatings that supported drops in the Cassie-Baxter state had lower adhesion than surfaces wetted in the Wenzel state, with increasing oleophobicity resulting in reduced adhesion compared to the flat control surfaces.

Layered surfaces showed the least amount of adhesion due to their oleophobic properties, with less than half the adhesion of the best flat control surfaces. Increasing the F-SiO_2 coverage concentration reduced adhesion to layered surfaces as well, with no visual adhesion to the highest coverage surface, with no film or drops adhering anywhere on the surface. Thus, the weight measurements for this surface were used to quantify adhesion for the consistently smooth sides and bottoms of samples that lacked any coating and were wetted by the dipping process. However, a few particles were seen to be

removed from the layered surfaces as the concentration was increased, suggesting that shear flow durability might be a potential issue with these surfaces.

4.5. Conclusion

While hexadecane and other low surface-tension liquids are more difficult to repel than water and other higher surface-tension liquids, surfaces that could repel hexadecane were produced by varying the adhesive matrix and additive particles in mixed and layered coatings. It was found that mixed surfaces could provide more consistent repellence; however, layered surfaces provided higher contact angles once the coverage concentration of fluorinated particles was high enough to hold drops in the Cassie-Baxter state. Dip testing of surfaces in a low surface-tension syrup showed that layered surfaces decreased fluid adhesion compared to mixed coatings and flat control surfaces, providing an encouraging starting point for further development of durable superoleophobic surfaces that can repel high viscosity oils when exposed to fluid shear.

5. FUTURE WORK

5.1. Ice Resistant Surfaces

5.1.1. De-icing Surfaces

As this work found, easy ice removal occurs on materials with low moduli and surface energies. However, these materials are inherently difficult to adhere to surfaces in a facile manner. Thus, these coatings could be improved by developing a primer that would enhance coating adhesion. Additionally, the use of a surface with domains with controlled modulus and texture could help reduce adhesion by encouraging the creation of defect sites for crack propagation. Textured surfaces are used for biofouling prevention (see the Sharklet company[182]), so this texturing combined with variable modulus could produce a useful material. Harder modulus domains might help further improve mechanical durability of the surface by protecting the low modulus surrounding material. The creation of a micro-pillared surface out of a high modulus elastomer and subsequent flooding and curing with a low modulus, non-sacrificial material would render a surface with small, hard domains. These domains and moduli could be tuned to balance increased surface area and modulus (which would increase adhesion strength) with increased defects (which would reduce ice adhesion strength) to make a surface with less ice adhesion strength and/or increased mechanical durability.

5.1.2. Anti-Ice Surfaces

Prevention of ice accumulation through anti-ice surfaces is the most widely researched area as it is highly attractive for the potential to not even need de-ice materials. While certain inherent limitations for anti-ice surfaces (extreme freezing temperatures, condensation within any texturing, wetting due to impact, etc.) will still require de-ice surfaces, developing a method to prevent or delay icing will serve adequate in some environments and applications and provide a good supplement to de-icing surfaces.

Additionally, the superhydrophobic nature of some anti-ice coatings will also serve useful at higher temperatures.

Use of hydrophilic surfaces and melting-point suppressing materials have the potential do create a liquid layer between the surface and the ice, creating an ice-skate effect resulting in decreased ice adhesion. Utilizing salts, sugars, and other polymers that can alter the melting point of materials while being miscible with low-modulus materials such as PDMS might offer a great combination of anti and de-icing properties for extended use (Section 6.3).

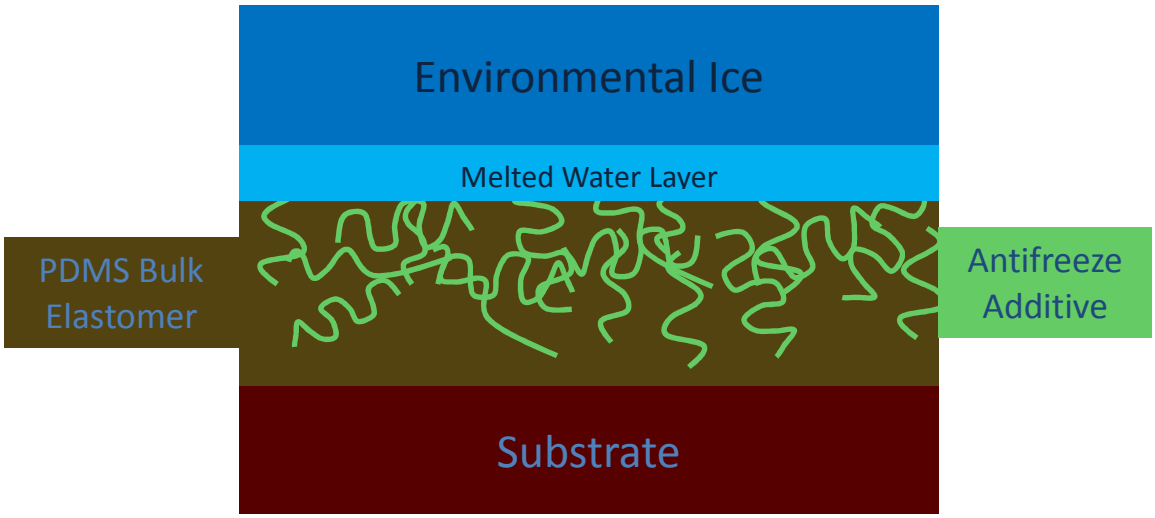

Figure 5.1: Anti and de-ice material idea.

5.2. Durable Superhydrophobic

5.2.1. Durability Improvement

Improvement of surface durability under a variety of abrasion methods (Section 5.3) would allow for wider application adoption of superhydrophobic surfaces, and improved lab testing as surfaces would not need to be replaced as often. With the tested spray-coating method, future work might include a comparison of the impact of carrier solvents on the cross-linking and texture of surfaces, along with the continual use of highly durable, low surface-energy materials. One idea would be to utilize the segregation of low surface-energy particles to the surface of a higher surface-energy matrix could serve

as an effective means for developing a durable superhydrophobic as highly adhesive materials tend to have higher surface energies, and low surface-energy additives could be potentially tuned to the material. Other additives beyond silica particles could also be considered to encourage segregation and coating adhesion while maintaining the superhydrophobic nature of surfaces. Improving the ductility of surface coatings so that they would "bend but not break" might also improve surface durability. If a low modulus, highly texturized surface with outstanding superhydrophobic behavior were developed, it could see great potential use for durable ice-resistant coatings. Combining the low bulk modulus of PDMS with the repellence of a texturized F-SiO_2 coating might produce such a surface. Conversely, using an even harder matrix material could also potentially increase durability by increasing the energy necessary to damage the material.

5.2.2. Control of Coating Methods

The current spray-coating method works decently well for small-scale testing with easy-spraying materials (Section 8.2). However, high-solids mixtures and mixtures with particles dispersed in solvents tend to clog the spray-guns and occasionally provide inconsistent surfaces. To ensure that coatings are repeatable, testing multiple coating methods with a single coating would ensure that anomalies are not being created by the spraying process. Use of an atomizer nozzle and rotating bed (with highly controlled height, pressure, and flow rate) could provide an easily repeatable coating method for testing. If production scaling-up is ever considered, tests with a larger commercial atomizing sprayer would provide information for coating specialists to correctly use superhydrophobic materials. Surface demonstrations, artwork, and other information dissemination methods could also be produced in tandem with these scaling tests to increase awareness and interest in developed coatings.

5.3. Durable Superomniphobic

5.3.1. Overview

While the creation of more repellent surfaces is necessary and always important, improving the durability of these coatings and (possibly more importantly) developing testing methods for defining durability must be considered for future works. Surface removal due to shear drag and fluid breakthrough due to pressure are likely failure modes for superoleophobic surfaces exposed solely to liquids. In order to control testing of these parameters and to test surfaces in an application environment, rotational fluid testing and eventual coated pipe flow testing are recommended future works. Additionally, mechanical abrasion testing with sandpaper under a normal force has been reported, but with varying types of setups, loading, abradants, and other conditions. Initial testing with a normal load and reciprocating motion of sandpaper on surfaces has shown that spray-applied superoleophobic surfaces tend to be quite sensitive to mechanical abrasion. Considering that the use of surfaces is quite variable, it is likely that this type of abrasion may not adequately simulate field conditions, either on the lower or higher scales of abrasion. Generally, a full review of established abrasion tests (crocking, Taber Rotary abrasion, etc.) in specific relation to superomniphobic surfaces is advised to provide fundamental methods for surface scientists to evaluate works by to determine appropriate applications for various surfaces.

After analyzing various durability testing methods, further mechanical abrasion testing and subsequent improvement of surfaces to withstand this abrasion is suggested. Considering other low surface-energy adhesive materials and other coating methods that may reduce the fragility of surfaces beyond just FPU and F-SiO_2 may allow for a study of material properties and coating properties that effect repellence and durability. Varying the existing abrasion setup by using different abradants (such as cloth or smooth surfaces) may help compare surfaces better during development.

5.3.2. Rotational Fluid Shear Testing

Fluid drag will impart much different surface forces than other testing methods, forces which may simulate certain field conditions better than non-fluid or static fluid testing (such as linear abrasion or dip-testing). To initially test surfaces during development in a cost, space, and time-effective manner, a rotational flow setup allowing for testing of surfaces in a variety of fluids is advised. By developing a fluid shear model related to geometry, fluid properties, and test parameters (rotational velocity, temperature, etc.), a test method that can be compared to external conditions would allow for quick surface development with comparable results. Use of a large cylindrical bowl with surfaces placed into a rotating fluid may be a simple and quick lab test if the test's parameters can be related to other external factors (shear stress, fluid drag, etc.). Weight change measurements and visual/optical inspection would allow for inspection of surface degradation, adhesion, and other effects.

5.3.3. Internal Flow Testing

For pipe-flow applications, creating a benchtop pipe flow test-bed will allow further analysis of high-performing surfaces in specific flow conditions. Pipe flow analysis of pressure drop has been used for testing the drag reduction effect of surfaces, so the inclusion of pressure transducers would enable drag reduction analysis. By utilizing small sections of pipe a few inches in length (as small as necessary for fully developed flow at specific conditions), fluid adhesion to internal surfaces could be tested via a similar weighing method as employed in the dip-coat testing method. An effective internal flow test-bed might include (relatively) facile switching of working fluids, easy changing of test pipe sections, multiple sizes of tested piping, a small footprint and size to decrease cost and location impact, low-cost component design for potentially producing multiple test-beds, easy fluid control through control valves, pressure gauges, drain valves, and more.

REFERENCES

[1] N. A. Patankar, Langmuir 2003, 19, 1249.
[2] N. A. Patankar, Langmuir 2004, 20, 8209.
[3] A. K. Kota, Colorado State University 2015 Spring.
[4] W. Barthlott, C. Neinhuis, Planta 1997, 202, 1.
[5] K. Golovin, D. H. Lee, J. M. Mabry, A. Tuteja, Angewandte Chemie 2013, 52, 13007.
[6] T. Jiang, Z. G. Guo, W. M. Liu, Journal of Materials Chemistry A 2015, 3, 1811.
[7] B. Leng, Z. Shao, G. de With, W. Ming, Langmuir 2009, 25, 2456.
[8] J. H. Li, R. Weng, X. Q. Di, Z. W. Yao, J. Appl. Polym. Sci. 2014, 131, 7.
[9] C. Neinhuis, W. Barthlott, Annals of Botany 1997, 79, 667.
[10] M. Nosonovsky, B. Bhushan, Current Opinion in Colloid & Interface Science 2009, 14, 270.
[11] T. L. Sun, L. Feng, X. F. Gao, L. Jiang, Accounts of Chemical Research 2005, 38, 644.
[12] J. P. Youngblood, N. R. Sottos, C. Extrand, Mrs Bull 2008, 33, 732.
[13] E. Almeida, T. C. Diamantino, O. de Sousa, Progress in Organic Coatings 2007, 59, 2.
[14] T. Arai, H. Harino, M. Ohji, W. J. Langston, *Ecotoxicology of Antifouling Biocides*, 2009.
[15] R. F. Brady Jr, Progress in Organic Coatings 2001, 43, 188.
[16] R. F. Brady, Jr., C. L. Aronson, Biofouling 2003, 19 Suppl, 59.
[17] M. Lejars, A. Margaillan, C. Bressy, Chemical Reviews 2012, 112, 4347.
[18] Y. Liu, C. Leng, B. Chisholm, S. Stafslien, P. Majumdar, Z. Chen, Langmuir 2013, 29, 2897.
[19] d. William W. Slater, S. Margaret, R. R. Brooks, M. J. Winter, Google Patents, 1994.
[20] M. Wouters, J. van Zanten, T. Vereijken, D. Bakker, J. Klijnstra, Surface Coatings International Part B: Coatings Transactions 2006, 89, 23.
[21] X. Yao, S. S. Dunn, P. Kim, M. Duffy, J. Alvarenga, J. Aizenberg, Angewandte Chemie 2014, 53, 4418.
[22] B. Bhushan, Y. C. Jung, Progress in Materials Science 2011, 56, 1.
[23] B. Dean, B. Bhushan, Philosophical Transactions of the Royal Society A: Mathematical, Physical and Engineering Sciences 2010, 368, 4775.
[24] C. Lee, C.-J. Kim, Physical review letters 2011, 106, 014502.
[25] M. A. K. Azad, D. Ellerbrok, W. Barthlott, K. Koch, Bioinspiration & Biomimetics 2015, 10.
[26] X. Heng, M. Xiang, Z. Lu, C. Luo, ACS applied materials & interfaces 2014, 6, 8032.
[27] L. Zhang, J. Wu, M. N. Hedhili, X. Yang, P. Wang, Journal of Materials Chemistry A 2015, 3, 2844.
[28] H. Vuollekoski, M. Vogt, V. A. Sinclair, J. Duplissy, H. Jarvinen, E. M. Kyro, R. Makkonen, T. Petaja, N. L. Prisle, P. Raisanen, M. Sipila, J. Ylhaisi, M. Kulmala, Hydrology and Earth System Sciences 2015, 19, 601.
[29] F. T. Malik, R. M. Clement, D. T. Gethin, W. Krawszik, A. R. Parker, Bioinspiration & Biomimetics 2014, 9.
[30] D. L. Hu, B. Chan, J. W. M. Bush, Nature 2003, 424, 663.
[31] H. Jin, A. Marmur, O. Ikkala, R. H. A. Ras, Chemical Science 2012, 3, 2526.
[32] H. Jin, M. Kettunen, A. Laiho, H. Pynnonen, J. Paltakari, A. Marmur, O. Ikkala, R. H. A. Ras, Langmuir 2011, 27, 1930.
[33] Y. Su, B. Ji, Y. Huang, K.-c. Hwang, Langmuir 2010, 26, 18926.
[34] X. Zhang, J. Zhao, Q. Zhu, N. Chen, M. Zhang, Q. Pan, ACS applied materials & interfaces 2011, 3, 2630.
[35] F. Zhang, L. Zhao, H. Chen, S. Xu, D. G. Evans, X. Duan, Angewandte Chemie 2008, 47, 2466.
[36] R. Helbig, J. Nickerl, C. Neinhuis, C. Werner, Plos One 2011, 6.

[37] S. Pan, A. K. Kota, J. M. Mabry, A. Tuteja, J. Am. Chem. Soc. 2013, 135, 578.
[38] A. K. Kota, G. Kwon, W. Choi, J. M. Mabry, A. Tuteja, Nature communications 2012, 3.
[39] G. Kwon, A. K. Kota, Y. Li, A. Sohani, J. M. Mabry, A. Tuteja, Advanced materials 2012, 24, 3666.
[40] J. Yang, Z. Zhang, X. Xu, X. Zhu, X. Men, X. Zhou, Journal of Materials Chemistry 2012, 22, 2834.
[41] X. Mao, Y. Chen, Y. Si, Y. Li, H. Wan, J. Yu, G. Sun, B. Ding, RSC Advances 2013, 3, 7562.
[42] A. C. Lima, J. F. Mano, Nanomedicine 2015, 10, 271.
[43] F. Mugele, J. C. Baret, Journal of Physics-Condensed Matter 2005, 17, R705.
[44] A. Mata, A. J. Fleischman, S. Roy, Biomed. Microdevices 2005, 7, 281.
[45] H. J. Butt, I. V. Roisman, M. Brinkmann, P. Papadopoulos, D. Vollmer, C. Semprebon, Current Opinion in Colloid & Interface Science 2014, 19, 343.
[46] J. Genzer, K. Efimenko, Biofouling 2006, 22, 339.
[47] A. K. Kota, W. Choi, A. Tuteja, Mrs Bull 2013, 38, 383.
[48] K. Liu, Y. Tian, L. Jiang, Progress in Materials Science 2013, 58, 503.
[49] B. Su, W. Guo, L. Jiang, Small 2015, 11, 1072.
[50] Z. Xue, M. Liu, L. Jiang, Journal of Polymer Science Part B-Polymer Physics 2012, 50, 1209.
[51] C. Antonini, M. Innocenti, T. Horn, M. Marengo, A. Amirfazli, Cold Regions Science and Technology 2011, 67, 58.
[52] R. Jafari, R. Menini, M. Farzaneh, Appl. Surf. Sci. 2010, 257, 1540.
[53] S. Jung, M. K. Tiwari, N. V. Doan, D. Poulikakos, Nature communications 2012, 3, 615.
[54] K. R. Khedir, G. K. Kannarpady, H. Ishihara, J. Woo, M. P. Asar, C. Ryerson, A. S. Biris, Appl. Surf. Sci. 2013, 279, 76.
[55] R. Menini, M. Farzaneh, Surface and Coatings Technology 2009, 203, 1941.
[56] A. J. Meuler, J. D. Smith, K. K. Varanasi, J. M. Mabry, G. H. McKinley, R. E. Cohen, ACS applied materials & interfaces 2010, 2, 3100.
[57] L. Mishchenko, B. Hatton, V. Bahadur, J. A. Taylor, T. Krupenkin, J. Aizenberg, ACS Nano 2010, 4, 7699.
[58] X. Sun, V. G. Damle, S. Liu, K. Rykaczewski, Advanced Materials Interfaces 2015, 2, n/a.
[59] P. Tourkine, M. Le Merrer, D. Quéré, Langmuir 2009, 25, 7214.
[60] J. Lv, Y. Song, L. Jiang, J. Wang, ACS Nano 2014, 8, 3152.
[61] A. Davis, Y. H. Yeong, A. Steele, I. S. Bayer, E. Loth, ACS applied materials & interfaces 2014, 6, 9272.
[62] Y. He, C. Y. Jiang, X. B. Cao, J. Chen, W. Tian, W. Z. Yuan, Appl. Surf. Sci. 2014, 305, 589.
[63] S. A. Kulinich, M. Farzaneh, Appl. Surf. Sci. 2009, 255, 8153.
[64] T. M. Schutzius, S. Jung, T. Maitra, P. Eberle, C. Antonini, C. Stamatopoulos, D. Poulikakos, Langmuir 2014.
[65] A. Alizadeh, M. Yamada, R. Li, W. Shang, S. Otta, S. Zhong, L. Ge, A. Dhinojwala, K. R. Conway, V. Bahadur, A. J. Vinciquerra, B. Stephens, M. L. Blohm, Langmuir 2012, 28, 3180.
[66] P. Eberle, M. K. Tiwari, T. Maitra, D. Poulikakos, Nanoscale 2014, 6, 4874.
[67] C. Laforte, J. Laforte, J. Carrière, "How a solid coating can reduce the adhesion of ice on a structure", presented at *Proceedings of the International Workshop on Atmospheric Icing of Structures (IWAIS)*, 2002.
[68] A. J. Meuler, G. H. McKinley, R. E. Cohen, ACS Nano 2010, 4, 7048.
[69] M. Nosonovsky, V. Hejazi, ACS Nano 2012, 6, 8488.
[70] F. Wang, C. Li, Y. Lv, F. Lv, Y. Du, Cold Regions Science and Technology 2010, 62, 29.
[71] L. Foroughi Mobarakeh, R. Jafari, M. Farzaneh, Appl. Surf. Sci. 2013, 284, 459.
[72] O. Gohardani, D. W. Hammond, Cold Regions Science and Technology 2013, 96, 8.
[73] S. A. Kulinich, M. Farzaneh, Cold Regions Science and Technology 2011, 65, 60.
[74] S. A. Kulinich, S. Farhadi, K. Nose, X. W. Du, Langmuir 2011, 27, 25.

[75] K. K. Varanasi, T. Deng, J. D. Smith, M. Hsu, N. Bhate, Appl Phys Lett 2010, 97, 234102.
[76] R. Menini, Z. Ghalmi, M. Farzaneh, Cold Regions Science and Technology 2011, 65, 65.
[77] S. Yang, Q. Xia, L. Zhu, J. Xue, Q. Wang, Q.-m. Chen, Appl. Surf. Sci. 2011, 257, 4956.
[78] S. R. Sivas, B. Thomaier, R. Hoover, K., NuSil Technology LLC, 2008.
[79] J. Chen, R. Dou, D. Cui, Q. Zhang, Y. Zhang, F. Xu, X. Zhou, J. Wang, Y. Song, L. Jiang, ACS applied materials & interfaces 2013, 5, 4026.
[80] V. Hejazi, K. Sobolev, M. Nosonovsky, Scientific reports 2013, 3, 2194.
[81] H. H. G. Jellinek, Journal of colloid science 1959, 14, 268.
[82] L. E. Raraty, D. Tabor, Proc R Soc Lon Ser-A 1958, 245, 184.
[83] M. Susoff, K. Siegmann, C. Pfaffenroth, M. Hirayama, Appl. Surf. Sci. 2013, 282, 870.
[84] C. Wang, T. Fuller, W. Zhang, K. J. Wynne, Langmuir 2014, 30, 12819.
[85] Wearlon, Wilton, NY.
[86] H. Jellinek, Canadian journal of physics 1962, 40, 1294.
[87] F. Arianpour, M. Farzaneh, S. A. Kulinich, Appl. Surf. Sci. 2013, 265, 546.
[88] T. Canada, Transport Canada Civil Aviation, 2014, 3.
[89] F. A. Administration, (Ed: FAA), 2014, 2.
[90] Boeing, in *Aero Magazine*, The Boeing Corporation, Seattle, Washington 2007, 15.
[91] A. Beisswenger, C. Laforte, J. Perron, 2011.
[92] M. Zou, S. Beckford, R. Wei, C. Ellis, G. Hatton, M. A. Miller, Appl. Surf. Sci. 2011, 257, 3786.
[93] H. Murase, K. Nanishi, Annals of Glaciology 1985, 6, 146.
[94] J. V. Nikkola, S. Pelto, J. Munter, T. Ropponen, J. Mangs, J. Mahlberg, R. Larismaa, J. Koivisto, J., 2014.
[95] D. N. Anderson, A. D. Reich, 1997.
[96] R. M. Fillion, A. R. Riahi, A. Edrisy, Renewable and Sustainable Energy Reviews 2014, 32, 797.
[97] N. D. Mulherin, R. B. Haehnel, DTIC Document, 2003.
[98] M. E. Farzaneh, *Atmospheric Icing of Power Networks*, Springer Netherlands, 2008.
[99] E. M. Petrie, Metal Finishing 2009, 107, 56.
[100] M. Nosonovsky, Nature 2011, 477, 412.
[101] P. W. Wilson, W. Lu, H. Xu, P. Kim, M. J. Kreder, J. Alvarenga, J. Aizenberg, Physical chemistry chemical physics : PCCP 2013, 15, 581.
[102] S. B. Subramanyam, K. Rykaczewski, K. K. Varanasi, Langmuir 2013, 29, 13414.
[103] N. Vogel, R. A. Belisle, B. Hatton, T.-S. Wong, J. Aizenberg, Nature communications 2013, 4, 1.
[104] T.-S. Wong, S. H. Kang, S. K. Y. Tang, E. J. Smythe, B. D. Hatton, A. Grinthal, J. Aizenberg, Nature 2011, 477, 443.
[105] E. H. Andrews, H. A. Majid, N. A. Lockington, J Mater Sci 1984, 19, 73.
[106] R. F. Brady Jr, Progress in Organic Coatings 1999, 35, 31.
[107] M. K. Chaudhury, J. A. Finlay, J. Y. Chung, M. E. Callow, J. A. Callow, Biofouling 2005, 21, 41.
[108] J. Kim, B. J. Chisholm, J. Bahr, Biofouling 2007, 23, 113.
[109] J. Y. Chung, M. K. Chaudhury, The Journal of Adhesion 2007, 81, 1119.
[110] K. H. Kim, M. K. Chaudhury, The Journal of Adhesion 2009, 85, 792.
[111] R. J. Pieper, A. Ekin, D. C. Webster, F. Cassé, J. A. Callow, M. E. Callow, Journal of Coatings Technology and Research 2007, 4, 453.
[112] D. L. Schmidt, n. Brady, K. Lam, D. C. Schmidt, M. K. Chaudhury, Langmuir 2004, 20, 2830.
[113] M. K. Chaudhury, K. H. Kim, The European Physical Journal E 2007, 23, 175.
[114] K. Kendall, J. Phys. D: Appl. Phys. 1971, 4, 1186.
[115] A. Colas, J. Curtis, Biomaterials science: an introduction to materials in medicine 2004, 2, 80.
[116] J. Mokkaphan, W. Banlunara, T. Palaga, P. Sombuntham, S. Wanichwecharungruang, ACS applied materials & interfaces 2014, 6, 20188.

[117] E. Yilgör, I. Yilgör, Progress in Polymer Science 2014, 39, 1165.
[118] S. Perutz, E. J. Kramer, J. Baney, C. Y. Hui, Macromolecules 1997, 30, 7964.
[119] C. Y. Hui, T. Tang, Y. Y. Lin, M. K. Chaudhury, Langmuir 2004, 20, 6052.
[120] A. K. Kota, G. Kwon, A. Tuteja, NPG Asia Mater. 2014, 6, 16.
[121] T. Young, The Royal Society 1805, 95, 65.
[122] J. Xi, L. Jiang, Industrial & Engineering Chemistry Research 2008, 47, 6354.
[123] F. Xia, L. Jiang, Advanced materials 2008, 20, 2842.
[124] M. H. Jin, X. J. Feng, L. Feng, T. L. Sun, J. Zhai, T. J. Li, L. Jiang, Advanced materials 2005, 17, 1977.
[125] E. Bittoun, A. Marmur, Langmuir 2012, 28, 13933.
[126] L. C. Gao, T. J. McCarthy, Langmuir 2006, 22, 2966.
[127] Y. Su, B. Ji, K. Zhang, H. Gao, Y. Huang, K. Hwang, Langmuir 2010, 26, 4984.
[128] D. Bonn, J. Eggers, J. Indekeu, J. Meunier, E. Rolley, Reviews of Modern Physics 2009, 81, 739.
[129] M. K. Chaudhury, G. M. Whitesides, Science 1992, 256, 1539.
[130] J. F. Joanny, P. G. Degennes, J. Chem. Phys. 1984, 81, 552.
[131] S. J. Gregg, The Journal of chemical physics 1948, 16, 549.
[132] C. G. Furmidge, Journal of Colloid Science 1962, 17, 309.
[133] A. B. D. Cassie, S. Baxter, Transactions of the Faraday Society 1944, 40, 0546.
[134] A. Woods, Archaeology 2012, 65.
[135] J. Genzer, K. Efimenko, Science 2000, 290, 2130.
[136] T. Nishino, M. Meguro, K. Nakamae, M. Matsushita, Y. Ueda, Langmuir 1999, 15, 4321.
[137] M. Nosonovsky, Langmuir 2007, 23, 3157.
[138] R. N. Wenzel, Ind Eng Chem 1936, 28, 988.
[139] A. K. Kota, Y. Li, J. M. Mabry, A. Tuteja, Advanced materials 2012, 24, 5838.
[140] S. P. R. Kobaku, A. K. Kota, D. H. Lee, J. M. Mabry, A. Tuteja, Angewandte Chemie International Edition 2012, 51, 10109.
[141] K. Koch, H. F. Bohn, W. Barthlott, Langmuir 2009, 25, 14116.
[142] S. Herminghaus, Europhys Lett 2000, 52, 165.
[143] P. S. Brown, B. Bhushan, Scientific reports 2015, 5.
[144] X. Deng, L. Mammen, H.-J. Butt, D. Vollmer, Science 2012, 335, 67.
[145] L. Ionov, A. Synytska, Physical Chemistry Chemical Physics 2012, 14, 10497.
[146] C. Jin, J. Li, S. Han, J. Wang, Q. Sun, Appl. Surf. Sci. 2014, 320, 322.
[147] Y. C. Jung, B. Bhushan, Acs Nano 2009, 3, 4155.
[148] M. Manca, A. Cannavale, L. De Marco, A. S. Arico, R. Cingolani, G. Gigli, Langmuir 2009, 25, 6357.
[149] N. V. Motlagh, F. C. Birjandi, J. Sargolzaei, N. Shahtahmassebi, Appl. Surf. Sci. 2013, 283, 636.
[150] T. Verho, C. Bower, P. Andrew, S. Franssila, O. Ikkala, R. H. A. Ras, Advanced materials 2011, 23, 673.
[151] H. Wang, Y. Xue, J. Ding, L. Feng, X. Wang, T. Lin, Angew. Chem.-Int. Edit. 2011, 50, 11433.
[152] L. Wu, J. Zhang, B. Li, L. Fan, L. Li, A. Wang, Journal of Colloid and Interface Science 2014, 432, 31.
[153] L. Wu, J. Zhang, B. Li, A. Wang, Polymer Chemistry 2014, 5, 2382.
[154] X. Yin, Z. Liu, D. Wang, X. Pei, B. Yu, F. Zhou, Journal of Bionic Engineering 2015, 12, 1.
[155] H. Zhou, H. Wang, H. Niu, A. Gestos, X. Wang, T. Lin, Advanced materials 2012, 24, 2409.
[156] J. Zimmermann, F. A. Reifler, G. Fortunato, L.-C. Gerhardt, S. Seeger, Advanced Functional Materials 2008, 18, 3662.
[157] S. A. Kulinich, M. Honda, A. L. Zhu, A. G. Rozhin, X. W. Du, Soft Matter 2015, 11, 856.
[158] M. Alonso Frank, A. R. Boccaccini, S. Virtanen, Appl. Surf. Sci. 2014, 311, 753.
[159] L. B. Boinovich, A. M. Emelyanenko, V. K. Ivanov, A. S. Pashinin, ACS applied materials & interfaces 2013, 5, 2549.

[160] R. Jagdheesh, B. Pathiraj, E. Karatay, G. R. Romer, A. J. Huis in't Veld, Langmuir 2011, 27, 8464.
[161] L. Li, V. Breedveld, D. W. Hess, ACS applied materials & interfaces 2012, 4, 4549.
[162] Z. YU, Y. YU, Y. LI, S. SONG, S. HUO, X. HAN, Surface Review and Letters 2010, 17, 375.
[163] J. G. Massey, Journal of Exotic Pet Medicine 2006, 15, 33.
[164] M. Bell, in *The Washington Post*, The Washington Post Company, Washington, D.C. 2010.
[165] F. M. Fowkes, Industrial & Engineering Chemistry 1964, 56, 40.
[166] D. K. Owens, R. C. Wendt, J. Appl. Polym. Sci. 1969, 13, 1741.
[167] A. Tuteja, W. Choi, M. Ma, J. M. Mabry, S. A. Mazzella, G. C. Rutledge, G. H. McKinley, R. E. Cohen, Science 2007, 318, 1618.
[168] L. Cao, T. P. Price, M. Weiss, D. Gao, Langmuir 2008, 24, 1640.
[169] A. Steele, I. Bayer, E. Loth, Nano Letters 2009, 9, 501.
[170] D. Wang, X. Wang, X. Liu, F. Zhou, Journal of Physical Chemistry C 2010, 114, 9938.
[171] J. Yang, Z. Zhang, X. Men, X. Xu, X. Zhu, New Journal of Chemistry 2011, 35, 576.
[172] J. Yang, Z. Zhang, X. Xu, X. Men, X. Zhu, X. Zhou, New Journal of Chemistry 2011, 35, 2422.
[173] J. Zhang, S. Seeger, Angew. Chem.-Int. Edit. 2011, 50, 6652.
[174] T. Fujii, Y. Aoki, H. Habazaki, Langmuir 2011, 27, 11752.
[175] A. K. Kota, A. Tuteja, in *Advances in Fluorine-Containing Polymers*, Vol. 1106, American Chemical Society, 2012, 171.
[176] X. Wang, X. Liu, F. Zhou, W. Liu, Chemical Communications 2011, 47, 2324.
[177] Y. Wang, B. Bhushan, ACS applied materials & interfaces 2015, 7, 743.
[178] H. Wang, H. Zhou, A. Gestos, J. Fang, T. Lin, ACS applied materials & interfaces 2013, 5, 10221.
[179] S. Peng, X. Yang, D. Tian, W. Deng, ACS applied materials & interfaces 2014, 6, 15188.
[180] S. Pan, R. Guo, W. Xu, Aiche Journal 2014, 60, 2752.
[181] V. G. Damle, A. Tummala, S. Chandrashekar, C. Kido, A. Roopesh, X. Sun, K. Doudrick, J. Chinn, J. R. Lee, T. P. Burgin, K. Rykaczewski, ACS applied materials & interfaces 2015, 7, 4224.
[182] C. M. Magin, S. P. Cooper, A. B. Brennan, Materials Today 2010, 13, 36.
[183] A.-L. Roth, in *Spiegel Online*, Spiegel Net, Der Spiegel, Hamburg, Germany 2015.
[184] I. Oliver Manufacturing CO, La Junta, CO 2014.

6. APPENDIX A- ICE ADHESION SUPPLEMENTARY

6.1. Additional Figures

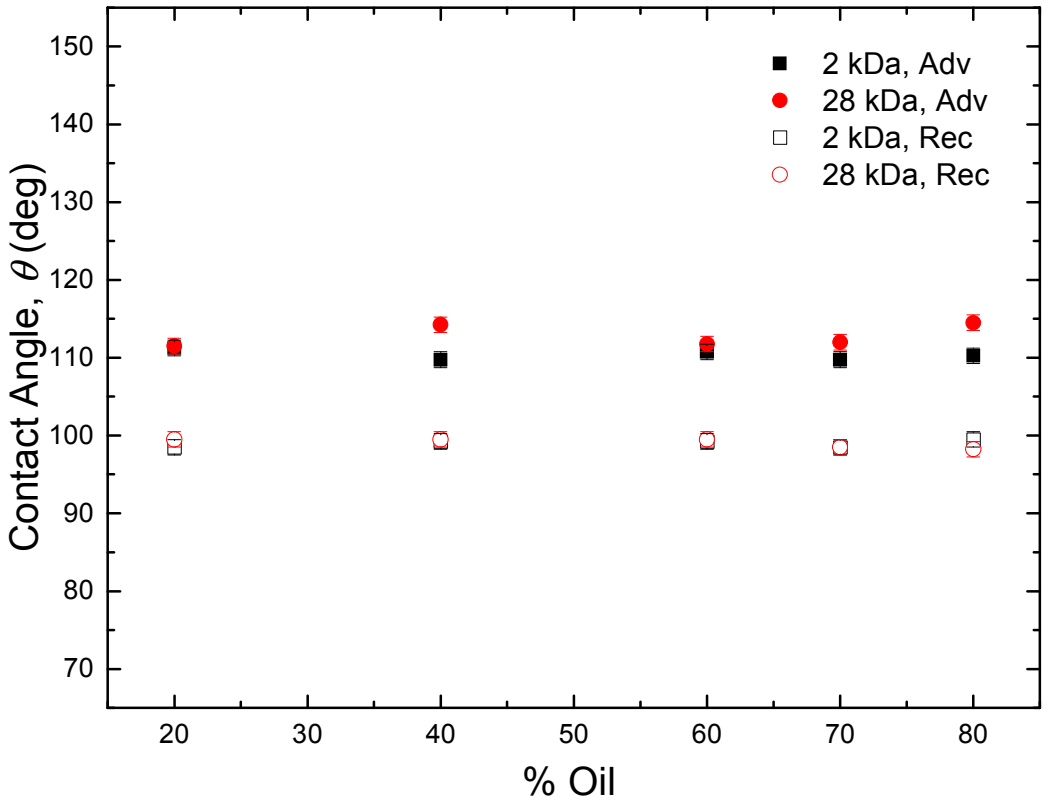

Figure 6.1: Advancing and receding contact angles for various materials tested. Tight grouping of contact angles (especially receding contact angles) highlights the constant surface energy for all materials.

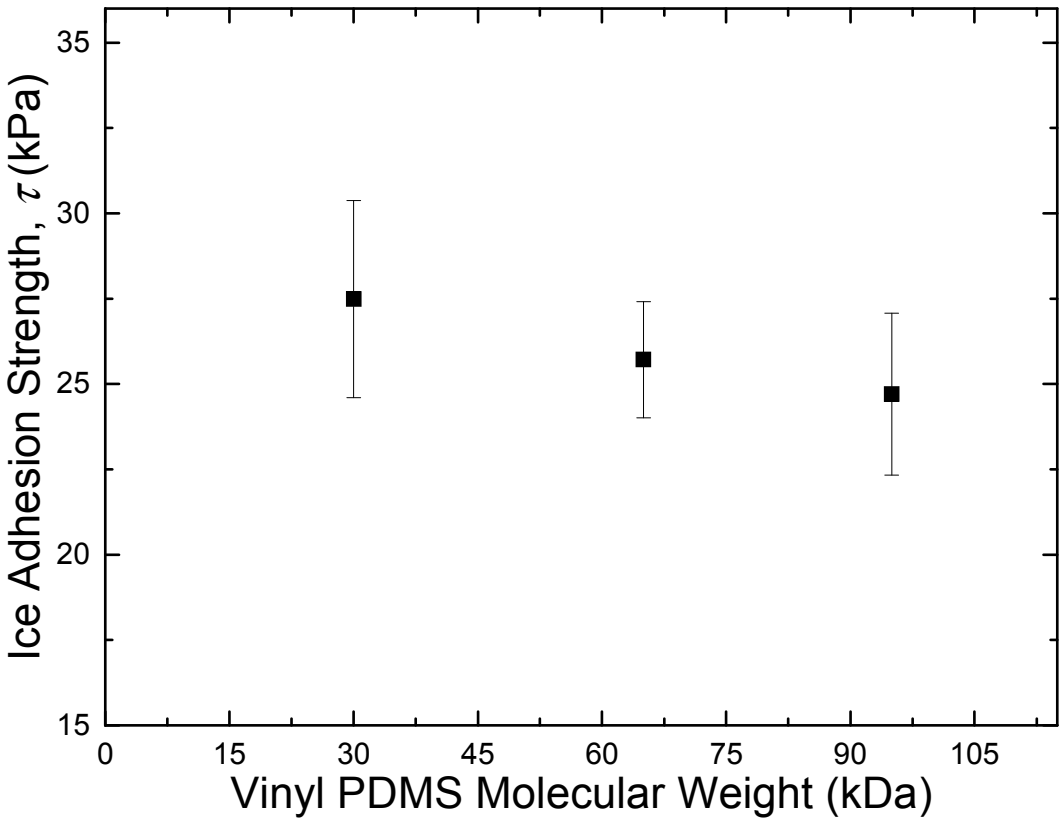

Figure 6.2: Ice adhesion strength for base vinyl silicone materials with varying molecular weights.

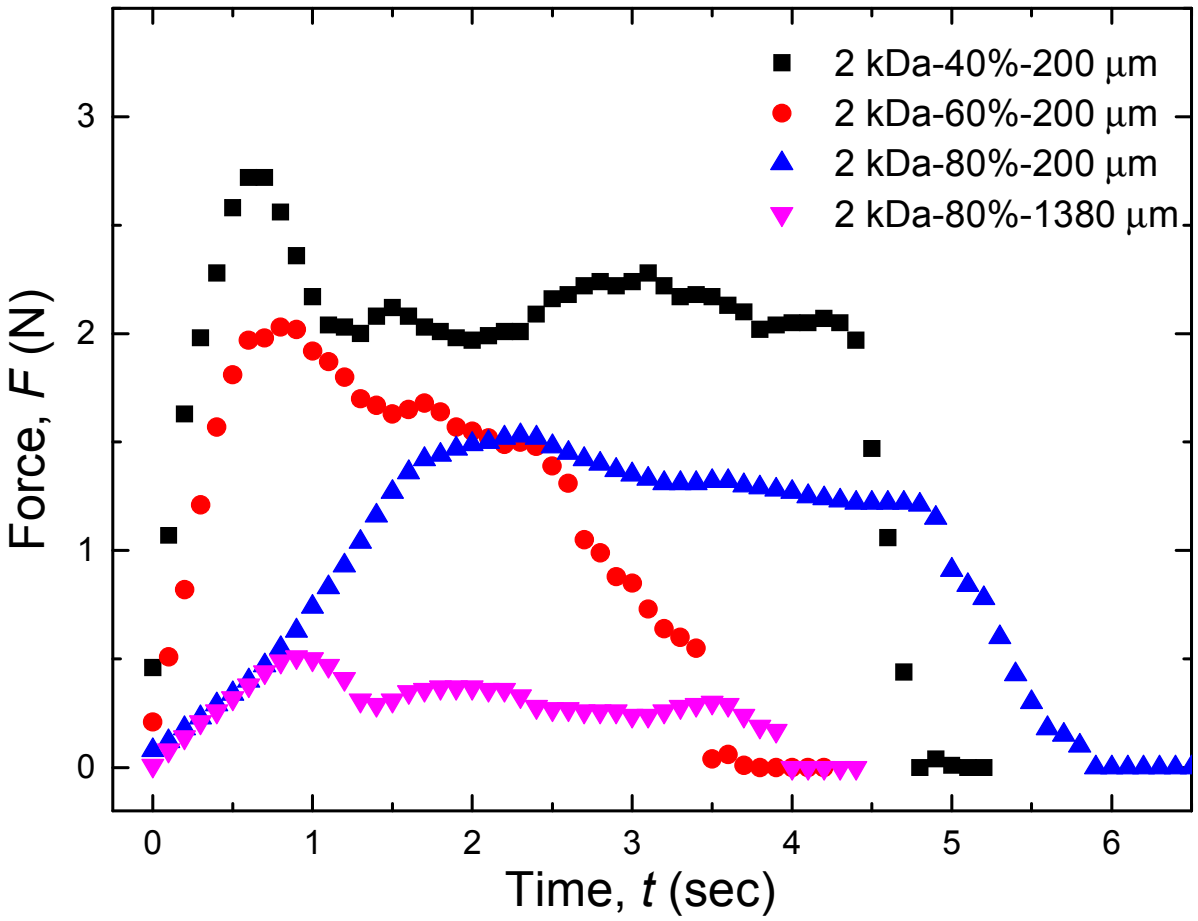

Figure 6.3: Characteristic load vs. time plots for ice adhesion strength testing for various materials showing maximum adhesion strength peak and subsequent sliding and detachment.

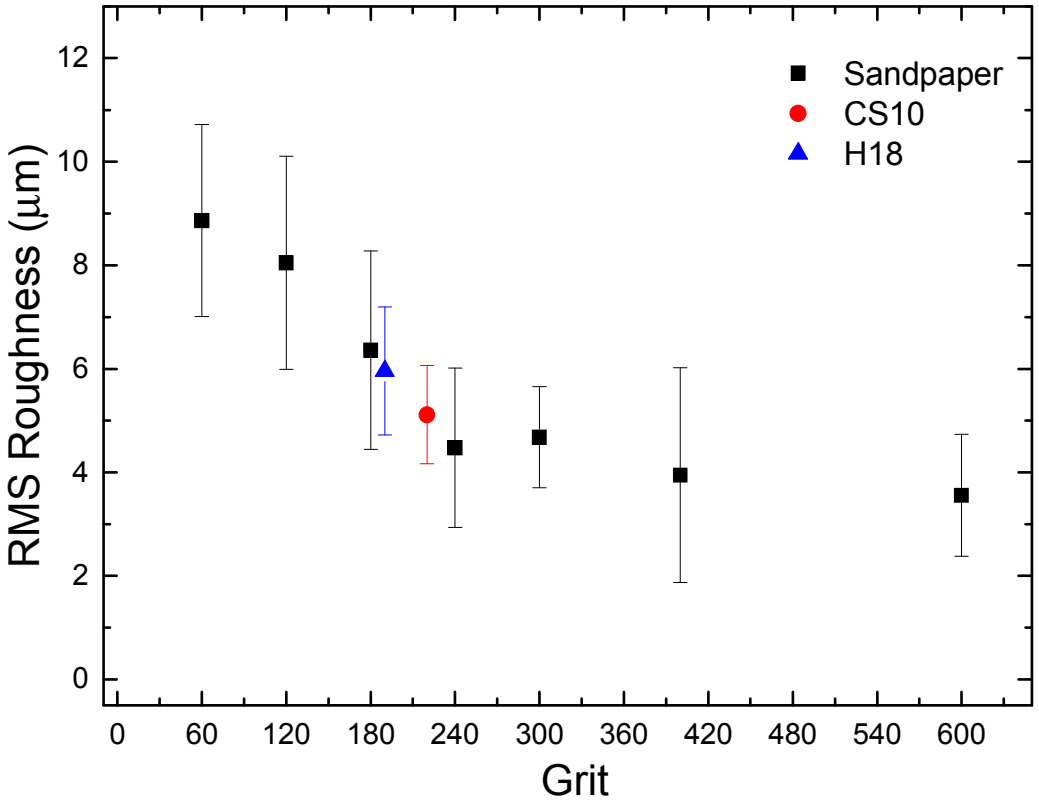

Figure 6.4: RMS roughness results for various grits of sandpaper and commercial abrasive wheels.

Table 6.1: Surface results before and after 180 grit abrasion, showing slight decrease in thickness and increase in roughness relative to material modulus.

	Ice Adhesion Strength [kPa]		**Thickness [µm]**		**RMS Roughness [µm]**	
Abrasion Cycles 180 Grit	0 Cycles	1000 Cycles	0 Cycles	1000 Cycles	0 Cycles	1000 Cycles
2 kDa-40%-200 µm	28.6	37.9	200	195	0.05	4.12
2 kDa-60%-200 µm	18.3	26.9	200	190	0.05	4.52
2 kDa-80%-200 µm	10.3	14.6	200	188	0.05	6.98
2 kDa-80%-1380 µm	5.4	9.6	1380	1350	0.05	6.98

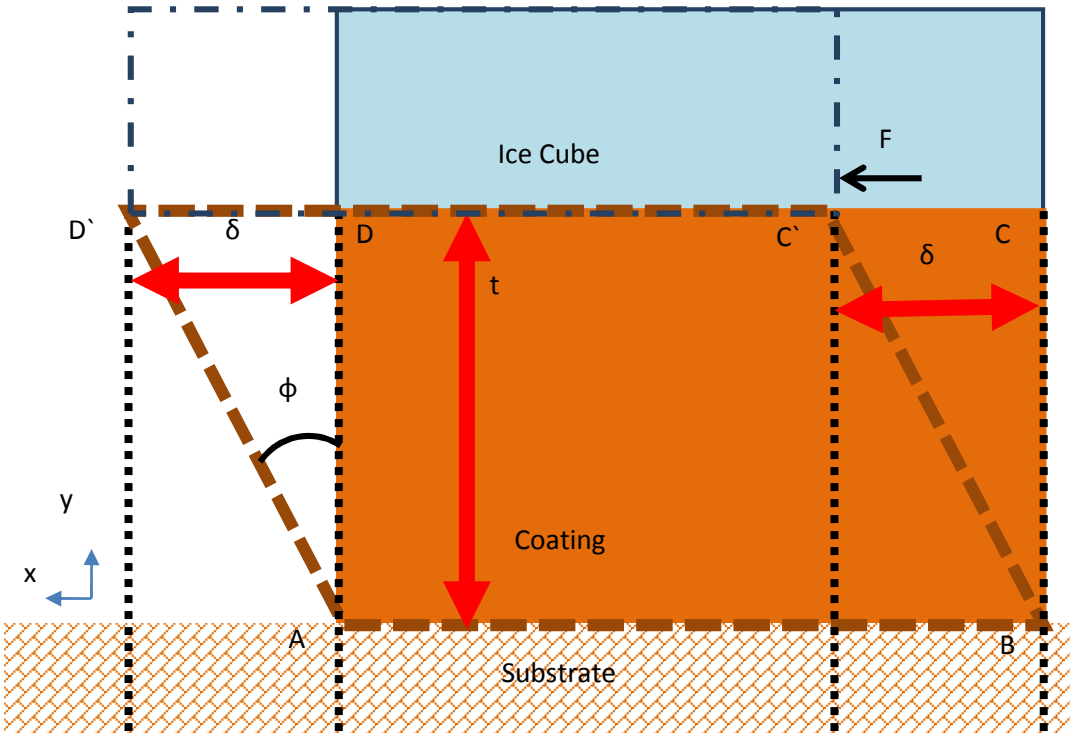

Figure 6.5: Schematic of shear displacement of a unit of elastic material constrained to a substrate.

Shear strain related to modulus and geometry of triangle ADD' (assume small angle ϕ):

$$\tan(\phi) = \frac{DD}{AD} = \phi = \frac{\delta}{t}$$

The elastic work done by the shear force in displacing the volume:

$$W_E = \frac{1}{2} \cdot F \cdot \delta$$

Shear modulus and stress:

$$G = \frac{\tau}{\phi} \qquad \tau = \frac{F}{A}$$

Elastic work displacing the volume per unit of end area:

$$W_E = \frac{\tau^2 \cdot t}{2 \cdot G}$$

At adhesive failure, the total work (or energy) of breaking the joint is exactly compensated by the gain in surface energy of the system. Total work of deflection is transmitted into the creation of two new surfaces (material elastically returns to its original position, with energy transmitted into the new surfaces):

$$W_A = W_E = \frac{\tau_{crit}^2 \cdot t}{2 \cdot G}$$

Unit Check:

$$\sqrt{\frac{\frac{J}{m^2} \cdot Pa}{m}} = 1\,Pa$$

Solving for critical shear stress, or the adhesion strength:

$$\tau_{crit} = \sqrt{\frac{W_A \cdot 2 \cdot G}{t}}$$

Force for removal is dependent on the area of adhesive contact (ice coverage area):

$$F_{crit} = \tau_{crit} \cdot A_{adh}$$

Figure 6.6:Derivation of critical adhesion strength for an elastic material.

6.2. PDMS Preparation

6.2.1. Overview

PDMS (polydimethylsiloxane) is an elastomer produced from combining a base fluid with a hardening agent. Uses include: pillared structures from molds, spin/spray coating anti-ice surfaces, using a syringe to produce micro-beads for dispersed structures, microfluidic devices, and more.

Cautions: PDMS is very sticky, so be sure to use gloves and avoid touching surfaces with sticky gloves. PDMS will also ruin pipettes, so never tilt the pipette tip up.

PDMS cures very hard to glassware, so avoid using glass for preparing PDMS. If glassware MUST be used, then use a strong solvent (such as AK) to clean the glassware after use. It is difficult to clean as PDMS smears off of surfaces, so use wipes and protective cloths under preparation area.

6.2.2. General Preparation

Prepare final containers (and samples to be coated) prior to beginning measurement of PDMS.

PDMS is usually mixed to a weight ratio of 10 units of base to each unit of hardener (10:1), although this can be varied to tune the modulus, and oils and other additives can be added. Regardless, always calculate the base: hardener ratio for the base BEFORE any plasticizers are added.

If adding silicone oil (or other additives), mix these in with the base material in the ratio/percent that you desire, degas this mixture, then add the cross-linker in the 10:1 ratio with the original base, degas again, then use as desired (spin coat, petri dish, mold, etc.).

The following recipe produces enough PDMS to fill 4 small petri dishes (47 mm) with PDMS, utilizing a plastic cup at least 2-3x the volume of PDMS for mixing. Bubbles will be removed with the vacuum oven. Approximate time: 20 minutes. Produces ~40 grams of PDMS.

1. If you are going to cure the PDMS at temperature, turn on your heating equipment to allow it to reach the desired temperature.
2. Create a database for PDMS production, and label final containers accordingly.

3. Layout tools and petri dishes:
    a. 4x 47mm petri dishes (or equivalent containers), mixing cup or plastic disposable beaker, Kim Wipes, multiple pairs of gloves, measuring spatula, 100-1000 μL micropipette (set to 250 μL measurement), balance (set to measure grams, put a Kim-wipe on the surface for protection), plasticizer oils.
4. Tare the mixing cup prior to measuring out base.
5. Measure out 36 grams of base into petri dish using spatula, then tare the balance again with the base in the petri dish. Clean the spatula with a Kim Wipe.
6. Add desired amount of plasticizer oil, mix well, and degas mixture.
7. Using the micropipette, measure out 3.6 grams of hardener into the base, producing a total mass of 39.6 grams of PDMS (not including plasticizer). Dispose of pipette tip. NEVER USE PIPETTE TO TRANSPORT BASE OR COMBINED PDMS (the high viscosity will not allow the PDMS to flow well, potentially sucking into the micropipette mechanics and clogging it…not fun).
8. Stir mixture thoroughly, many air bubbles should be produced from the reaction between the base and hardener.
9. Once stirred, place the mixture in the vacuum oven and put under vacuum to release these bubbles. Once bubbles rise to top and start to enlarge release the vacuum quickly then pull a vacuum again. Repeat until bubbles are mostly gone under vacuum. Cycling between atmospheric pressure and vacuum will disturb the bubbles enough to pop them quicker.
10. Using spatula, pour PDMS into final petri dishes (or other desired container).
11. Throw away gloves, wipes, and mixing cup. Return materials to cabinet.
12. Do not cure in plastic petri dishes in oven above 120 ^{o}F, it will melt. Hot plate can be used to cure at ~70 ^{o}C.
13. Coat sample as desired.

14. Oven Curing: 48 hrs. 100 °F
15. Hot Plate Curing: 70 °C: 1-3 hours

6.2.3. Notes

Tape samples to the bottom of petri dishes in order to get best results. If multiple layers of forming sheets are used adhere the sheets together with JB Weld or another bonding agent. Uncured superglue deactivates the PDMS hardener. Do not make samples too thin. Doing so will make it very difficult to peel PDMS off of the mold.

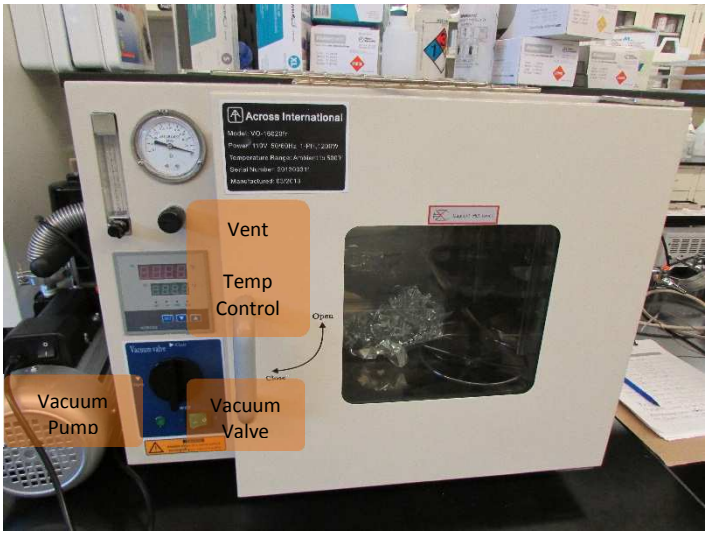

Figure 6.7: Vacuum oven for degassing and curing.

Spin-coat sample immediately after degassing for consistent viscosities.

Check boiling point of plasticizers by putting a glass slide covered with the plasticizer on a hot petri dish (whatever temperature is of interest).

High molecular weight and low % plasticizer mixtures are very viscous and difficult to degas.

6.3. Anti-Icing Time and Time Dependent Ice Adhesion Strength Testing Procedure

6.3.1. Introduction

The purpose of this test is to compare the amount of time to freeze a drop of constant volume on surfaces in a constant environment in order to evaluate the anti-icing effects of surfaces. There are a couple of options for single-trial tests or multiple tests.

Samples should be prepared ahead so that they are completely cured and ready for testing.

6.3.2. Setup

Equipment: Samples to test, 10-100 µL pipette, fresh pipette tips, fresh DI water in 20 mL vial, plastic transfer pipette (for IAS testing), walk-in refrigerator at 4 ^{o}C, 60% Relative Humidity, stop-watch, Peltier plate cart.

6.3.3. Test environment

1) Walk-in environmental chamber: 4 ^{o}C, 60% Relative Humidity
    I. To allow for analysis of the surfaces and to eliminate outside heat transfer effects, tests are to be performed under consistent conditions in a cool environmental chamber.
    II. A refrigerator, not a freezer, should be used so that freezing is initiated from the surface and not the ambient environment. This is to simulate conditions where surfaces are well below the ambient freezing temperature and surfaces have potential to ice. This also eliminates the effect of freezing initiation from air.
        i) Future testing can be done in a freezer if studying delay of ambient freezing is of interest.
        ii) The environmental chamber on the southwest side of the 1st floor is ideal as there is already a thermometer and humidity control. The second floor chamber has the same conditions, as tested with the lab thermometer/relative humidity hygrometer, but other groups do light-sensitive work in this chamber.
2) Setup/Preparation- THERMAL EQUILIBRIUM!!
    I. Take the entire setup cart into the chamber, with water, samples, Peltier plate…everything.
    II. Plug the Peltier plate in, set the target temperature to be -22 ^{o}C and let the Peltier plate sit for 15 minutes, or until it reaches thermal equilibrium.
        i) The true goal test temperature is -20 ^{o}C, so the set temperature and time to equilibrium may need to be modified to bring the temperature within at least 1 degree.

III. Leave surfaces and the DI water exposed to the ambient the entire time so that they can drop to the ambient temperature. It is important that the water be at ambient temperature for heat-transfer reasons.

3) Surface Preparation for endurance testing (washing of the surface to remove frost)

I. After sitting for 15 minutes, clamp samples onto the Peltier plate

II. Cover the surface with a film of water and allow this water to freeze.

III. Once frozen, remove the film to expose a clean surface.

i) This is done to remove all frost from the surface and serve as a washing step. Ideally, durable, repeatable surfaces should be able to withstand complete water exposure and ice removal and still be able to perform. If surfaces cannot do this, or if a different test is desired skip step c.

6.3.4. Procedure

1) Pipette 50 µL of DI water onto surface as one full drop.

I. Multiple 50 µL drops can be placed on the surface, but spaced at least a half inch apart. For strict testing, only test one drop at a time and remove all frost with a film of water after each test.

2) Start timing as soon as the drop is put on the surface.

3) Observe the drop's freezing progress. Air bubbles should rise to the top of the drop and a freeze-front should be visibly moving upwards.

Figure 6.8: Anti-ice test on Peltier plate with DI drops.

4) Stop the timer once the drop has visually completely frozen.

I. This should be visible from the air bubbles causing the drop to freeze to a point at the top.

II. Wear warm-gear as the cold and humidity can be dangerous, and you will have to stand in the chamber during testing.

5) Remove frost (if desired and applicable) or place another drop on a clean part of the surface (most likely the same spot).
6) Repeat at least 3 times for statistical significance.
7) Test Ice Adhesion Strength following time delay tests, if desired. Freeze surfaces for a consistent 10 minutes in the same manner as general ice adhesion strength tests, with the probe measuring the maximum adhesion strength while pushing the block as close to the surface as possible a rate of 5 cm min^{-1}.
    I. Ice Adhesion Strength tests can also be used to clean the frost off of the surface.

6.3.5. Notes

Thicker surfaces may take longer to reach equilibrium, so the film freeze is also important to ensure that surfaces are completely at equilibrium. Let this film freeze completely and sit for a few minutes before removal.

This test can be modified for purely anti-icing surfaces, as these surfaces may want to evaluate frost prevention.

If confirmation of repeated anti-icing is needed beyond simply freezing and removing the initial film, then another method may be advised. Frost formation during equilibrating is an issue though, as water drops will wet on the frost and possibly even move across the surface due to this wetting.

6.4. Rheometry Procedure

6.4.1. Lab Key

Connected to aluminum plate with big hole cut in it. Return to lab manuals drawer in Scott 365 after use.

Figure 6.9: Lab key

6.4.2. Machine Startup

The rheometer needs air pressure to be > 60 psi. Check gauge on the east wall. If pressure is low turn off the valve to the right of the door (above the sink), disconnect the line ahead of the oil trap, reconnect the line, and reopen the valve.

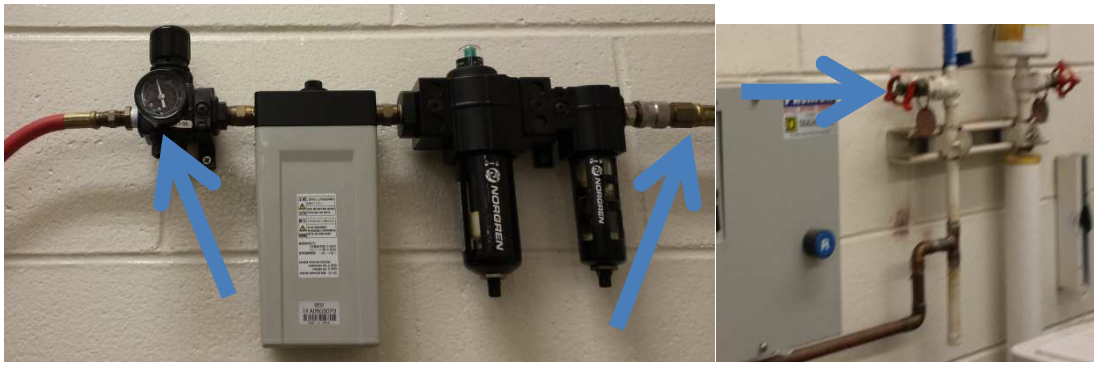

Figure 6.10: Pressure source, regulator, and connection.

6.4.3. Starting the Oven

IMPORTANT- it takes a while to fill the liquid nitrogen dewar, so get this started as soon as possible!

- Open the valve on the liquid nitrogen tank and check level before starting (connect line first, if disconnected).

Figure 6.11: Liquid nitrogen valve, gauge, and connection.

- Start the TA Orchestrator Software, open the Instrument Control Panel from the Control toolbar.
  - Set desired temperature for first phase (either curing temperature or testing temperature)
  - Ensure control is set to Oven, turn on Environmental Controller and Liquid Nitrogen Dewar.
  - Leave Motor Power off until after zeroing the machine.

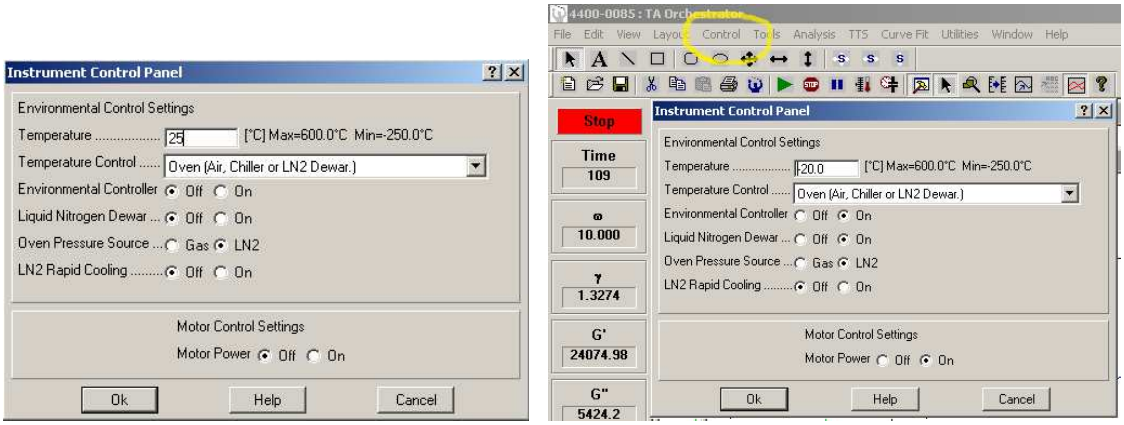

Figure 6.12: Setting up the instrument control.

6.4.4. Installing Plates/Cup Holder

Use the 25 or 8 mm parallel plates for samples that do not flow and can be cured outside of the machine. The 25 mm parallel plates are the ideal attachment for firmer materials while the 8mm plate is better for softer materials. Choose based on which geometry will allow you to compress the entire surface area with a reasonable force.

Find the plates in the “Rheometer Supplies” Cabinet. If using the cup holder, find the cup in the accessories bag. Use a parallel plate upper with the cup, and set the diameter to the plate size.

Figure 6.13: Rheometer supply cabinet with plates.

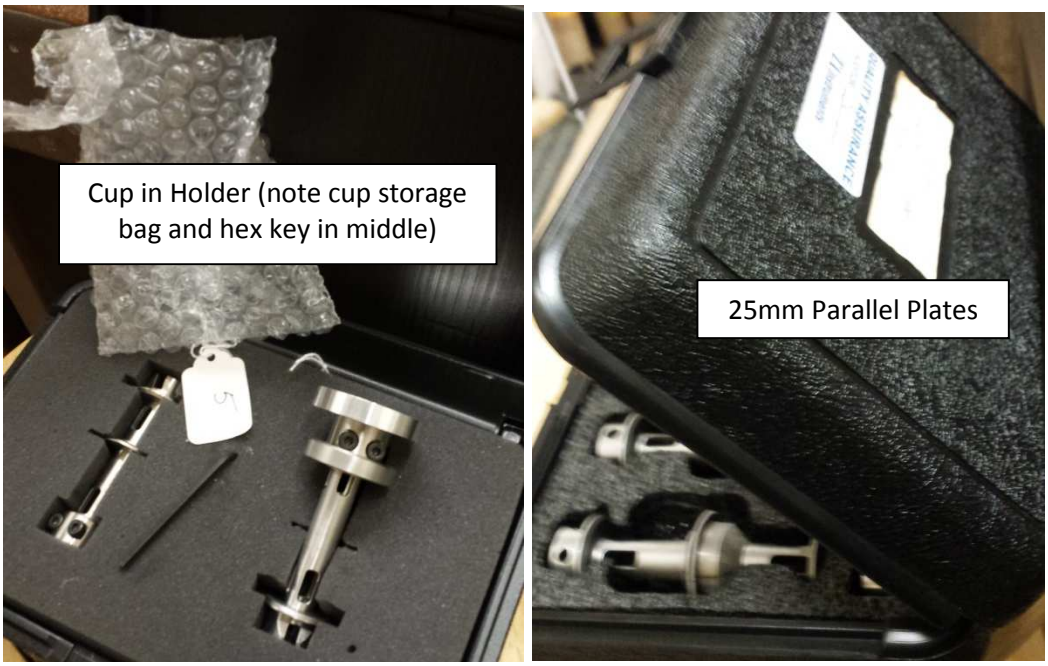

Figure 6.14: Boxes with rheometer accessories.

Insert the temperature probe (the small one) into the base. Rotate the probe until it slides all the way into hole as shown. Check to make sure that the machine is reading the room temperature (no probe shows -250 ^{o}C, so this will be obvious).

Put plates on, and hand-tighten nuts (blue arrows). Make plates parallel by bringing them into contact with each other. Do not overload (watch the bar on the machine feedback indicator (not on the computer). Tighten nuts with screwdriver, separate the plates a little bit. Make sure the deflector fins (red arrows) are close to the plates so that they do not contact and damage the oven ceramic.

Note: The middle button of the motor controller accelerates whichever directional button is pressed. Do fine adjustments by holding the directional button and tapping the acceleration button. Directional buttons move the machine a few 10's of µm per second, so is useful for fine control.

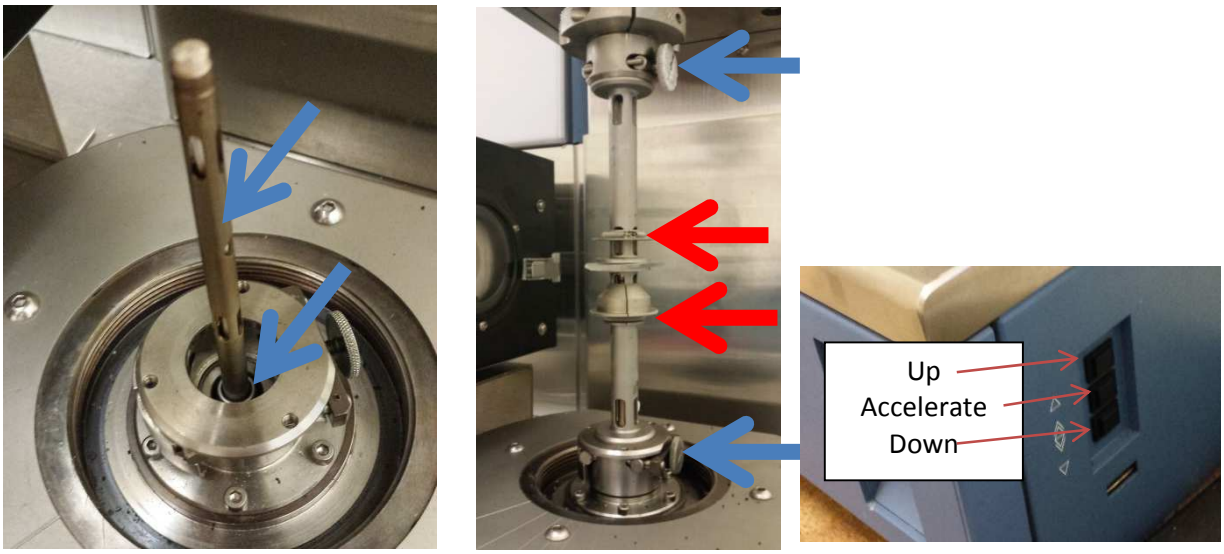

Figure 6.15: Thermometer in lower plate clamp, parallel plates in place and tightened with guards clearing the oven, positioning buttons.

6.4.5. Placing the Oven/Zeroing the Plates

It is important to zero the plates after they have come to thermal equilibrium, as they will have thermal expansion/contraction. Get the plates equilibrating as soon as the oven is ready-to-go.

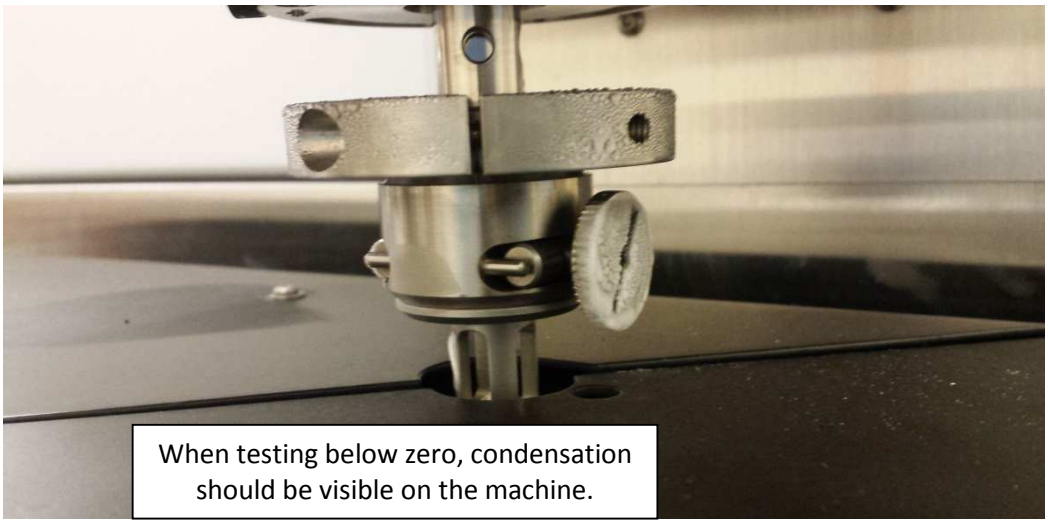

Figure 6.16: Upper plate connection at thermal equilibrium.

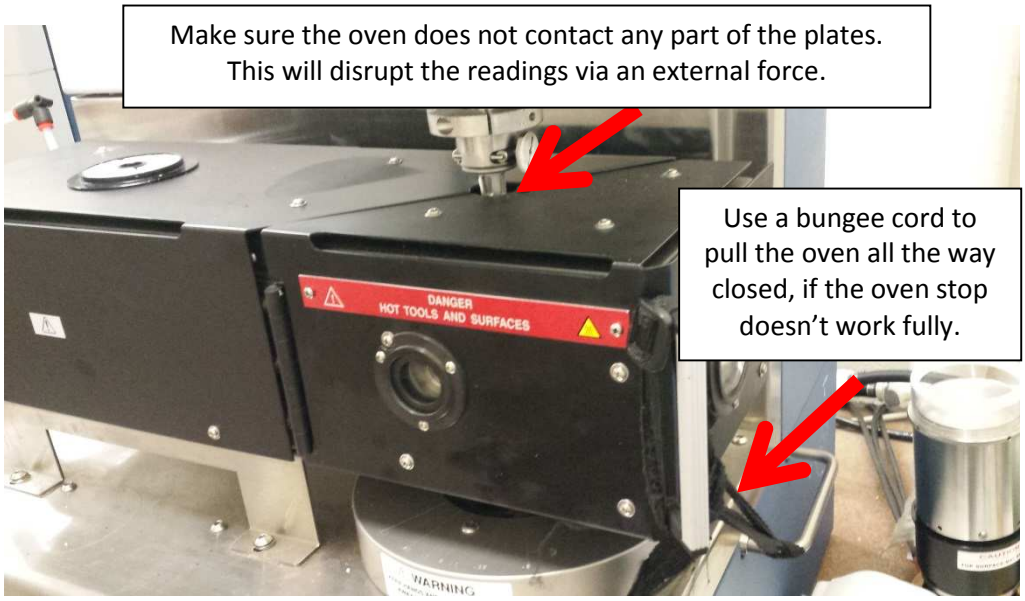

Figure 6.17: Oven in place.

Wait 15 minutes to allow for thermal equilibrium. This is a good time to prepare your sample and setup the tests (see below). You can setup the tests before zeroing the plates so that you can test as soon as you zero them.

Zeroing- The machine runs a program which brings the plates into contact. It measures the force to know when they are in contact and zero the gap accordingly. Test results are based on the sample volume, so a quality zeroing is important. Load your sample after zeroing and re-zero FORCE ONLY.

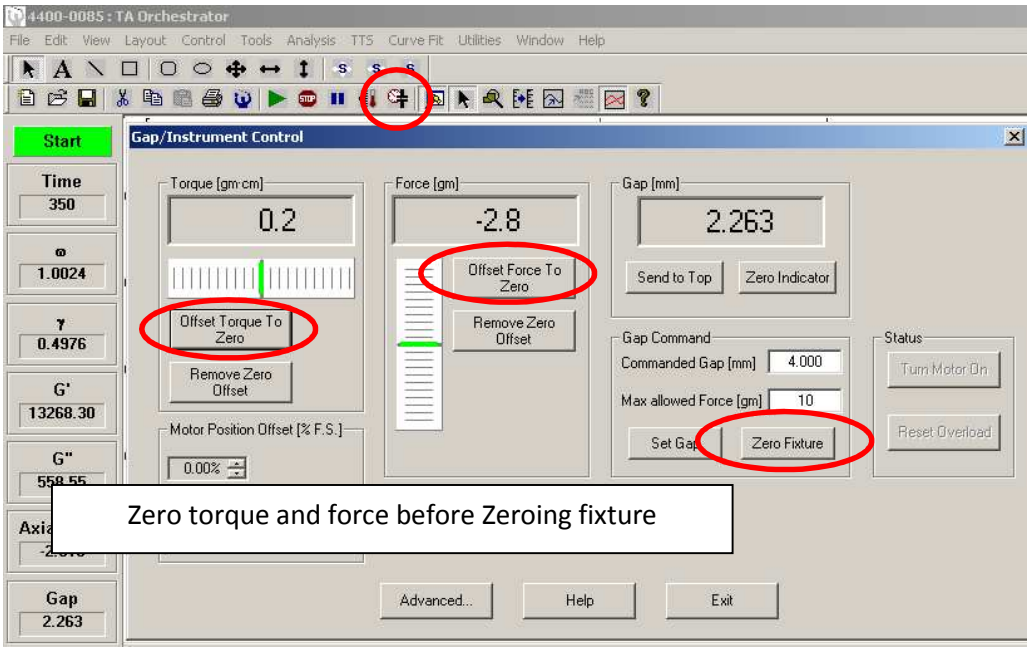

Figure 6.18: Gap control for zeroing fixture.

6.4.6. Preparing Tests

Open Edit/Start Test from the Control Toolbar

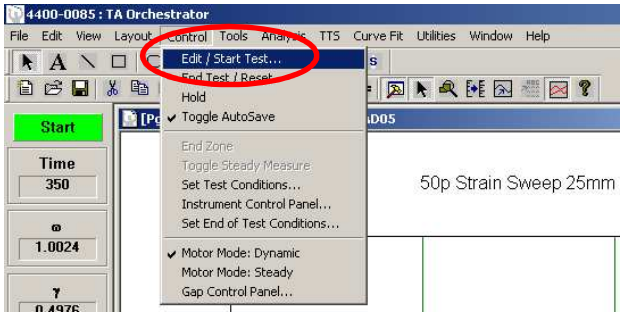

Figure 6.19: Edit test menu selection.

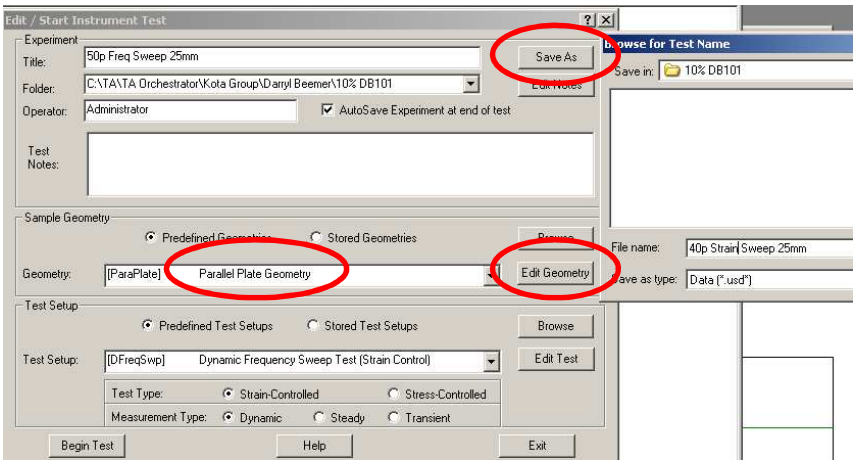

Figure 6.20: Frequency sweep setup and geometry control.

Save the test with the material, test, plate geometry, and test rev.

General file path is below. Make a folder with your name, and subfolders based on material.

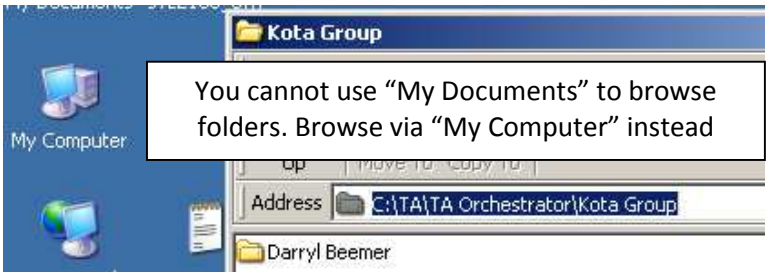

Figure 6.21: Note on file folder access.

Edit Parallel Plate Geometry, set the Diameter, and ensure “Read Test Fixture Gap” is checked

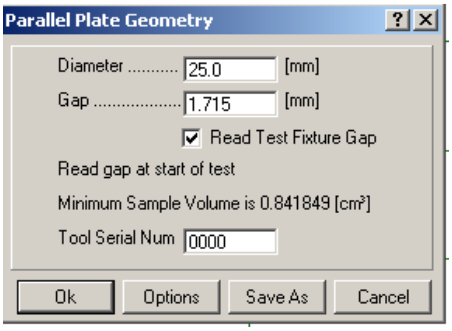

Figure 6.22: 25mm parallel plate settings.

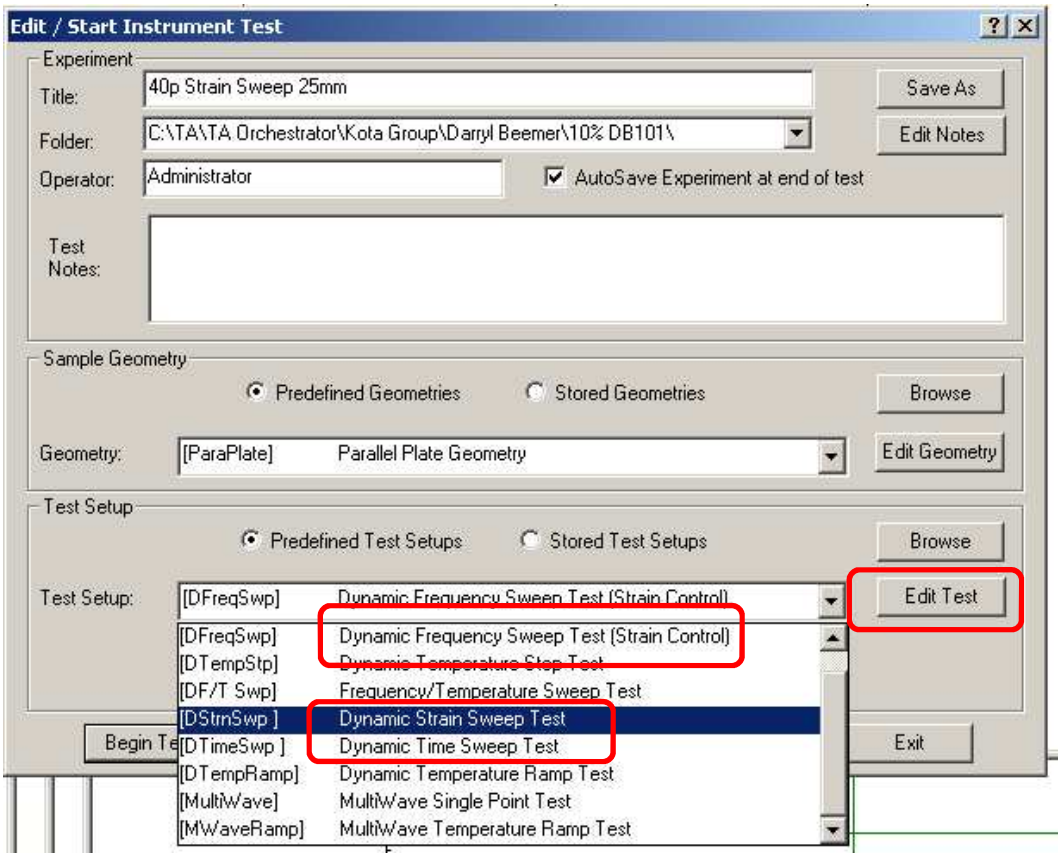

Figure 6.23: Test setup showing frequency and strain sweep options.

6.4.7. Dynamic Strain Sweep Setup

Setup accordingly. Be sure not to exceed 10% final strain for polymers, doing so will damage the sample. Use the Dynamic Strain Sweep to find the constant modulus point for testing.

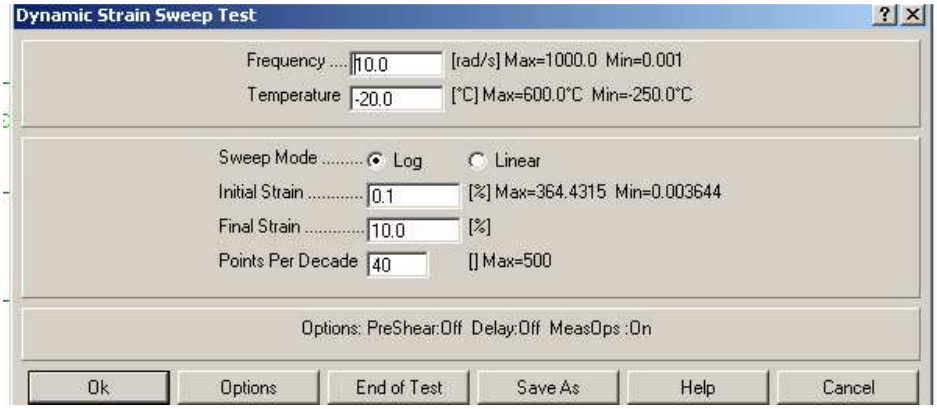

Figure 6.24:Strain sweep test parameters.

Make sure the oven is not contacting the plates, the sample is loaded, temperature is as desired, the test is setup correctly, etc.

Load the sample to ensure that the plates are in good contact with the material, with a 3%-5% strain offset from when the plates first contact the material. This is an important step, and the load should be between 10-30 Newton.

Start the test. Note that there is a 10 second delay before readings are taken.

6.4.8. Modifying plots

Double click on the graph to bring up the Plot Layout window, where you can change axes, adjust lines, symbols, layout, etc. It is useful to change the graph from symbols to lines using the Color/Symbols/Lines tab.

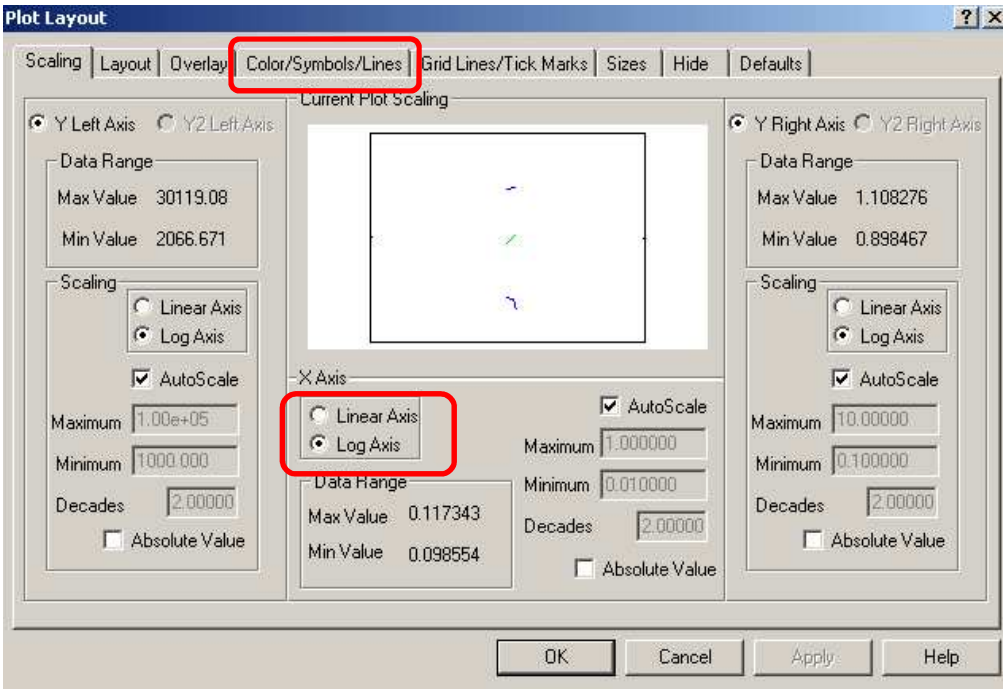

Figure 6.25: Modifying the plot view in TA Orchestrator.

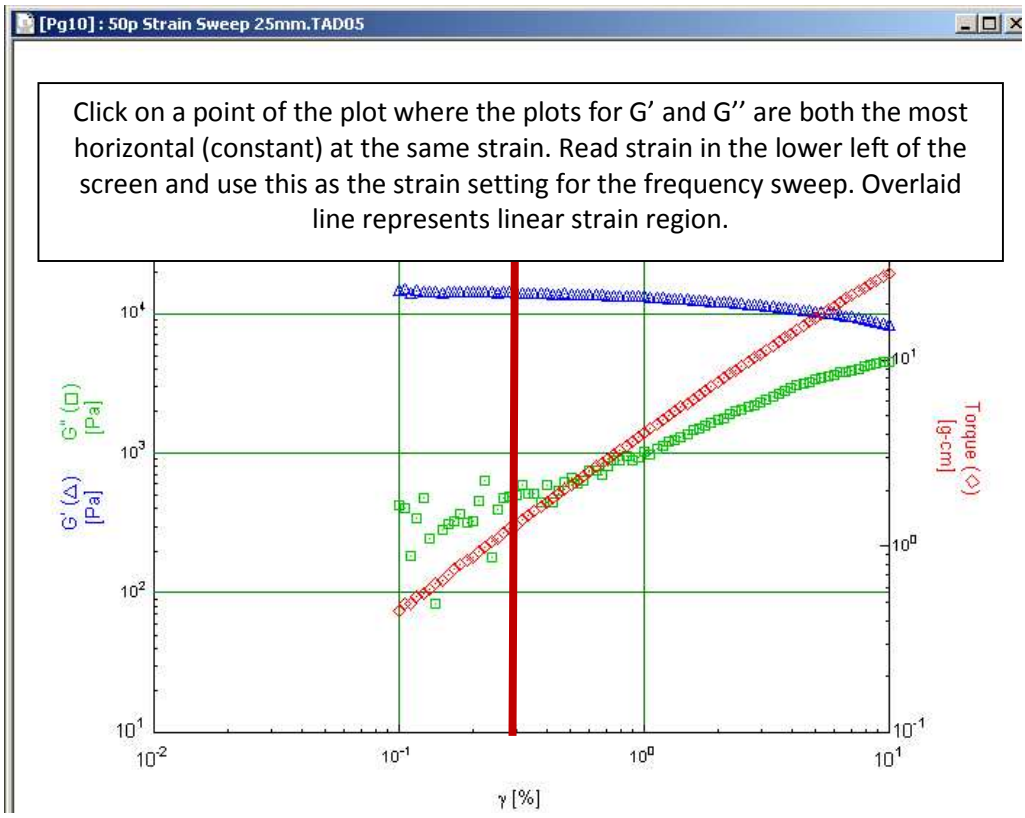

Figure 6.26: Strain sweep example plot.

Save the data, and export the data to a text file. Same folder, same name.

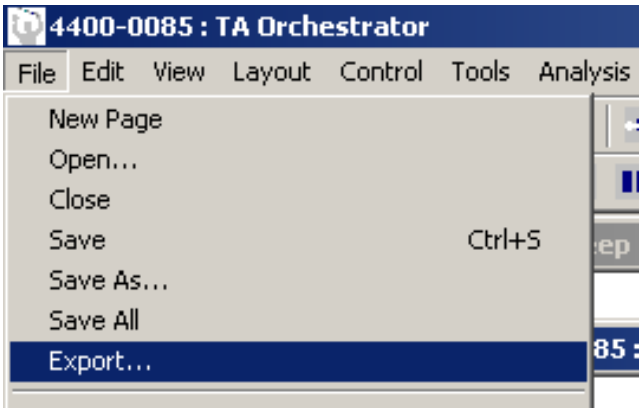

Figure 6.27: File export for saving .txt file.

6.4.9. Frequency Sweep Setup

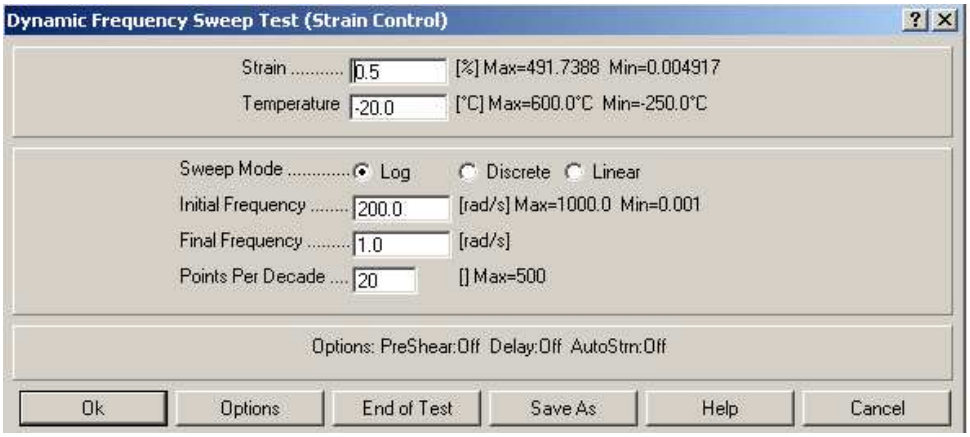

Figure 6.28: Frequency sweep settings (set strain from dynamic strain sweep results).

Run the frequency sweep test, save, export as text.

Copy all of the text files to a USB drive.

Turn the oven and motors off, close the liquid nitrogen valve, remove the sample, take the plates off and put them back into the cases and cabinet. Clean everything up nicely, and put stuff back where it came from. Close out of test windows in the software. Take the key with you when you leave so as to not be locked out.

Process/email data.

6.4.10. Rheometer Cup Fabrication

Use aluminum, 6061 for fabrication. Drawings and image below:

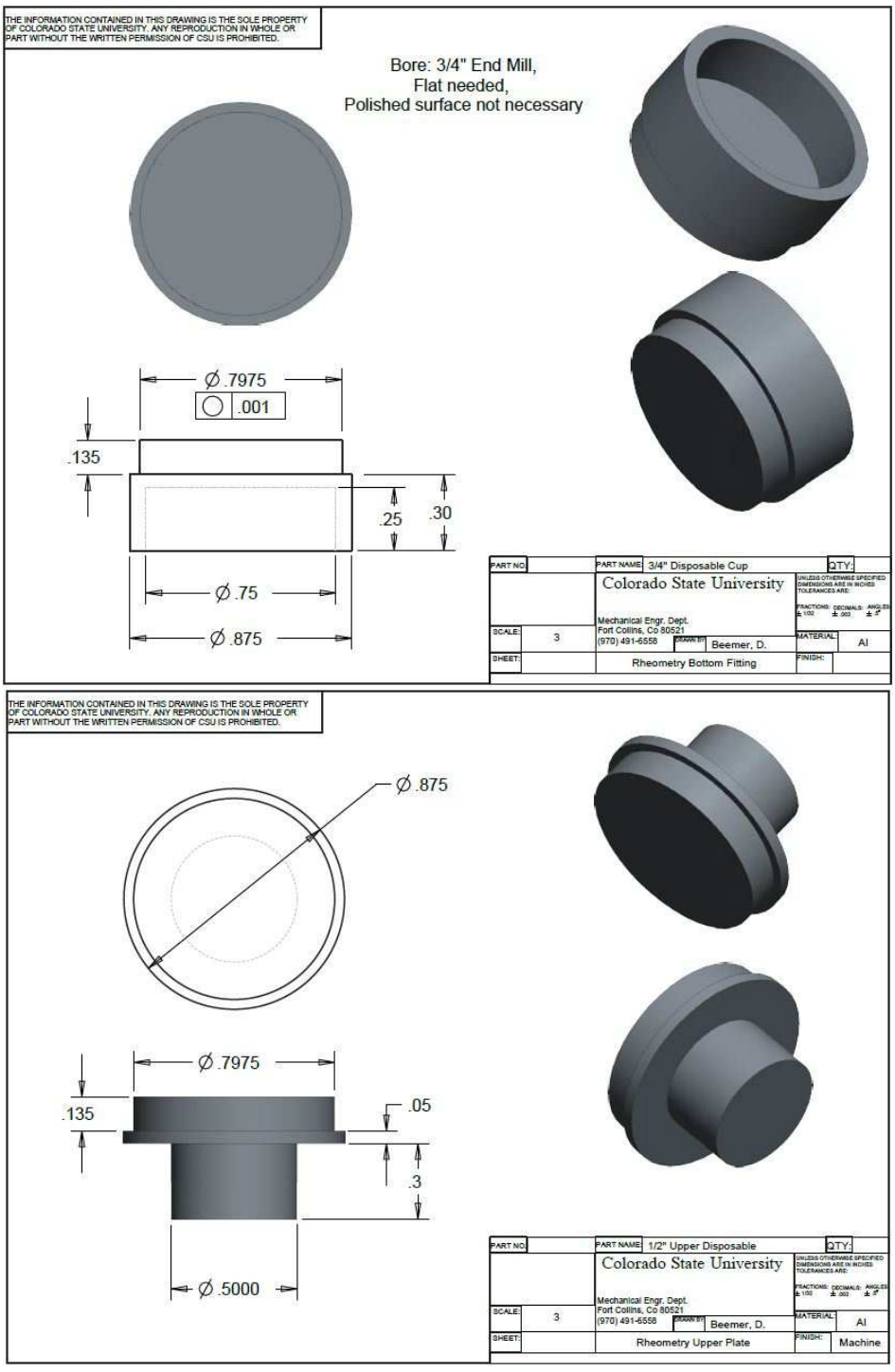

Figure 6.29: Top and bottom disposable cup fabrication drawings.

Figure 6.30: Fabricated disposable aluminum rheometer cups.

6.4.11. Freeze Plate Drawing

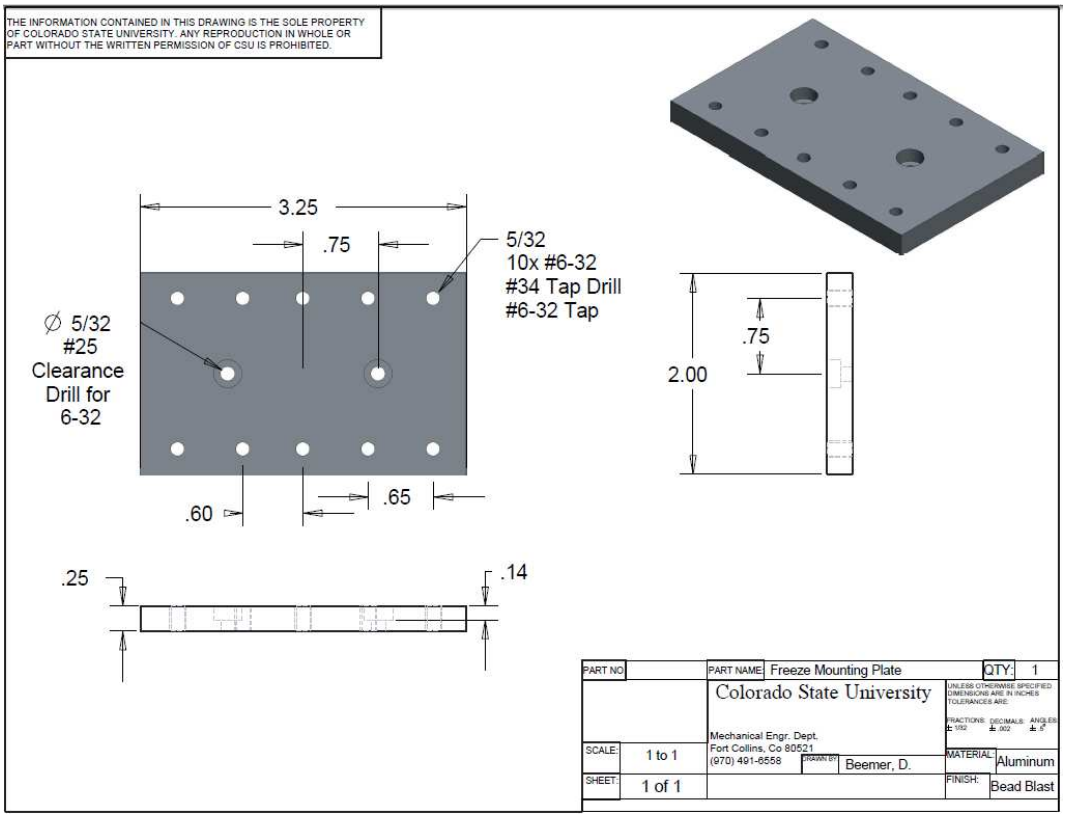

Figure 6.31: Peltier freeze mounting plate manufacturing drawing.

6.4.12. Spec Sheet for Peltier Plate

The Peltier plate is a TECA model AHP-150cp: http://www.thermoelectric.com/2010/pdf/ahp-300cp-ahp-150cp.pdf

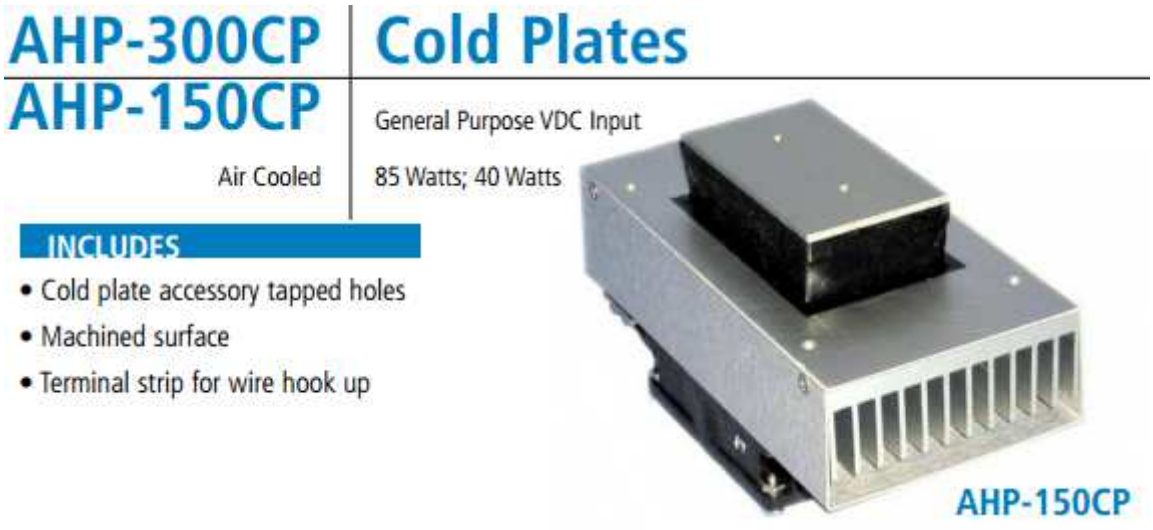

Figure 6.32: Peltier plate information from specifications sheet.

6.5. Linear Taber Procedure

6.5.1. Introduction

Linear Taber abrasion is meant to provide a controlled abrasion on a variety of surfaces. For de-ice surfaces, it is desired to measure ice adhesion strength before and after abrasion, so care must be taken to use non-sacrificial abrasives (waterproof sandpaper works well) and clamping needs to be done with care. Tests can be performed with the sample clamped to the stationary base or adhered to the moving arm with the abrasive on the base. The linear abrader translates circular motion into a linear actuation, with a loaded shaft allowing for vertical displacement. A variety of accessories are available for the equipment to control load and pressure, so consult the user manual for more operation information.

6.5.2. Setup

Mount the sample using the supplied mounting brackets. Place a flat piece of cloth under the sample to prevent material from dirtying the mounting plate. Using double sided tape, adhere adhesive

sandpaper onto the universal attachment and trim edges. Curl the edges sticking out up so that they do not cut the surface. Align the sample using the laser aligner, and make sure the abrasive head does not hit the clamps at the toggle points. Buehler CarbiMet 2 sandpaper is the ideal abrasive. Replace abrasive paper at least every 250 cycles, with more frequent replacement if the abrasive gets wet or contaminated.

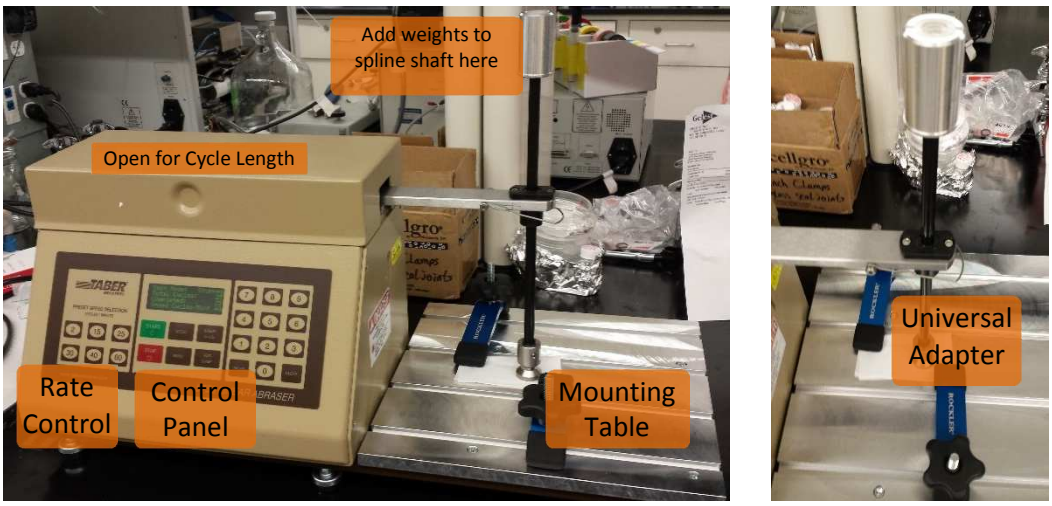

Figure 6.33: Taber linear abraser setup.

6.5.3. Procedure

For ice adhesion strength abrasion testing, use a stroke length of 1 inch and a speed of 25 cycles min^{-1}. 400/P800 grit sandpaper provides a moderate abrasion, while 180/P180 paper gives a heavier abrasion. Use a load of 350 grams. Test adhesion strength every 250 cycles, at least.

6.6. Optical Profilometer Procedure

6.6.1. General Setup

First, you have to be trained by a member of the Henry group, so default to their instructions for running the optical profilometer.

Turn on the air (just open the valve), log into the computer, record the start time in the user log, open the software and initialize the equipment. It will automatically

Figure 6.34: Henry lab door.

home, which takes a few minutes. Tape a piece of paper to the bed so that no material can contaminate the bed. Cut a sharp step in the material for thickness testing with a razor blade, and clean the bottoms of samples so that they sit flat.

Bring the z-axis close to the surface so that the laser dot is in the center of the viewing screen. Switch to the 20- lens and turn on the field-stop to help find the fringes. Once you have found the surface and are in the location of interest, gauge the thickness by finding the fringes on the glass and the top of the material.

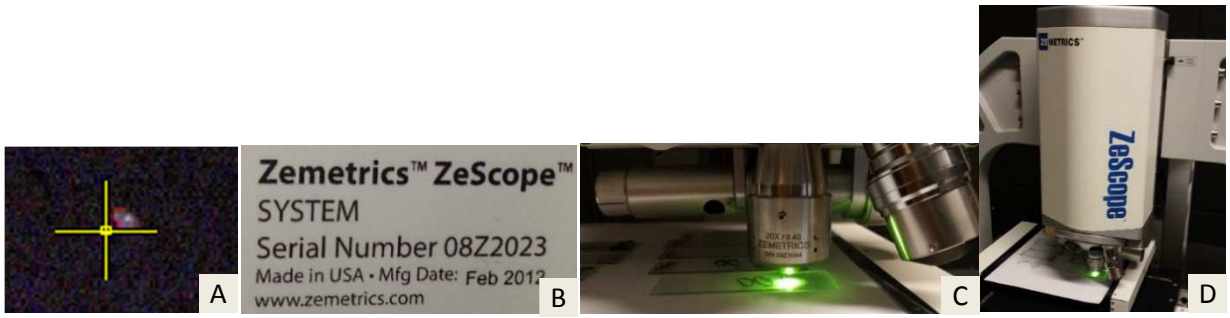

Figure 6.35: A) Laser dot aligning with crosshairs, B) profilometer equipment tag, C) profilometer in action, D) vertical column of profilometer with lens in action.

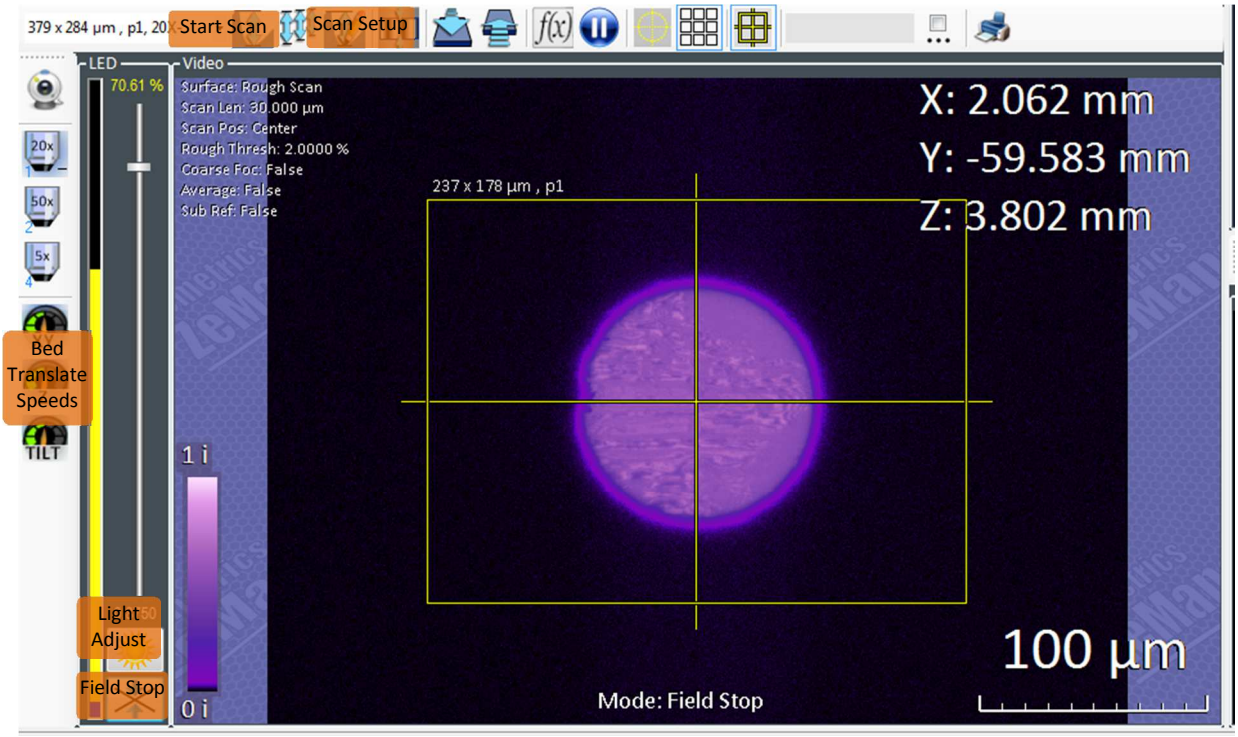

Figure 6.36: Video screen with field stop in use for initial focusing of fringes.

6.6.2. Thickness

For thickness measurements, setup a rough scan and a stitch large enough to measure the surface as well as the substrate. Exceed the estimated thickness by ~50-100 µm to ensure that you see both extremes of fringes. Once the scan is complete, be sure to use the "Remove Tilt" tool to remove any tilts of the substrate or the coating. Then, use the "Area Difference" tool to find the thickness (dZ). Measure at least 3 spots on different parts of the surface. It is usually easiest to do a top or bottom scan for thickness measurements.

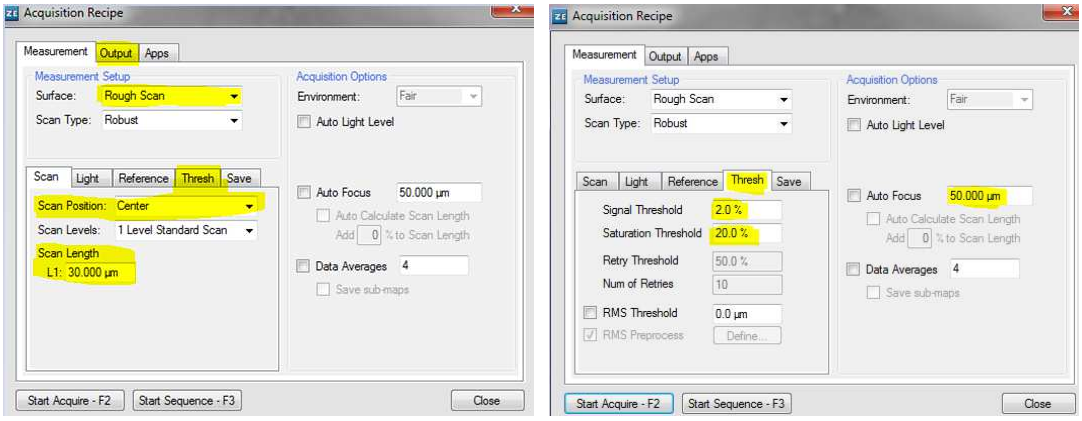

Figure 6.37: Scan acquisition setup with options highlighted.

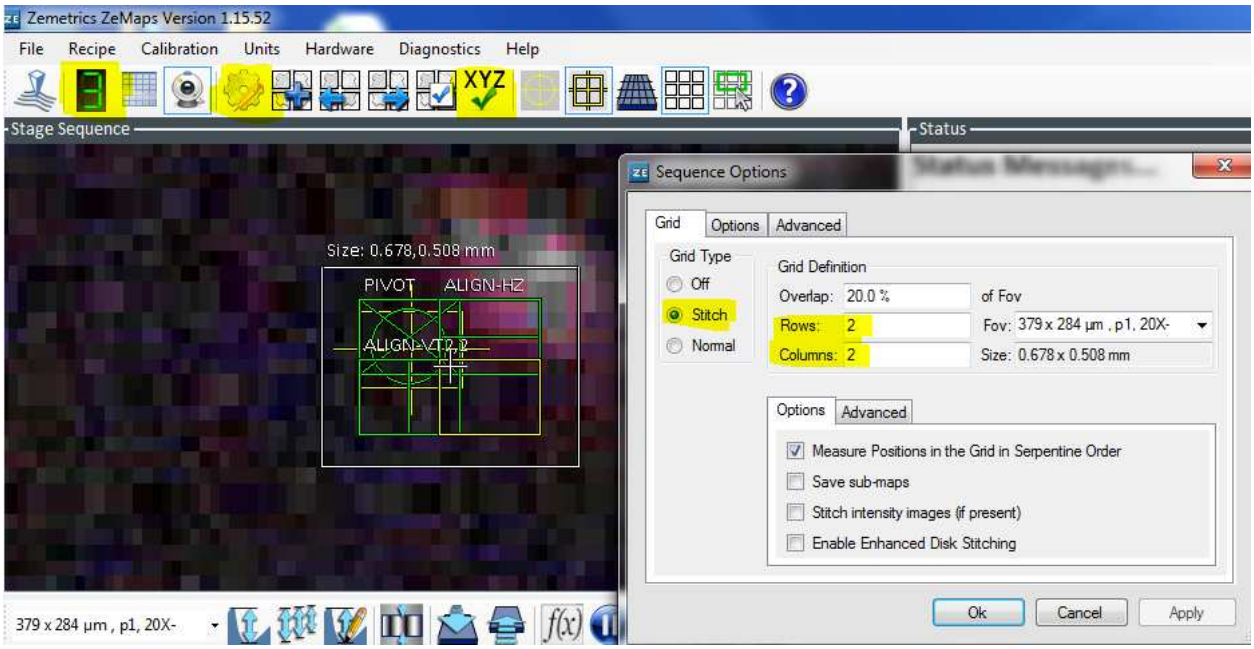

Figure 6.38: Stitch setup options, with position zeroing highlighted.

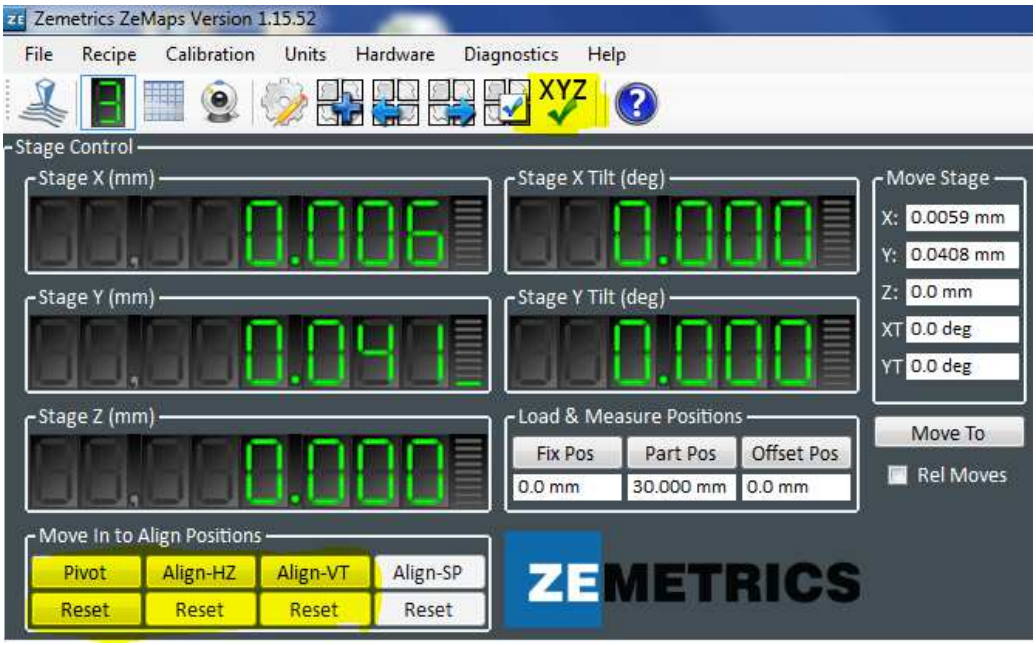

Figure 6.39: Stitch position control menu.

6.6.3. Roughness

Roughness measurements are performed similarly to the thickness measurements, except a fine, middle scan is used. Set the scan as a middle scan in the rough scan settings, then switch to fine scan. Use a signal threshold of 2.5% and a saturation threshold of 10%.

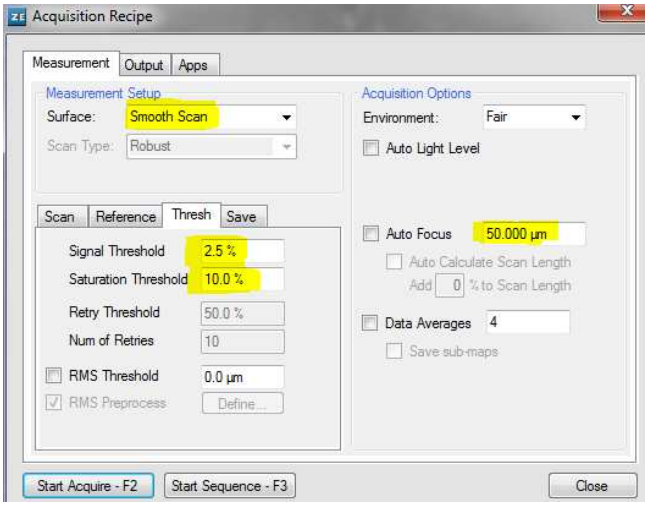

Figure 6.40: Smooth scan acquisition menu.

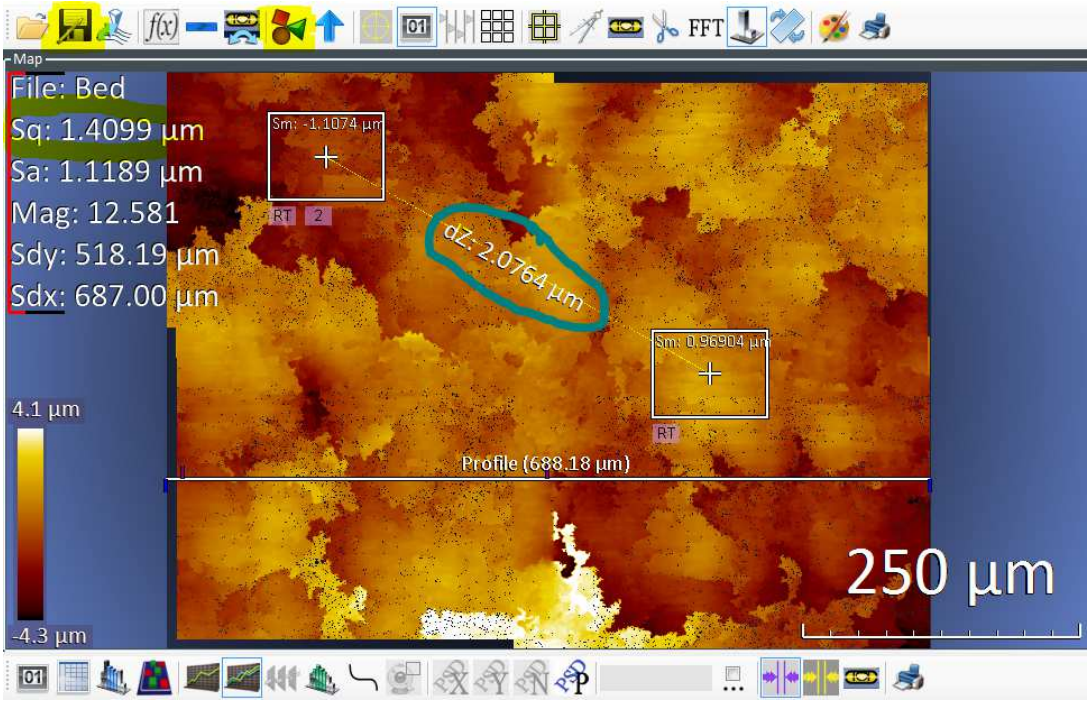

Figure 6.41: Roughness results showing RMS roughness (Sq) and area height difference (dZ).

6.7. Materials Database (PDMS, Silicone Oils)

Below is a summary of the PDMS materials in the lab. Mixtures of different bases and oils can be used to make silicones with varying properties. When adding oils, keep in mind that the base: cross-linker ratio is based on the amount of base before hardener is added. This value is usually 10:1, unless otherwise noted (some mixtures are 1:1). If the base already has plasticizer in it from the manufacturer

the cross-linker also has an equivalent of plasticizer, so still use a 10:1 ratio. B100, B200, and B300 mixed with oils are the most common materials for controlled modulus variation.

Table 6.2: PDMS material database.

PDMS Materials								
Source	Material	Ratio	MW Vinyl	MW Hydride	Q-Resin	Silica	Plasticizer	Type
	Internal ID	Base: CL	kDa	kDa	%	%	%	
Dow Corning	Sylgard 184	10:1	NG	NG	NG	NG	NG	Elastomer
Si Inc.	P-4	10:1	65	1.3	25%	0	0	Elastomer
Si Inc.	XP-573	10:1	71	1.3	0	27	39%	Elastomer
Si Inc.	XP-537	10:1	71	1.3	0	25	30%	Elastomer
Si Inc.	P-157	10:1	30	1.3	0	0	33%	Elastomer
Si Inc.	XP-634	10:1	95	1.3	25%	0	0	Elastomer
Si Inc.	XP-565	10:1	95	1.3	20%	0	28%	Elastomer
Si Inc.	XP-536	10:1	95	1.3	18%	0	28%	Elastomer
Si Inc.	B100	10:1	30	1.3	0	0	0	Elastomer
Si Inc.	B101	10:1	30	1.3	0	0	60%	Elastomer
Si Inc.	B102	10:1	30	1.3	0	0	50%	Elastomer
Si Inc.	B103	10:1	30	1.3	0	0	40%	Elastomer
Si Inc.	B104	10:1	30	1.3	0	0	10%	Elastomer
Si Inc.	B200	10:1	65	1.3	0	0	0	Elastomer
Si Inc.	B201	10:1	65	1.3	0	0	60%	Elastomer
Si Inc.	B204	10:1	65	1.3	0	0	10%	Elastomer
Si Inc.	B300	10:1	95	1.3	0	0	0	Elastomer
Si Inc.	B301	10:1	95	1.3	0	0	60%	Elastomer
Si Inc.	B304	10:1	95	1.3	0	0	10%	Elastomer
Si Inc.	B308	10:1	95	1.3	0	0	80%	Elastomer
Si Inc.	XP-729	1:1	85	0.475	25%	0	0	Sticky Elastomer
Si Inc.	XP-656	1:1	30	1.3	0	21%	48%	Elastomer
Si Inc.	XP-429	1:1	93	0.33	0	<1%	65%	Gooey Gel
Si Inc.	XP-429 5%	1:1	93	0.33	0	5	65%	Gel
Si Inc.	XP-429 10%	1:1	93	0.33	0	10	65%	Gel
Si Inc.	XP-429 15%	1:1	93	0.33	0	15	65%	Gel
Si Inc.	XP-429 20%	1:1	93	0.33	0	20%	65%	Gel

Table 6.3: Silicone fluids database.

Silicone Fluids (Plasticizer Oils)						
Source	Material	Viscosity	MW Oil	Surface Tension	Specific Gravity	Flashpoint
Company	ID	cSt.	Da	mN/m		°C
Gelest	DMS-T00	0.65	162	15.9	0.761	-1
Gelest	DMS-T03	3	550	19.2	0.898	100
Gelest	DMS-T12	20	2000	20.6	0.95	232
Gelest	DMS-T31	1000	28000	21.2	0.971	315
Silicones Inc.	34900	20	3500	20	0.95	232

6.8. Spin Speed vs. Thickness

The spin-coating thickness of materials is viscosity-dependent, and variable with cure time, molecular weight, and amount of plasticizer used. Below are thickness-spin speed curves for a few materials developed.

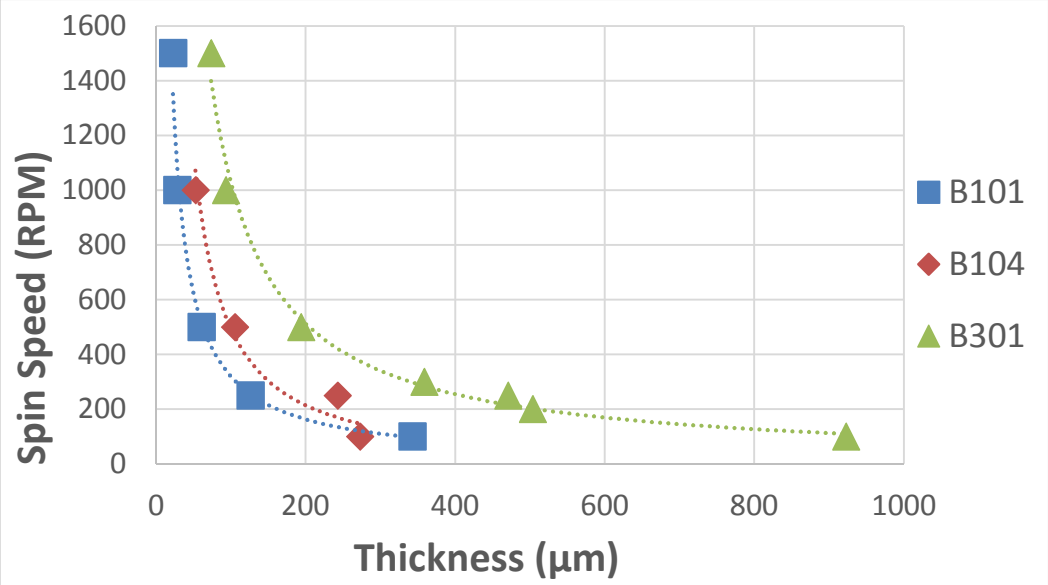

Figure 6.42: Spin speed chart for varying base materials.

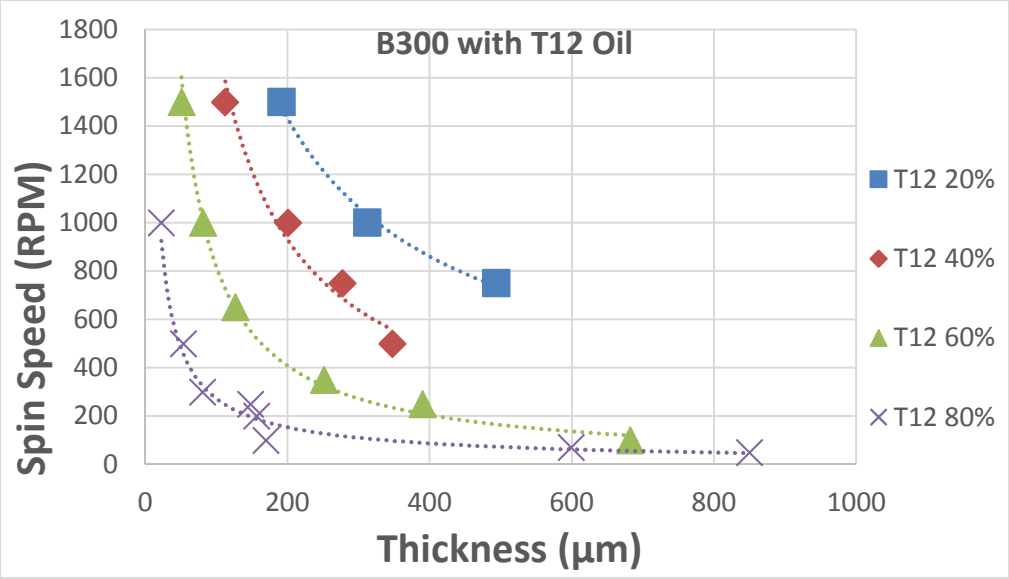

Figure 6.43: Spin speed chart for B300 base with varying amounts of DMS T12 oil.

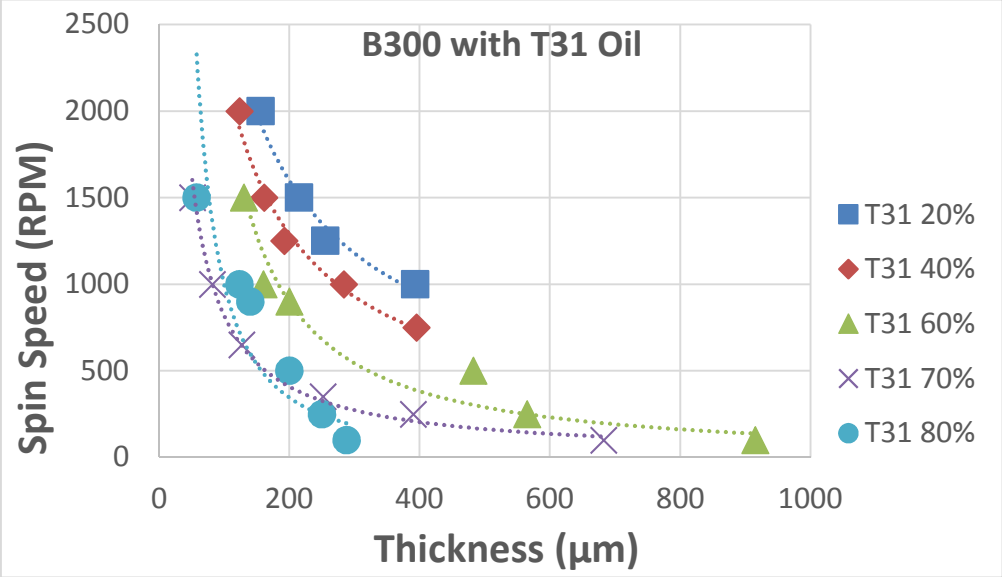

Figure 6.44: Spin speed chart for B300 base with varying amounts of DMS T31 oil.

7. APPENDIX B- ACID ETCHING SUPPLEMENTARY

7.1. HF Etching Procedure

7.1.1. Introduction

Hydrofluoric acid is a deadly chemical when even a moderate amount is spilled as it can cause corrosive burns and the fluoride ions can penetrate through the skin and form insoluble salts, breaking down calcium and destroying tissue. It can essentially kill from the inside-out. Thus, safety is very important for working with HF. Consult another training manual, such as the CSU EHS training, and do not just look at this procedure. Here is a useful site from the University of Tennessee, Knoxville: HF Safety. All etching with HF must be done in the Popat Lab's HF hood. NEVER PUT HF IN GLASS BOTTLES. It will dissolve the silica and spill. Plastics (LDPE, HDPE, PTFE, PP, among others) are the only HF-resistant materials.

7.1.2. Setup

Fully clean samples after surface treatments (such as bead blasting) and before HF etching for uniform etching. If etching at high temperature, get the hot plate turned on so that it has time to get to temperature.

Figure 7.1: HF etching equipment with hot plate in fume hood and PTFE beakers on hot plate.

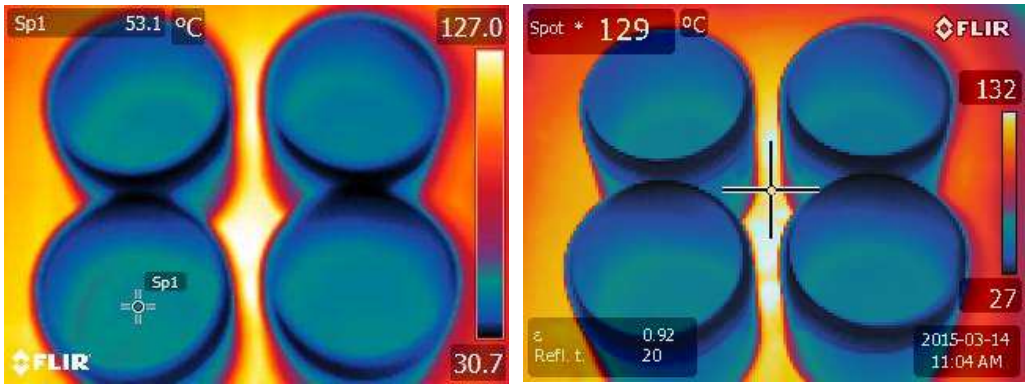

Figure 7.2: FLIR images showing hot plate temperature vs. fluid temperature.

Equipment: Hot plate (in hood), HF tongs (Teflon), Teflon beaker(s), HF acid, HF disposal bottle, DI squirt bottle, sink, thick rubber gloves, basic lab gloves, safety glasses, lab coat, face shield, funnel, timer, thermometer (if needed).

Get everything laid out nicely, with DI water, an extra Teflon beaker, tongs, waste disposal bottle, PPE, and samples ready in the fume hood before bringing the HF out.

7.1.3. Procedure

Place samples on the bottom of Teflon beaker(s). Fill with enough HF to completely cover the samples. Return the HF bottle to the acids cabinet and start the timer.

Figure 7.3: HF acid cabinet below fume hood.

Watch etching progress, noting color changes during reaction and bubbling. These are signals of etching progress. Often, when steels turn a darker shade of green quality etching has occurred. As you get to

the end of the etching process, prepare the waste disposal bottle with the funnel in it, turn on the nitrogen air, and get the DI water ready.

Remove the sample with tongs and thoroughly wash the surface. You can wash into the etching beaker so as to dilute it and help stop the etching process. Readjust the sample in the tongs and wash the sample thoroughly at least three times. Use the nitrogen to evenly dry the sample of all of the DI water. Place sample on a piece of cardboard and clean the other samples.

Dispose of HF, and triple wash all of the equipment in the fume hood, disposing of waste as you go.

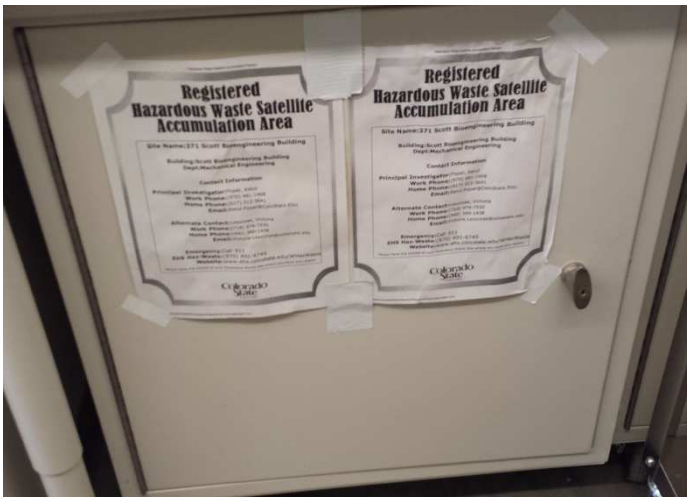

Figure 7.4: HF hazardous waste cabinet.

Wash gloves and equipment in the sink using detergent soap, return to storage cabinet.

Do a final wash of etched surfaces with acetone, ethanol, and DI water before continuing to subsequent steps.

7.1.4. Silanization of Stainless Steel

Expose the surfaces to oxygen plasma for 15 minutes to ensure that the surface has adequate hydroxyl groups for silanization. Meanwhile, turn a hot plate on at 125 ^{o}C. Cut a small piece of glass large enough to hold the amount of silane needed. Prepare the pipette and tips, and get the silane with Parafilm so that it can be re-sealed immediately after use. After oxygen plasma is completed, place the samples on the hot plate, with a glass slide propping one end of the samples up so that the entire

surface gets silanized. Pipette 100 µL of silane per square inch of metal surface onto the cut glass slide and immediately place a glass bowl over everything to isolate the silanization environment from the ambient.

Flow nitrogen into the silane bottle to prevent it from being ruined by ambient humidity. Cap the bottle and use Parafilm to seal the bottle. Be sure to stretch the Parafilm over the cap for a good seal.

Figure 7.5: Hot plate silanization setup.

Allow for 1hr of silanization, then remove the samples with tongs (they will be hot) and do a quick rinse with DI water (5 seconds) then place it back on the hot plate to dry for 5 minutes. Dispose of the silane-holding slide. Finish by washing surfaces with acetone, ethanol, and DI water.

7.2. $FeCl_3$ Etching Procedure

7.2.1. Introduction

Iron chloride is used for etching a variety of metals, particularly soft metals like copper. Etching is dependent on time, temperature, and concentration, so all of these parameters must be varied for finding the optimal etching conditions. Iron chloride will "pit" steels at medium to high concentrations, creating holes periodically across the surface that can grow and even extend through the material. Thus, lower concentration etching for longer time is usually ideal for this etchant.

Aqueous iron chloride acidic solution is produced by dissolving iron chloride crystals into water. This is an exothermic reaction, so add enough water to the solution to absorb the heat of reaction. Weighing boats can also be used to measure out the crystal so that it can be added to the water. This is the preferred method for higher concentration mixtures as the heat can be more easily controlled.

Iron chloride will etch steel tools, so designate certain tools to only be used for this process. Glass is resistant to the etching, so glass beakers are best for mixing.

7.2.2. Setup

Materials: $FeCl_3$ crystals, balance, weighing boat, beakers (1 for mixing, 1 for measuring water), magnetic stir bar and stir plate, metal spatula, DI water, cleaning towels, proper PPE.

Plan out the desired molarity and volume of mixture ahead of time, using the molar mass of 162 mg/mole for $FeCl_3$. Use the following equations to determine the mass of crystals and volume of water and molarity. Usually, the volume of solution will be set to 200 mL and molarity will be known, allowing for calculation of the mass of crystals needed:

$$\text{Moles}_{\text{solute}} = \frac{\text{Molarity}}{\text{Volume}_{\text{solution}}} \qquad \text{Mass}_{\text{solute}} = \frac{\text{Moles}_{\text{solute}}}{\text{W}_{\text{solute}}}$$

Figure 7.6: Molarity equations.

Get all tools and equipment ready, with aluminum foil covering the balance and the stirring hot plate to protect the surfaces from any spills.

7.2.3. Procedure

1) Measure out desired amount of liquid into a beaker. Do not fill the beaker more than half full.
2) Weigh out desired amount of $FeCl_3$ crystal. Minimize time that the jar is open and flood the jar with nitrogen before sealing. Use the dark crystals, not any oxidized crystals that turn brighter yellow.
3) Slowly add crystals to the water, then add magnetic stir bar and allow the salt to full dissolve before removing the spin bar.

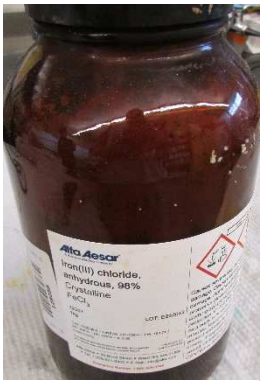

Figure 7.7: $FeCl_3$ jar.

4) If etching at temperature, turn the hot plate on and allow the etchant to reach the desired temperature before adding cleaned samples into the solution.
5) Add samples, observing changes in color during etching process.

6) Clean all tools and equipment thoroughly, disposing of acidic waste. Throw away any solids (contaminated gloves, wipes, etc.).
7) Remove samples after etching and initially clean with water, followed by acetone, ethanol, and water again.
8) Dispose of used etchant and completely clean glassware. It can be difficult to impossible to clean stains off of glassware, so use soap and elbow grease.
9) Make fresh solution every time, as the ions in the solution will degrade with time, reducing etching effectiveness.

7.3. Metal Preparation (shearing, bead blasting)

7.3.1. Introduction

Easy use of metal surfaces starts with quality initial processing of surfaces. Having properly sized samples large enough for analysis without edge effects but small enough to fit multiple surfaces in etching beakers and on hot plates will reduce chemical waste. Removing burs and sharp edges is necessary for safety and for easier analysis of contact angles. Relieving surface residual stresses from cold-working is often necessary for homogenous etching and abrasive blasting will also make a uniform surface. Metal preparation in the machine shop can be performed relatively quickly and easily if the proper tools are used for the proper materials and with the right work flow. You must talk to "Doc" Schaeffer to get access to the EMEC, and abide by all lab rules and training protocol. This is solely supplementary to the EMEC handbook, and certainly not a replacement for its information. This procedure will take you through cutting samples to size and abrasive blasting the samples to relieve stresses and produce a homogenous surface.

7.3.2. Setup

Materials/Equipment: Metal stock (usually in long thin sheets), shop rags, Pexto/Roper Whitney Model 137 L sheet metal stomp shear, sheet metal bender, bead blast cabinet, horizontal band saw.

7.3.3. Procedure

1) Prepare stomp shear. I find it useful to use the interior of the shear as the blade is often sharper here due to less use. Create a guide surface by bending a scrap piece of metal and wedging it into one of the slots in the bed. Bring this guide surface close to the yellow material clamp, with the guide face positioned so that the metal clamp will hold the sample during cutting.
2) Cut medium length pieces small enough to fit into the bead blaster. (Skip to cutting to the final size if you will not be bead blasting surfaces. Use a shop rag to protect surfaces from the biting of the metal clamp.
3) The horizontal band saw must be used for mild steel and softer metal thicker than 16 gauge (0.057”), with a maximum thickness of 21-22 gauge (0.035”) for stainless steels.
4) Bead blast surfaces from a distance of 1 inch, with a pressure of 70 psi and adequate time to consistently bead blast the entire surface. Clean surfaces of all grease before bead blasting to prevent ruining of the abrasive media.

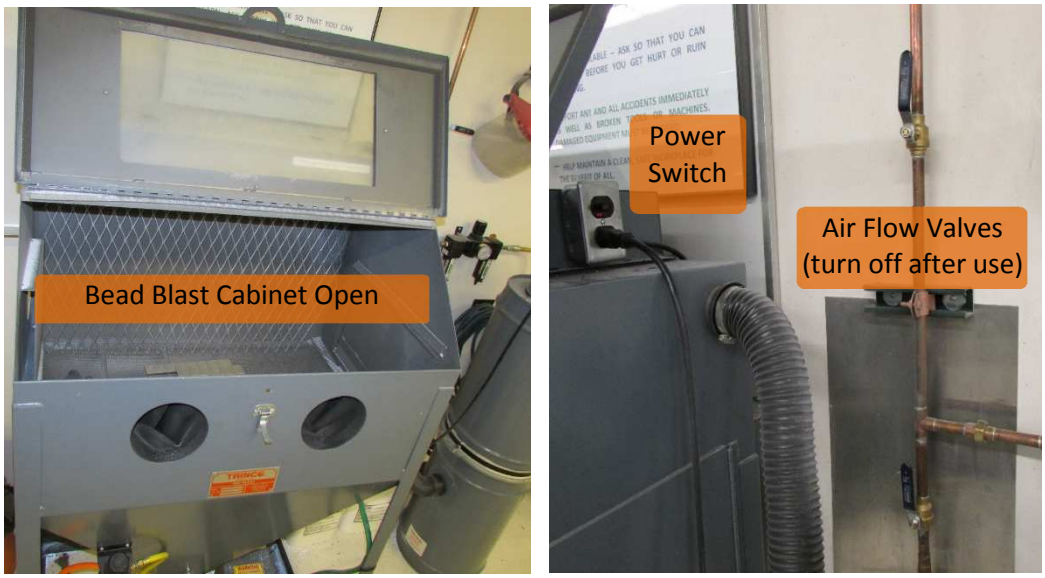

Figure 7.8: Bead blast cabinet overview.

Figure 7.9: Pressure and flow control for bead blasting. Pull and rotate regulator dial to set pressure.

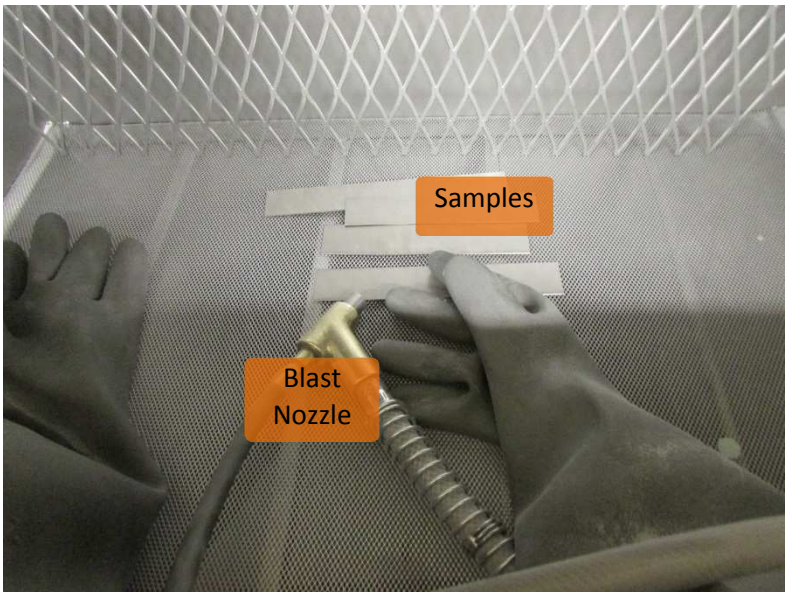

Figure 7.10: Interior of bead blast cabinet showing equipment, samples, and blast gun.

5) Finish cutting metal to the desired size on the stomp shear. Usually 1 in^2 is the largest size that will be used. It is often helpful to keep the sizes of different metal types different and consistent to help with distinguishing metals. Notches can also be marked into metals (like pig ear notch marks) to distinguish metal grades after etching (which would remove non-mechanical markers). Cutting can be done after abrasive blasting if the blasted side is protected from any clamping faces.

   I. Use the stop behind the blade to set a consistent size, allowing for quick shearing.

7.3.4. Notes

The horizontal band-saw takes a long time to use as surfaces need to be de-burred after cutting with this equipment, so acquire metals thin enough to allow for cutting on the sheet metal break. This will save hours of work.

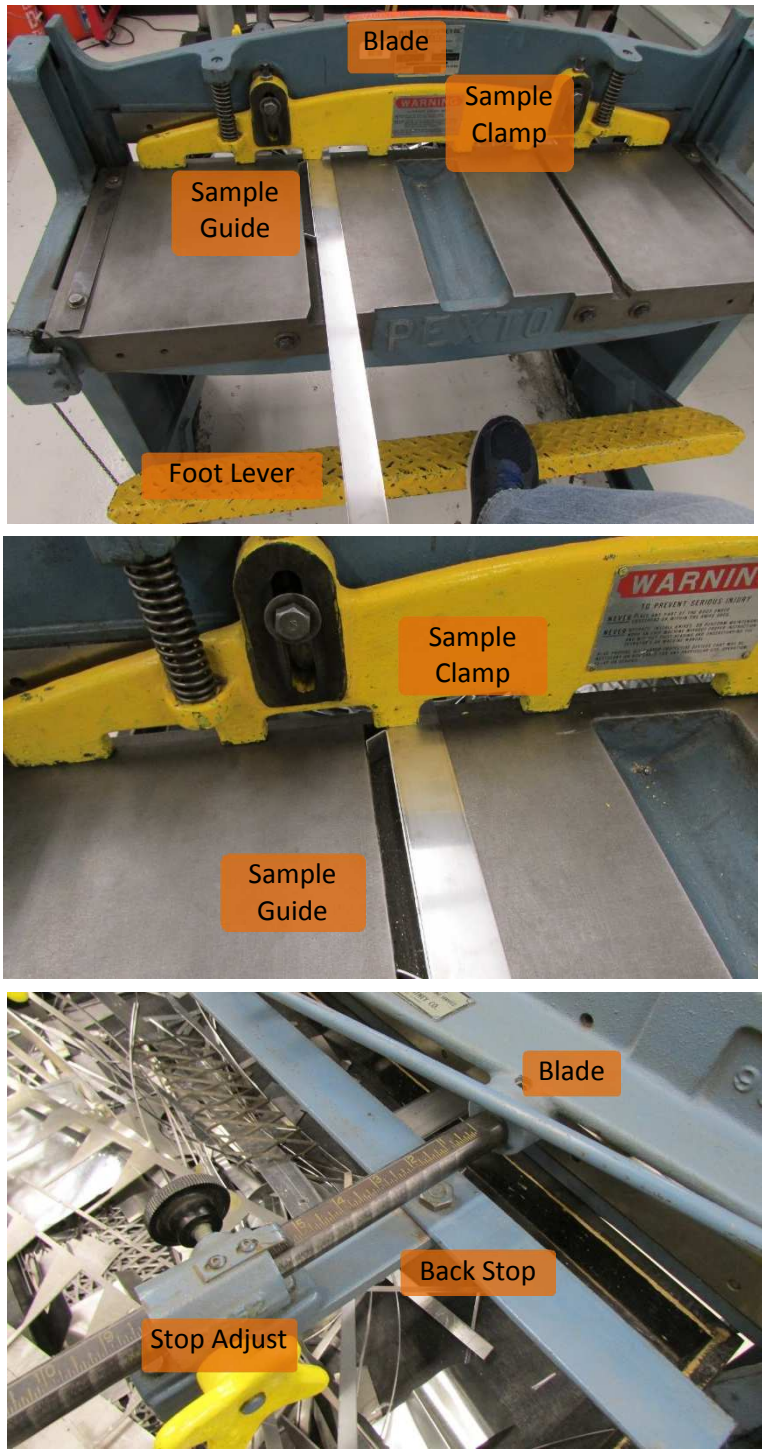

Figure 7.11: Stomp shear components.

7.4. Metals Database

Metals are easiest to cut with the metal break, so thickness needs to be less than the capacity of the equipment. Additionally, 1 inch wide strips are best for early testing as they can be processed easier than large square sheets. Following is a table of metals of the optimal thickness for processing, with a few different sizing options for early testing and for eventual scaling-up. Certification is available for some metals at about twice the cost, so see the company site for more information on costs and benefits.

Table 7.1: Thin, shearable metals database.

Metal	Type	Vendor	Part #	Thickness		Width	Length	Cost	Cost/in^2
				Inches	Gauge	inch	inch	$	$
SS	304	McMaster	1421T61	0.03	22	1	36	$ 6.81	$ 0.19
SS	304	McMaster	1421T63	0.03	22	4	36	$ 20.01	$ 0.14
SS	304	McMaster	1421T64	0.03	22	6	36	$ 25.23	$ 0.12
SS	316	McMaster	9090K55	0.03	22	1	24	$ 7.68	$ 0.32
SS	316	McMaster	9090K85	0.03	22	4	24	$ 25.04	$ 0.26
SS	316	McMaster	9090K45	0.03	22	6	24	$ 32.82	$ 0.23
SS	430	McMaster	8457K49	0.025	24	1	12	$ 1.77	$ 0.15
SS	430	McMaster	8457K13	0.025	24	6	12	$ 9.09	$ 0.13
SS	430	McMaster	1294T24	0.035	21	6	12	$ 10.49	$ 0.15
Al	* 6061	McMaster	89015K161	0.04	18	2	24	$ 5.76	$ 0.12
Al	* 6061	McMaster	89015K45	0.04	18	2	48	$ 10.22	$ 0.11
Al	* 6061	McMaster	89015K162	0.04	18	4	24	$ 10.08	$ 0.11
Al	* 7075	McMaster	8885K811	0.032	20	6	6	$ 4.95	$ 0.14
Al	* 7075	McMaster	8885K813	0.032	20	6	24	$ 16.67	$ 0.12
Al	* 7075	McMaster	8885K814	0.032	20	8	8	$ 8.25	$ 0.13
Ti	*Grade 5	McMaster	9039K15	0.032	21	6	6	$ 74.66	$ 2.07
Ti	*Grade 5	McMaster	9039K16	0.032	21	12	12	$ 195.16	$ 1.36
Ti	*Grade 5	McMaster	9039K29	0.032	21	24	24	$ 683.05	$ 1.19
* Can get with certification of traceable lot number and material test report (see site)									

7.5. Cost Analysis

7.5.1. Introduction

Cost for production of etched surfaces (not including the metal) was evaluated for the optimal etching recipes and based on lab-scale processes and chemical costs. This analysis was used as a baseline for comparison to other coating options and for initial scaling considerations, in addition to an internal knowledge of the costs for each surface produced in the lab.

Chemical		HF	DI Wash	Acetone Wash		Silane
Price		2041	1	20		1000
Volume (L)		16	4	4		0.6
Density (kg/L)		1.15	1.00	0.79		0.83
Weight (kg)	Total	18.40	4.00	3.14		0.5
$/kg		110.92	0.25	6.36		2000.00
$/gram		0.11	0.00	0.01		2.00
$/L		127.56	0.25	5.00		1666.67
$/mL		0.13	0.00	0.01		1.67
Weight Used (g)	**0.00**					
Volume Used (mL)	**36.55**	6.45	20.00	10.00		0.10
Part Cost ($/unit)	**$ 1.04**	$ 0.82	$ 0.01	$ 0.05	$ -	$ 0.17
% Cost	**100%**	**79%**	**0%**	**5%**	**0%**	**16%**
Cost/mL Chemicals	**$ 0.03**	$ 0.02	$ 0.00	$ 0.00	$ -	$ 0.00
$/L Chemicals	***$ 28.58***	$ 22.51	$ 0.14	$ 1.37	$ -	$ 4.56
$/gal Chemicals	***$ 108.16***	Coverage (sq in)		Coverage (sq ft/gal)		Depth (cm)
Cost ($/sq ft)	***$ 3.13***	2		34.5		0.5
		cm^2 12.9				

Figure 7.12: Cost analysis for HF-etching process.

Chemical		HCl	DI Wash	Acetone Wash	Glycerin	Nitric Acid	Silane
Price		300	5	20	255	170	1000
Volume (L)		19	4	4	12	2.5	0.6
Density (kg/L)		1.18	1.00	0.79	1.26	1.26	0.83
Weight (kg)	Total	22.42	4.00	3.14	15.12	3.15	0.5
$/kg		13.38	1.25	6.36	16.87	53.97	2000.00
$/gram		0.01	0.00	0.01	0.02	0.05	2.00
$/L		15.79	1.25	5.00	21.25	68.00	1666.67
$/mL		0.02	0.00	0.01	0.02	0.07	1.67
Weight Used (g)	**0.00**						
Volume Used (mL)	**92.45**	12.90	40.00	20.00	12.90	6.45	0.20
Part Cost ($/unit)	**$ 1.40**	$ 0.20	$ 0.05	$ 0.10	$ 0.27	$ 0.44	$ 0.33
% Cost	**100%**	**15%**	**4%**	**7%**	**20%**	**31%**	**24%**
Cost/mL Chemicals	**$ 0.02**	$ 0.00	$ 0.00	$ 0.00	$ 0.00	$ 0.00	$ 0.00
$/L Chemicals	***$ 15.14***	$ 2.20	$ 0.54	$ 1.08	$ 2.97	$ 4.74	$ 3.61
$/gal Chemicals	***$ 57.31***	Coverage (sq in)		Coverage (sq ft/gal)		Depth (cm)	
Cost ($/sq ft)	***$ 2.10***	4		27.3		0.5	
		cm^2 25.8					

Figure 7.13: Cost analysis for glyceregia etching process.

8. APPENDIX C- DURABLE SPRAY-COATING SUPPLEMENTARY

8.1. Materials

Table 8.1: Spray-coat chemical/material information.

Chemical	Vendor	Item #	Volume L	Mass kg	Unit Cost $
Luxecolor FPU	Helicity Tech. Inc.	4FVBA-800	NA	4	$ 150.00
Silane	Gelest	SIH5841.0	NA	0.5	$ 1,000.00
Fumed Silica 7 nm	Sigma Aldrich	S5130-500G	NA	0.5	$ 69.50
Fumed Silica 200 nm	Sigma Aldrich	S5505-500G	NA	0.5	$ 57.90
n-Hexane 95%	Fisher Scientific	H306-SK4	4	NA	$ 274.02
Chloroform	Fisher Scientific	C295-4	4	NA	$ 409.30
Acetone	Fisher Scientific	A18-P4	4	NA	$ 206.33

8.2. Spray-Coating Procedure

8.2.1. Introduction

Spray-coating is a coating method that allows for full atomization of sprayed fluids (paints, coatings, liquids, etc.) to provide a smooth, even coat, or to control the texturing of a coating if texture is of interest. To control the flow rate and spray size, the fluid viscosity can be controlled with thinning solvents, air pressure can be adjusted, nozzle sizes and nozzle shapes can be changed. A commercial airbrush is described here, but there are multiple other spray-coating nozzles, such as atomizers and ultrasonic sprayers. This procedure will present a method for preparing materials for repellent mixed and layered surfaces and their subsequent spraying. Concentrations and recipes can all be varied, but general suggestions will be consistent. One comical example of a spray-coated surface that has received much internet publicity where walls in Hamburg, Germany were coated so they could pee back at passing inebriated urinators.[183]

8.2.2. Material Preparation

Equipment: 20 mL glass vials, hexane 95%, chloroform, centrifuge, shaker mixer, silica particles, spatula, balance, pipette, silane, fume hood, PPE.

1) Silica silanization- 3 days, 1 gram silica/ 1 mL of silane, dispersed in 25 mL hexane/ 1 gram silica
   I. Weigh silica into vials in fume hood, do not breathe silica particles.
   II. Add hexane to vial(s), use as little water (as pure of hexane) as possible.
   III. Add silane to vials, seal silane and seal vials.
   IV. Shake-mix for 3 days

Figure 8.1: 7 nm fumed silica bucket.

2) Particle dispersion in chloroform
   I. Measure out desired volume of “silica mix before centrifuge” into vial.
   II. Centrifuge particle mixture at 350g for 5 minutes (balance weights evenly), separate hexane and excess silane into separate vial and dispose.
   III. Fill vial ¾ full w/Chloroform, shake on vortex mixer, sonic mix 2 minutes, centrifuge, dispose of excess liquid.

IV. Add fresh chloroform to ¾ full, sonic mix 2 minutes, centrifuge again.

i) Recycle excess chloroform into next vial of particles for their first chloroform dispersion.

Figure 8.2: Centrifuge in operation at 350g, with 7 minutes remaining.

3) Coating preparation

I. Add solvents to the centrifuged particles per "% solids" and "final mg/mL Silica in Chloroform" ratio, mix well with vortex mixer.

II. Pour solvents and silica particles into spray jar

III. Add FPU to solvents and particles, mix well

i) 3064:236 Base: Hardener ratio (8.36 grams base = 0.64 grams of hardener)

IV. Mix well, spray at 20 psi or below

V. Working time is 15-20 minutes

Figure 8.3: FPU components (left) and silica particles on vortex mixer (right).

8.2.3. Spraying Procedure

1) Clean and prepare equipment (spray bottles, siphon lids, hose, acetone wash jars, air-brush, backdrop of newspaper and cardboard, sample substrates).
   I. Completely clean bottles and air-brush with acetone (and chloroform, if used) before spraying to eliminate contamination. Spray acetone after washing to ensure air-brush is cleared.
   II. Use pipe cleaner wire brushes to clean tubing and air-brush. Mechanically wipe surfaces.
2) Read user's manual prior to using Paasche H-series air-brush for full operation instructions.
   I. Connect spray jar to air-brush, turn on air flow, start air flowing by pushing down on trigger. Flow material by pushing down then pulling back. Aim away from surface when first pulling down on the trigger, and start coating surface once a good flow has started.
   II. Shake to keep mixture well mixed during spraying.
   III. Spray from further than 6 inches away from the surface, and far enough to allow solvents to evaporate before contacting the surface

3) Clean between surfaces by spraying acetone (and other solvents used) through the air-brush.

4) Clean everything after spraying by spraying solvents through the air-brush (use this spraying fluid to clean jars and equipment) and wiping everything with solvents.

    I. Open up the air-brush and clean the needle, tip, and all surfaces thoroughly.

5) Place samples to the side to cure and finish cleaning the entire area. Dispose of chemicals and vials accordingly.

Figure 8.4: Paasche air brush with spray jar.

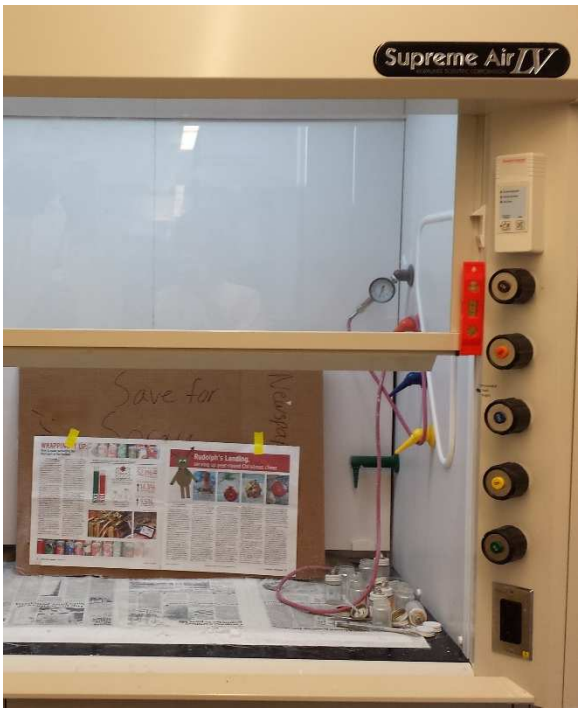

Figure 8.5: Spray coating fume hood with protective cardboard and newspaper.

8.2.4. Notes

Clean everything completely and often. The best way to have clean equipment when you need it is for everyone to thoroughly clean after use. Don't just spray solvent in and hope the jet dissolves contamination, use your hands and muscle to wipe down jars and scrape off contamination.

Best results are found when Silanized silica particles are sprayed at the 3 day mark. After this, the silica begins to degrade. Other solvents can be used for silanization and spraying, but try to use as little content of water (minimal aqueous solvents) as possible.

8.3. Mixture Ratio Calculations

The figure below highlights calculations for determining all characteristics of FPU-Silica mixed surfaces and is used for designing recipes for these mixtures. The FPU: Silica ratio, amount of FPU, % solids in the mixture, and silica/chloroform thinning ratio are the controlling parameters for these surfaces, with amounts of materials determined from these controls.

FPU:SiO2		10	
INPUT	**CALCULATION**		**OUTPUT**
FPU Total (g)	**Base (g)**	**Hardener (g)**	**Silica (g)**
6	5.57	0.43	0.600
FPU % Solids	4.0%	**Final (mg SiO2)/(mL Chloroform)**	15
0.6 g silica in 20 mL suspension		**Silica Mix Before Centrifuge (mL)**	20.0
Acetone (mL)	3.50	**Chloroform (mL)**	40.00
Coverage (in^2)	9.00	**Coverage (cm^2)**	58.05
6600	mg -Total Solids (FPU & SiO2)- mg		152
43.50	mL -Total Solvents (Acetone & Chloroform)- mL		
10	Ratio Solids (FPU:SiO2)		**mg/cm^2 Solids**
11.43	Ratio Solvents (Chloroform:Acetone)		113.70
90.9%	FPU % of Solids		**wt % Silica**
92.0%	Chloroform % of Solvents		9.09%

Total After Centrifuge			
Name	**% Weight**	**Mass (grams)**	**Volume (mL)**
Chloroform	86%	59.60	40.00
Acetone	4%	2.77	3.50
Silica Particles	1%	0.60	5.00
PU Base	8%	5.57	4.64
PU Hardener	1%	0.43	0.36
Total	***100%***	***69.0***	***53.5***
		AFTER CENTRIFUGE	

Part A			
Name	**% Weight**	**Mass (grams)**	**Volume (mL)**
PU Base	8%	5.57	4.64
Silica Particles	1%	0.60	5.00
Chloroform	91%	59.60	40.00
Total	***100%***	***65.8***	***49.6***

Part B			
Total	**% Weight**	**Mass (grams)**	**Volume (mL)**
PU Hardener	13%	0.43	0.36
Acetone	87%	2.77	3.50
Total	***100%***	***3.2***	***3.9***

Hardened (less solvents)			
Name	**% Weight**	**Mass (grams)**	**Volume (mL)**
PU Base	84%	5.57	4.64
PU Hardener	7%	0.43	0.36
Fumed Silica	9%	0.60	5.00
Total	***100%***	**6.6**	**10.0**

Figure 8.6: Mixed coating calculations sheet.

8.4. Layered Surface Calculations

The figure below highlights calculations for determining characteristics of FPU-Silica layered surfaces and is used for designing recipes for these materials. This is similar to the mixture calculations, except that the amount of FPU is not directly coupled to the amount of silica. As the thickness and concentration of the base FPU layer can be controlled independently of the top layer, these calculations use the coverage area for determining the recipe. These calculation sheets are in the excel file “FPU and Silica Calculations” for future group use.

Full FPU Base Layer (spray, pour, or spin coat, FPU and Silica de-coupled			
Coverage (in^2) (3 X #Slides)	6	mg/cm^2 SiO_2	15
FPU % Solids	18.0%	Final (mg SiO2)/(mL Chloroform)	30
INPUT	**CALCULATION**		**OUTPUT**
FPU Total (g)	Base (g)	Hardener (g)	Silica (g)
6	5.57	0.43	0.581
$FPU:SiO_2$	10.3	Coverage (cm^2)	38.70
0.6 g silica in 20 mL suspension		Silica Mix Before Centrifuge (mL)	19.4
Acetone (mL)	5.00	Chloroform (mL)	19.35
6581	mg -Total Solids (FPU & SiO2)- mg		270
24.4	mL -Total Solvents (Acetone & Chloroform)- mL		
10.3	Ratio Solids (FPU:SiO2)		mg/cm^2 FPU
3.9	Ratio Solvents (Chloroform:Acetone)		155.04
91.2%	FPU % of Solids		mg/cm^2 Silica
79.5%	Chloroform % of Solvents		15.00

Layer 1			
Name	% Weight	Mass (grams)	Volume (mL)
PU Base	56%	5.57	4.64
PU Hardener	4%	0.43	0.36
Acetone	40%	3.95	5.00
Total	***100%***	***10.0***	***10.0***
Layer 2			
Total	% Weight	Mass (grams)	Volume (mL)
Silica Particles	2%	0.58	4.84
Chloroform	98%	28.83	19.35
Total	***100%***	***29.4***	***24.2***
Hardened (less solvents)			
Name	% Weight	Mass (grams)	Volume (mL)
PU Base	85%	5.57	4.64
PU Hardener	7%	0.43	0.36
Fumed Silica	9%	0.58	4.84
Total	***100%***	**6.6**	**9.8**

Figure 8.7: Layered surface calculation sheet.

8.5. Cost Analysis of Spray-Coat Surfaces

Similar to the chemical etching analysis earlier, a cost analysis of a layered and mixed spray coating process were performed for lab-scale application, with a template produced for analysis of various surfaces.

Chemical		Acetone	Hexane	FPU	Silica	Chloroform	Silane
Price		20	50	150	70	275	1000
Volume (L)		4	4	3.8		4	0.6
Density (kg/L)		0.79	0.65	1.05		1.48	0.83
Weight (kg)	Total	3.14	2.60	4	1	5.92	0.5
$/kg		6.36	19.23	37.50	70.00	46.45	2000.00
$/gram		0.01	0.02	0.04	0.07	0.05	2.00
$/L		5.00	12.50	39.47	#DIV/0!	68.75	1666.67
$/mL		0.01	0.01	0.04	#DIV/0!	0.07	1.67
Weight Used (g)	**10.45**			10.00	0.45		
Volume Used (mL)	**70.20**	8.00	11.25	9.50	1.00	40.00	0.45
Part Cost ($/unit)	**$ 4.09**	$ 0.04	$ 0.14	$ 0.38	$ 0.03	$ 2.75	$ 0.75
% Cost	**100%**	**1%**	**3%**	**9%**	**1%**	**67%**	**18%**
Cost/mL Mix	**$ 0.06**	$ 0.00	$ 0.00	$ 0.01	$ 0.00	$ 0.04	$ 0.01
$/L Mix	***$ 58.22***	$ 0.57	$ 2.00	$ 5.34	$ 0.45	$ 39.17	$ 10.68
$/gal Mix	***$ 220.37***	Spray Area (sq in)		Coverage (sq ft/gal)			
Cost ($/sq ft)	***$ 2.04***	12		107.9			

Figure 8.8: Layered surface cost analysis.

Chemical		Acetone	Hexane	FPU	Silica	Chloroform	Silane
Price		20	50	150	70	275	1000
Volume (L)		4	4	3.8		4	0.6
Density (kg/L)		0.79	0.65	1.05		1.48	0.83
Weight (kg)	Total	3.14	2.60	4	1	5.92	0.5
$/kg		6.36	19.23	37.50	70.00	46.45	2000.00
$/gram		0.01	0.02	0.04	0.07	0.05	2.00
$/L		5.00	12.50	39.47	#DIV/0!	68.75	1666.67
$/mL		0.01	0.01	0.04	#DIV/0!	0.07	1.67
Weight Used (g)	**10.67**			10.00	0.67		
Volume Used (mL)	**49.53**	6.00	16.67	9.20	1.00	16.00	0.67
Part Cost ($/unit)	**$ 2.86**	$ 0.03	$ 0.21	$ 0.36	$ 0.05	$ 1.10	$ 1.11
% Cost	**100%**	**1%**	**7%**	**13%**	**2%**	**38%**	**39%**
Cost/mL Mix	**$ 0.06**	$ 0.00	$ 0.00	$ 0.01	$ 0.00	$ 0.02	$ 0.02
$/L Mix	***$ 57.73***	$ 0.61	$ 4.21	$ 7.33	$ 0.94	$ 22.21	$ 22.43
$/gal Mix	***$ 218.49***	Spray Area (sq in)		Coverage (sq ft/gal)		Ratio FPU:SiO2	
Cost ($/sq ft)	***$ 1.43***	12		152.9		15	

Figure 8.9: Mixed surface cost analysis.

8.6. Corn Washing Procedure

8.6.1. Introduction

Shell corn is never completely clean. Little red flakes of chaff from where the kernel connects with the cob will always break off from corn. When getting corn out of a large grain bin or in processing equipment, this chaff flies around in a cloud of dust. Early testing with corn abrasion saw this chaff as a fouling agent that served to soften the abrasion as it created a protective layer over the surface. As Oliver uses a variety of seeds, which are well washed prior to coating, it is not desirable to test with chaff in the abradant mixture. Chaff can be removed by washing with water or with air. Using air is very convenient for removing the chaff as gravity helps separate pieces; however, chaff also makes the surrounding very dirty and dusty, so this is not feasible for the laboratory. Intact kernels will sink to the bottom water while bad kernels and chaff will float and can be removed. It is very important to completely dry the corn after washing as it can absorb water quite well.

8.6.2. Setup

Equipment: Large 5 gallon bucket(s), shell corn, sink, powder soap, white 2 gallon bucket with grated edge, concrete mixer, disposable hand towels.

8.6.3. Washing Procedure

Use the white bucket to wash the corn as water and chaff can drain out through the grating, with the grating catching floated kernels and preventing them from clogging the sink drain.

Figure 8.10: Corn washing bucket in sink with a trapped kernel.

1) Place the bucket in the sink and fill it about 1/3 full with unwashed corn.
2) Fill the bucket with corn, stirring the corn by hand by turning/folding it in. Some chaff will not float without mixing.
3) Add a small amount of soap without the water running, then continue stirring. Remove chaff off of the surface with the soap bubbles and any undesirable organic matter.
4) Continue rinsing until no more soap is present, dump out the water, as much as you can dump out.
5) Pour into mixer for drying and wash a new batch while the previous batch starts to dry.

8.6.4. Drying Procedure

1) Mix without any towels for a few minutes to allow water to drain out (put cardboard under the mixer).
2) Add towels into the mixer to absorb water and pull them out as they soak up liquid.
3) Continue mixing for a while (a few days), turning the mixer on and off so as not to burn out the motor. Corn will be dry and hard to the touch, and should not yield when pinched with fingernails.

8.6.5. Notes

Corn moisture content is actually a very specific science that effects long-term storage, corn can be too dry or too wet for long term storage. For laboratory use, it is OK to be on the drier side as this will provide a heavier abrasion due to the corn being harder.

8.7. Corn Mixer Abrasion Procedure

8.7.1. Introduction

A standard 3.5 gallon cement mixer (CM) from Harbor Freight (Item #67536) was used to simulate accelerated seed abrasion by tumbling seeds over surfaces mounted collinearly along the interior of the CM. 5 pounds of washed shell corn is tumbled for 1 hour to abrade the surface, with contact angle measurements before and after mixing.

8.7.2. Setup and Operation

1) Weigh 5 pounds of corn into the mixer, and put the tilt on the first tilt setting, resulting in an approximate 45^{o} angle with the horizontal.
2) Place a bucket or piece of cardboard under the mixer to catch any removed chaff for disposal.
3) Mount samples on the black line inside the mixture (redraw if this line starts to fade) using double sided wall mounting strips (with pull tabs for easy removal). Point the arrows opposite of the direction of rotation so that the abrasive motion does not remove the sample.
4) Run the mixer for 30 minutes with a 15 minute cool-down period to prevent overheating of the drive motor. Run the test for 1 hour of active abrasion, then measure contact angles.

8.7.3. Notes

If the motor overheats, allow it to cool for around an hour then press the motor reset button and it will work again. Cooling with a fan will help expedite cooling. Clean the specimen mounting spot with a slightly damp towel for enhanced adhesion, but avoid wetting the corn.

Figure 8.11: Concrete mixer in operating position.

Figure 8.12: Concrete mixer in operation. Note that samples are mounted on the black line and not on the black rubber gasket.

Figure 8.13: Oliver Manufacturing seed dryer.[184]

Figure 8.14: Seeds flowing inside an Oliver seed dryer.[184]

8.8. Corn Shaker Abrasion Procedure

8.8.1. Introduction

A shaking mixer was tilted and fitted with a seed hopper and director to flow seeds over a shaking surface in an effort to simulate conditions experienced on a vibratory shaker. Use 2 petri dishes to tilt the shaker to an angle of 5°. Set the shaker to its maximum speed of 350 RPM. The flow needs to be adjusted by controlling the tilt angle and the gap for the seeds above the surface so that seeds slowly but consistently trickle across the surfaces being tested. It should take around 10 minutes for a gallon of seeds to flow through the system, but this rate can be adjusted for different levels of abrasion.

Figure 8.15: Shaker abrasion setup showing tilt and operation with hopper.

8.8.2. Hopper Setup and Operation

1) Place the plywood hopper table on a pair of large lab jacks over the shaker.
2) Place the hopper on the table with the outlet about 1 inch above the surface of the shaker. Use the lab jack screws to adjust the height of the hopper feed.

3) Start the shaker with the above settings. Make sure that the surface does not strike the hopper outlet.
4) Put a 5-gallon bucket under the outlet of the shaker to catch the seeds BEFORE adding seeds to the hopper.
5) Slowly pour seeds into the hopper and get the desired seed flow by adjusting the hopper height.
6) Add a fan to blow chaff away as it falls from the shaker to the bucket, if desired.
7) The hopper may need to be tapped or jostled if it begins to clog during use.
8) A stepstool may be necessary for pouring corn into the hopper.
9) Run abrasion test for 1 hour in standard method. Use longer time if desired for refined testing of a single surface.

8.9. Syrup Dip Test Procedure

8.9.1. Introduction

This dip testing procedure is designed to compare the adhesion of surfaces under basic submergence conditions. The test consists of weighing and measuring a sample before and after dipping into and out of a fluid (the drink syrup will be described here, but fluids are interchangeable). Outputs are measured adhesion per unit of surface area of the coating.

It is suggested that the "Dip Coat Template" be copied and modified for specific coatings and fluids. Find a control sample (if possible) that obviously completely repels the fluid and use this sample to calculate the control amount of fluid adhered to the sample bottom and edges for use in the "less edges" calculation.

8.9.2. Setup

Materials: Syrup mixture in beaker (large enough for complete dipping), iron stand, fishing line (or other thin rope) with alligator clips or paper clamps on each end, syringe pump, sensitive scale, cleaning wipes, weighing paper, gloves.

Prepare syrup by completely stirring with a magnetic stir bar. Setup iron stand to allow for fishing line with clamps to pull the sample vertically out of the fluid (Figure 8.16). Clip an alligator clip to the moving portion of the syringe pump.

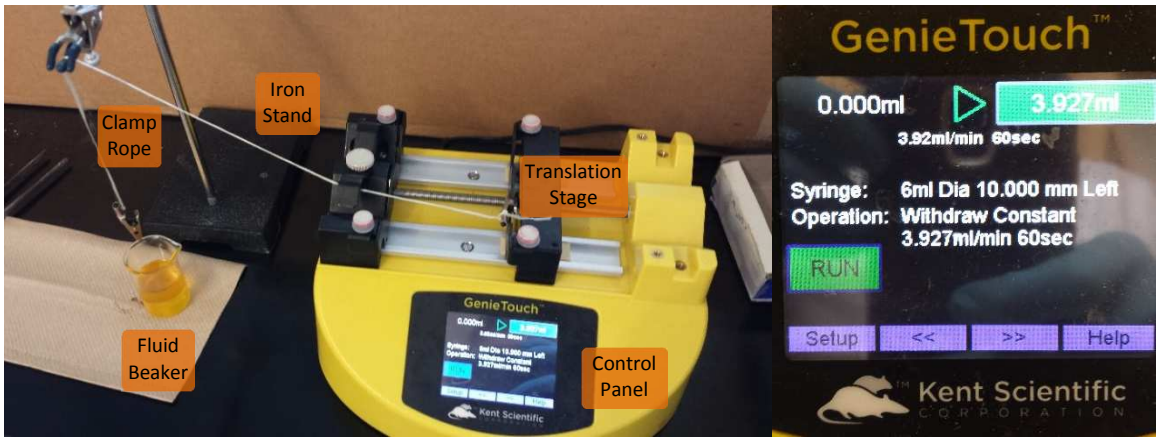

Figure 8.16: Dip test setup showing syringe pump settings.

Syringe Pump: 10 mm diameter, facing left, 5 cm min^{-1} (3.92 ml min^{-1}), 60 second withdrawl, 6 mL capacity. Set zero position to left side of syringe pump so that the pump will pull the rope at a constant rate.

8.9.3. Procedure

1) Weigh and measure samples before testing (surface area and initial weight are needed for calculations. 1" X 1" samples are the ideal size for testing. Try to keep sizes consistent.
2) Get a wipe ready, and put weighing paper/boat on the balance (needs to be a sensitive balance).
3) Clip the sample at an edge. Reverse the syringe pump to submerse the sample.
4) Immediately run the syringe pump and let the sample be completely removed from the fluid and let the syringe pump stop on its own.
5) Unclip the sample and wipe excess fluid off the bottom and sides of the sample.
6) Weight the sample for final weight.
7) Repeat as desired.

8.9.4. Notes

Be careful to not run the syringe pump moving stage into the edges, this will cause the motor to stall and possibly damage the pump. If this happens, remove the side and use a screwdriver to manually retract the stage. If using syrup, know that everything will be sticky. Perform test at consistent temperature (room temperature is ideal).

8.10. Syrup Mixture Preparation

8.10.1. Introduction

The drink syrup is a 2:1 (by volume) mixture of Sucrose Acetate Isobutyrate [Sucrose Acetate Isobutyrate](#) (SAIB) and Terpene Hydrocarbons (Terpene).

The SAIB is soluble in the terpene and in acetone, but not much else. It is also VERY STICKY. SAIB is a food-grade sugar that has a very high viscosity at room temperature (think of tree sap).

Figure 8.17: Coca Cola SAIB label and drum.

Terpene is a lemon hydrocarbon that is insoluble in water:

TERPENE HYDROCARBONS, N.O.S.

CAS #: 84292-31-7, Flammability Hazard: 3

Aka: Lemon Terpenes, used for soft drinks and juices

Insoluble in Water, Avoid strong oxidizing agents

Reference Florida Chemical Product Code 304000, Source: Coca Cola

Figure 8.18: Terpene hydrocarbons in drum and in glass bottle.

8.10.2. Procedure

Materials: SAIB can, Terpene Jar, 1-2 L beaker (depending on desired volume), 2 hot plates, large stir bar, a lot of cardboard, a lot of wipes, a lot of gloves, lab coat, storage jars for final mixture.

1) Cover working area with cardboard. You will thank yourself as it is a messy process. The SAIB can be used outside of the fume hood, but I would suggest doing the final mixture in a fume hood.
2) Turn on a hot plate to ~250 ^{o}C. Partially fill a sink with water to distribute heat across the can.
3) Clean the bottom of the SAIB can, then place it on the hot plate. Every 5 minutes remove it from the hot plate and stir the mixture by tilting the can on the floor and rolling it. The SAIB will become less viscous in the bottom of the can than at the top, so it is important to roll it and mix it well to be able to pour it easily.
4) Heat for 10-20 minutes. Try pouring the SAIB into the beaker to check viscosity.
5) Once the fluid is flowing easily, fill each beaker ~half full, then place half full beakers on another hot plate at ~50 ^{o}C. Cap the can, clean it up, and put the can away.
6) Add Terpene (half of the volume of the SAIB, 2:1 ratio SAIB: Terpene by volume) on top of the SAIB. With a spatula, mix well.

7) Add a magnetic stir bar and keep stirring until the mixture will stir by itself with the magnetic stir bar. Let the mixture stir for ~1 hour.

8) Pour into storage jar, cap, and label as “SAIB/Terpene Syrup, Date”

9) Clean everything with acetone and disposable towels. You will need a lot of acetone.

10) Enjoy the lemony smell.

Figure 8.19: Syrup mixture on hot plate for mixing with magnetic stir bar.

8.10.3. Notes

IN CASE OF SPILL- Pour large silica particles onto spill and rub with towel and gloves. Silica will pick up the syrup and allow it to be scraped off of the surface and thrown away. Everything is food grade, but fluid still needs to be disposed of as a hydrocarbon (non-halogenated). Please be careful not to make everything sticky. Make the mixture in large batches as it is a pain to work with the SAIB. There should be sufficient mixture for a lot of dip tests, but large-scale flow tests will require more to be made.

9. APPENDIX D- GENERAL LAB SUPPLEMENTARY

9.1. Chemical Management Information

9.1.1. Lab Safety Training

Complete the CSU Environmental Health Services Hazardous Waste Generator Training by registering here. Training consists of reading a manual and going through slides and training videos before taking an exam.

9.1.2. *Chemical and Lab Inventory*

Access the group's chemical inventory here. Familiarize yourself with the chemical and lab inventory and where items are located in the laboratory. EHS has a separate chemical inventory system that we keep up to date in parallel with the group inventory. It can be accessed via the Chemical Management button (see below) after logging into the EHS Main Portal (link) after completing the Lab Safety Training. There is also a "Chemical Management" PowerPoint in the group folder with more detailed instructions.

Figure 9.1: EHS management portal with management options.

9.1.3. Lab Hazardous Waste

Follow the EHS instructions for hazardous waste and for chemical compatibility, but following are a few lab-specific suggestions for hazardous waste:

Use larger labels than provided by EHS so that you can easily write the responsible individual, start date, and contents so that these items can be easily read. Include percentages on constituents to make disposal easier.

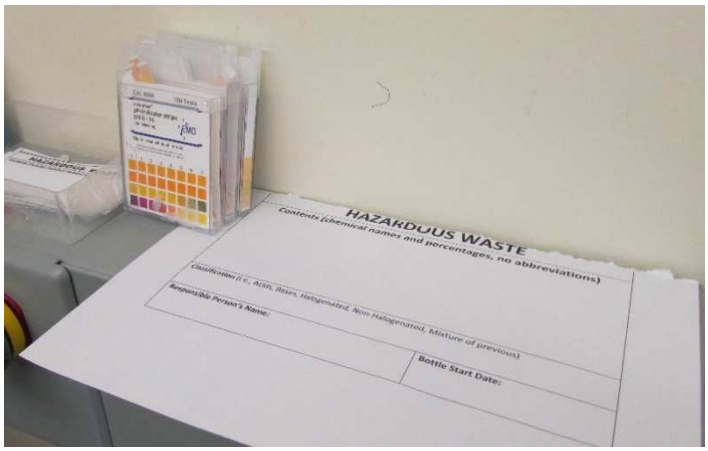

Figure 9.2: Enlarged hazardous waste in-use labels with pH strips.

Segregate incompatible chemicals into acids, bases, non-halogenated solvents, and halogenated solvents. Some chemicals are inherently mixed during use, such as hexane, silane, and chloroform, or acids and aqueous solvents. For pre-mixed chemical types that are compatible, create a separate waste bottle with the mixture clearly labeled, and include a note to not add anything other than pre-mixed materials as it is best to minimize the amount of mixed chemicals produced.

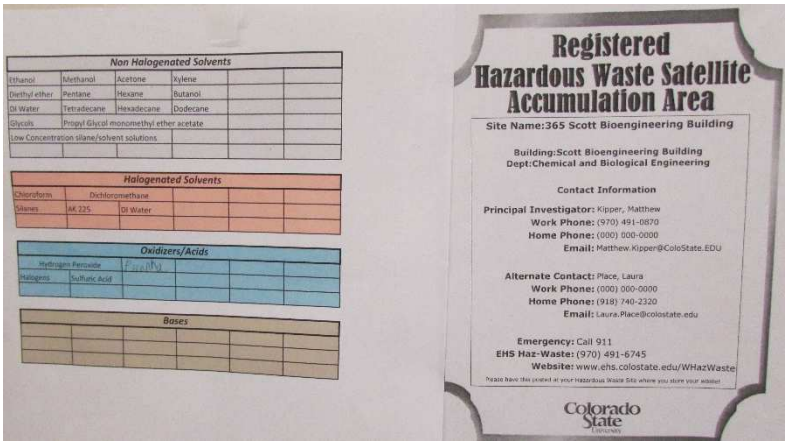

Figure 9.3: Chemical categories and haz-waste satellite area certificate.

Keep the waste bottles and secondary containers clean by using a funnel for disposal and by regularly checking and cleaning the waste area. Dispose of bottles once fluids reach the tapering neck of the bottle to prevent over-filling.

Figure 9.4: Haz-waste containment area with secondary containment and disposal boxes clearly marked.

Request as many new bottles as are disposed of, unless there are an excess of empty bottles. It is good to always have at least 2 extra empty bottles to be prepared for a spill. Keep all single boxes that chemicals are shipped in, as these are highly convenient for packaging for disposal. Try to dispose of multiple bottles at a time for efficiency. When a chemical bottle is emptied, remove it from the inventory electronically, but also use a Sharpie to make large, obvious X's on the label so that it can be used for waste disposal.

Figure 9.5: Empty disposal bottles as-received from EHS.

9.2. Goniometer Procedure

9.2.1. Equipment Introduction

The ramè-hart model 260-F4 contact angle goniometer is a useful tool for a variety of surface measurements, with more capabilities than are described here. It utilizes a fiber optic light to illuminate a drop placed on a controllable stage by a micro syringe. A video camera captures the image and sends it to a connected computer, which uses software to measure the contact angle and make subsequent calculations for surface energy, surface tension, and more.

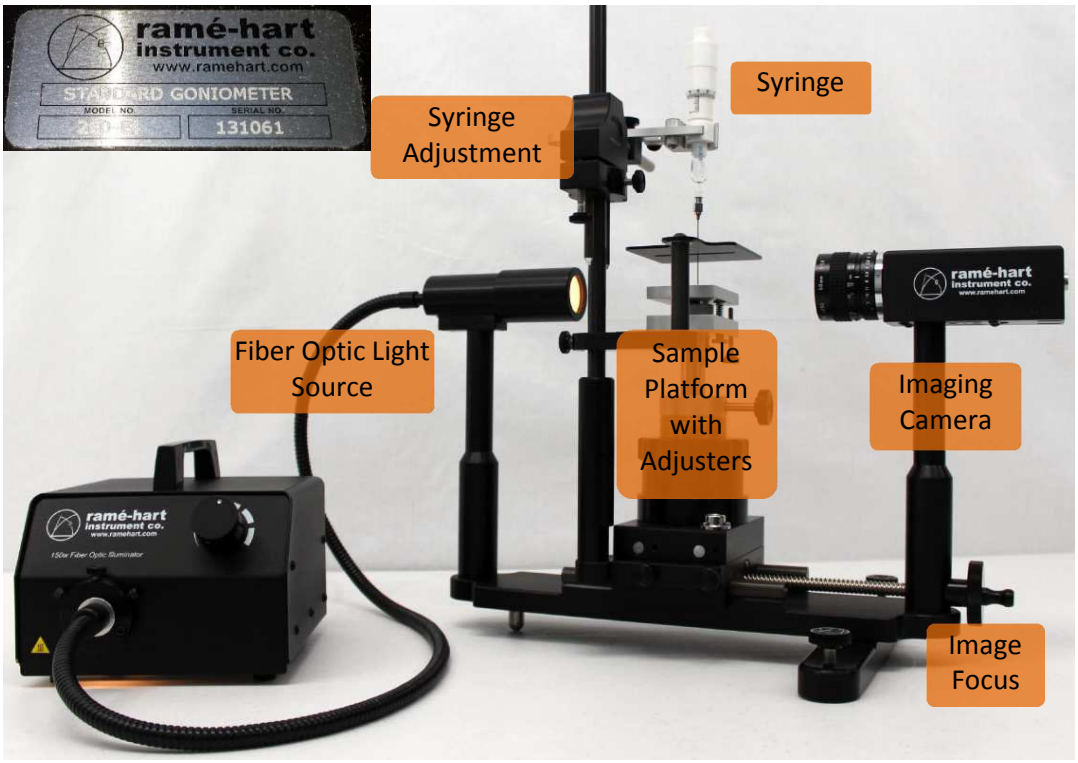

Figure 9.6: Goniometer components overview with equipment tag.

9.2.2. Equipment Operation

After placing the sample on the platform and centering the syringe and needle over the sample, close to the sample surface, turn on the fiber optic light and get the Drop Image software running so that you can see the silhouette of the surface on the software camera screen.

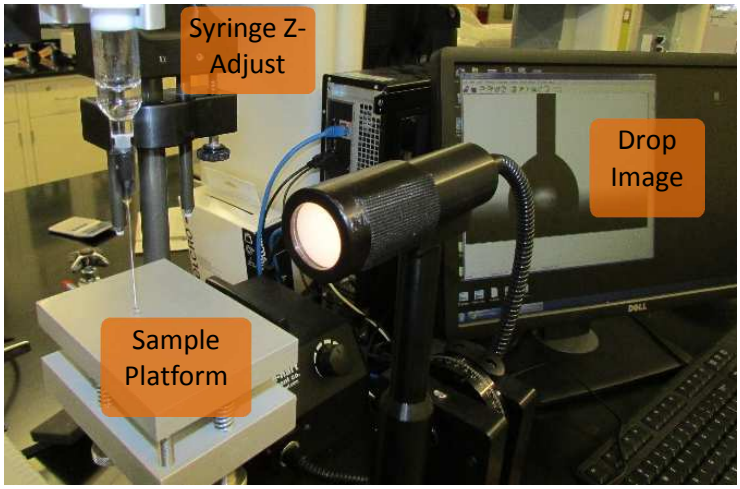

Figure 9.7: Goniometer analysis overview.

Once the syringe and surface are visible on the screen, finely adjust the syringe so that the needle is centered on the screen. Using the macro and micro platform Z-adjustments, bring the sample so that the surface is in the lower third of the screen. Bring the needle into focus with the focusing screw under the camera.

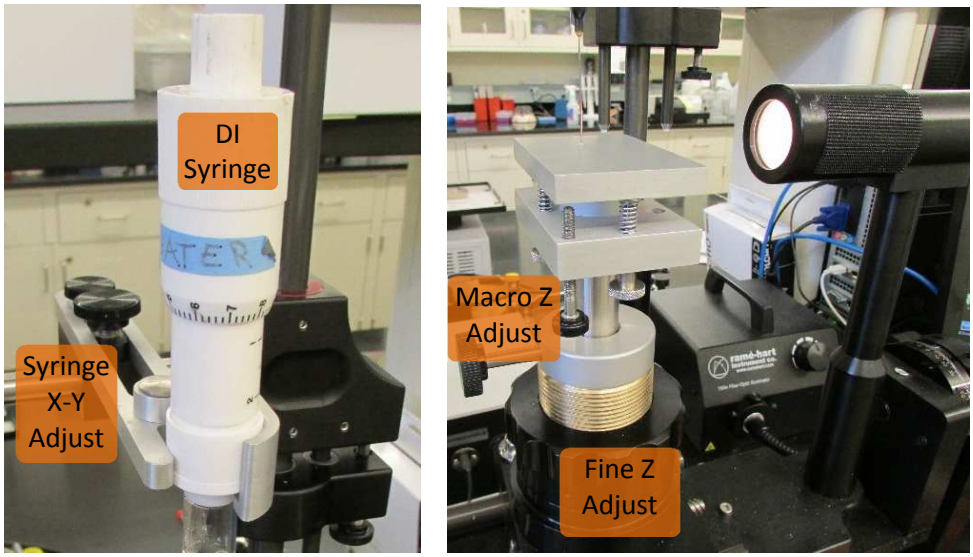

Figure 9.8: Goniometer positioning tools.

With the image now in focus, prime the syringe by putting a drop on the surface and removing it. Use the platform Y-translation crank to move to a fresh position on the surface. Perform contact angle measurements (see the software section). Raise the needle and place a static drop on the flat surface.

Using the tilt crank, tilt the system until the drop rolls off of the surface, record the indicated angle as the roll-off angle.

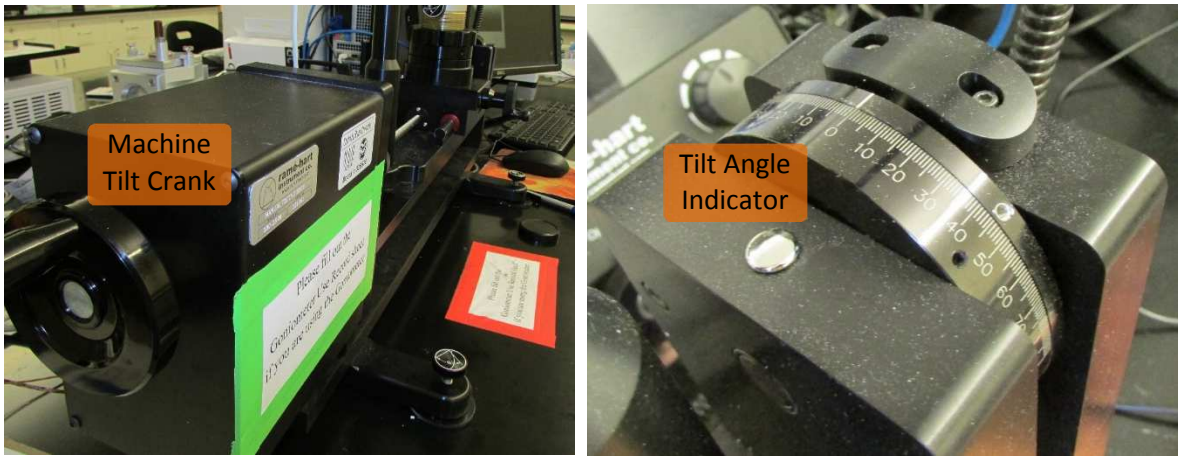

Figure 9.9: Roll-off angle crank and indicator.

9.2.3. Software Use

Open “Contact Angle” from the “CA Tools” menu. Click “measure” to bring up two vertical lines and a horizontal line for measuring contact angles. Left-click to place the left vertical line through the drop but to the left of the needle, with the right vertical line to the right of the needle (right-click). Neither vertical line should be touching the needle; doing so will result in an error. Align the horizontal line with the solid-liquid interface (shift + left-click).

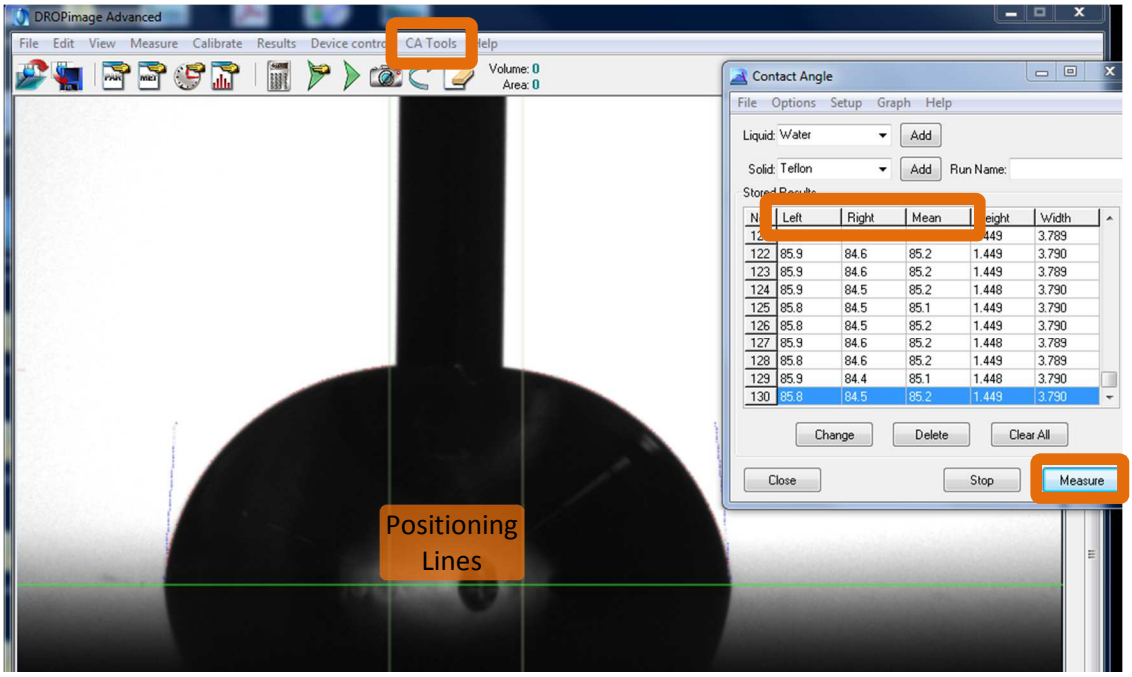

Figure 9.10: Contact angle measurement window and setup.

Measure advancing contact angles while adding fluid to the drop and repeatedly clicking “Measure” while monitoring when the drop de-pins and advances. Record maximum angle measured just prior to drop advancement. Similarly, measure the minimum angle during drop retraction for the receding contact angle measurements. Receding angle measurements may require bringing the needle closer to the surface. Dimming the light will show the curves used to calculate the contact angles, so check this image to be sure that the angles are based on the droplet curvature and not refracted light from the surroundings.

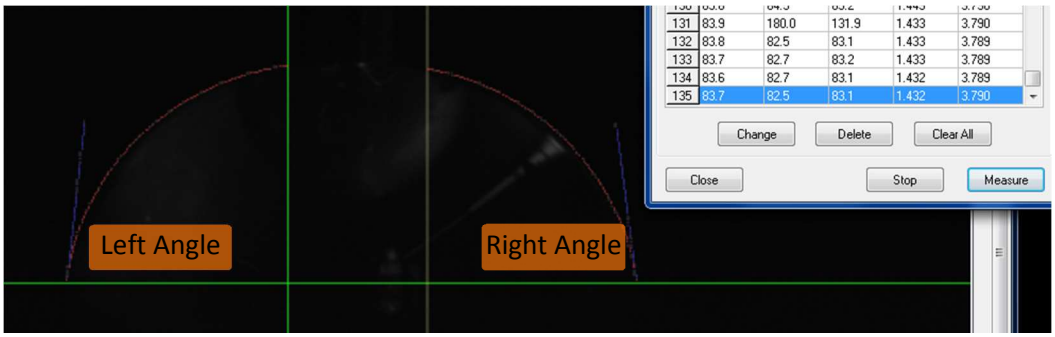

Figure 9.11: Contact angle lines shown on blackened screen showing droplet curvature.